

Review on High-Loading and High-Energy Lithium–Sulfur Batteries

Hong-Jie Peng, Jia-Qi Huang, Xin-Bing Cheng, and Qiang Zhang*

Owing to high specific energy, low cost, and environmental friendliness, lithium–sulfur (Li–S) batteries hold great promise to meet the increasing demand for advanced energy storage beyond portable electronics, and to mitigate environmental problems. However, the application of Li–S batteries is challenged by several obstacles, including their short life and low sulfur utilization, which become more serious when sulfur loading is increased to the practically accepted level above 3–5 mg cm⁻². More and more efforts have been made recently to overcome the barriers toward commercially viable Li–S batteries with a high sulfur loading. This review highlights the recent progress in high-sulfur-loading Li–S batteries enabled by hierarchical design principles at multiscale. Particularly, basic insights into the interfacial reactions, strategies for mesoscale assembly, unique architectures, and configurational innovation in the cathode, anode, and separator are under specific concerns. Hierarchy in the multiscale design is proposed to guide the future development of high-sulfur-loading Li–S batteries.

1. Introduction

A constantly increasing energy demand and formidable environmental crisis are igniting global interest in various advanced technologies, such as electrified transportation and smart grids, aiming at efficient storage and sustainable utilization of clean, renewable energy sources based on solar and all of its derivative forms, such as wind, wave, geothermy, and so on.^[1] High-energy-density rechargeable batteries are the critical elements in these cutting-edge energy technologies.^[2] Conventional lithium-ion batteries (LIBs), based on ion-insertion materials such as lithium metal oxides (e.g., LiCoO₂ and LiNi_xCo_yMn_{1-x-y}O₂) or lithium phosphates (e.g., LiFePO₄) as the cathode and graphite as the anode, have transformed portable electronic devices for more than thirty years.^[3,4] Under continuous research and development, LIBs are approaching the theoretical limitation of electrode materials. Hence, this stern reality hinders the pervasive deployment of LIBs in aforementioned emerging

applications that demand exceptional specific energy (energy per unit weight) or energy density (energy per unit volume). Therefore, alternative battery chemistries to LIBs are attracting unprecedented attention to break through the ceiling.

The lithium–sulfur (Li–S) battery, normally comprised of a sulfur cathode and a lithium anode, is capable of exerting multielectron conversion electrochemistry between elemental sulfur and lithium to deliver considerably higher specific energy than LIBs (Figure 1a).^[5,6] Both sulfur and lithium are lightweight elements, resulting in very promising gravimetric capacities of 1672 and 3860 mA h g⁻¹, respectively; much higher than that of insertion-type electrodes (e.g., cathodes at the delithiated state such as Li_{1/2}CoO₂ (142 mA h g⁻¹), Li_{1/3}Ni_{1/3}Co_{1/3}Mn_{1/3}O₂ (195 mA h g⁻¹), Li₀FePO₄ (178 mA h g⁻¹),

and anodes at the fully lithiated state such as graphite (LiC₆, 340 mA h g⁻¹)).^[3] Considering an average voltage of 2.15 V, theoretical specific energy and energy density of the Li–S battery are 2500 W h kg⁻¹ and 2800 W h L⁻¹, respectively, going much further beyond conventional LIBs. In addition, sulfur is cheap and abundant, making Li–S batteries a promising low-cost technology for widespread deployment. Unlike another alternative high-energy rechargeable battery, namely the lithium–oxygen/air battery, the Li–S battery is a closed system, preventing exposure to atmospheric contamination and potential explosive danger.

The first Li–S battery was proposed in 1960s.^[7] However, Li–S batteries were plagued with low capacity and rapid capacity fading in the next few decades. In 2009, Nazar and colleagues achieved a major breakthrough by introducing a highly ordered, nanostructured, mesoporous carbon host to encapsulate sulfur.^[8] The mesoporous carbon, CMK-3, precisely constrained sulfur nanofillers within its conductive channels, rendering Li–S batteries with high capacity and stable cycling. Since then, a growing number of efforts and achievements have been made, significantly promoting the understanding toward Li–S batteries and expanding the whole field.^[9–11] Up to now, high sulfur utilization (>90%),^[12] high weight percentage of sulfur (>90%),^[13,14] extraordinary high-rate capability (>10 C, 1.0 C = 1672 mA g⁻¹),^[15] and long service life (>1000 cycles)^[16–19] have been realized with the remarkable progress in material chemistry and electrochemistry. Nevertheless, most of these achievements were obtained with relatively low areal loadings of sulfur (<2.0 mg cm⁻²). The low areal loading

H.-J. Peng, Prof. J.-Q. Huang, X.-B. Cheng, Prof. Q. Zhang
Beijing Key Laboratory of Green Chemical Reaction
Engineering and Technology
Department of Chemical Engineering
Tsinghua University
Beijing 100084, China
E-mail: zhang-qiang@mails.tsinghua.edu.cn

The ORCID identification number(s) for the author(s) of this article can be found under <http://dx.doi.org/10.1002/aenm.201700260>.

DOI: 10.1002/aenm.201700260

raises an inevitable question: is the Li–S battery really as promising as it presents theoretically?

Unfortunately, the answer would be no as long as the areal sulfur loading remained low, even if unprecedented cell performance was obtained. To pave the way to practically viable Li–S batteries, a high areal loading of sulfur is essential.^[20,21] According to the estimation from Wang and co-workers, an areal capacity of at least 4.0 mA h cm^{-2} is required for Li–S batteries to be comparable to commercial LIBs.^[22] More than just areal capacity, the areal sulfur loading further determines the gross specific energy of a packaged Li–S cell, as it strongly affects the weight percentage of active materials.^[23] In fact, it has been accepted that in the scope of the whole device, instead of materials only, cell parameters, such as the areal loading of sulfur, the weight percentage of sulfur in the cathode, the excess mass of lithium, and the electrolyte/sulfur (E/S) ratio have profound influence on the specific-energy/energy-density.^[24] For example, Hagen et al. systematically investigated the effect of these parameters on cell specific energy using prototype 18650 Li–S cells, and validated the huge gap between the state-of-art results and the expectations (cell specific energy of $\approx 500\text{--}600 \text{ W h kg}^{-1}$).^[20] Pope and Aksay statistically analyzed the projected specific energy as a function of sulfur loading and E/S ratio, indicating that the sulfur loading must be higher than 2.0 mg cm^{-2} to gain a specific energy higher than 400 W h kg^{-1} , while E/S ratio would exhibit a more prominent impact on the specific energy if the sulfur loading was increased to $3.0\text{--}5.0 \text{ mg cm}^{-2}$ or higher (Figure 1b).^[25] Eroglu et al. described a set of cell parameters that are even more challenging for Li–S batteries being deployed in electric vehicles: sulfur loading of $>7.0 \text{ mg cm}^{-2}$, a limited excess of lithium ($\approx 50\text{--}100\%$), and E/S ratio of $<1.9 \text{ mL g}^{-1}$.^[26] Although the standards used for these estimations vary slightly, the important role of sulfur loading and E/S ratio in shaping the future of Li–S batteries is unambiguously identified.^[27]

Despite many impactful and insightful reviews, in which nanostructured sulfur cathodes,^[10,28] anodes,^[29] separators,^[30–32] and electrolytes^[33] have been summarized, none of them particularly focus on and comprehensively introduce the strategies and approaches toward advanced high-loading Li–S batteries. The scope of this review is to provide an overview of major progress in recent high-loading and high-energy Li–S battery research and to intentionally extract valuable concepts from these advancements. A threshold of at least 2.0 mg cm^{-2} sulfur loading is adopted to explore potential solutions for addressing Li–S batteries with even higher loadings. With the increase of sulfur loading, issues that are possibly incubative under low loading raise in not only the sulfur cathode side but also in the anode, as well as at the interfaces between the separator and cathode/anode. Therefore, a hierarchical design principle is presented with branches lying on 1) the cathode with its basic electrochemistry, host–sulfur/polysulfide/Li₂S guest interfacial engineering, particle design, and electrode architectures being discussed; 2) the anode classified into lithium metal and the nonmetallic counterpart; 3) the interlayer/separator with modulation of either sides in contact with the cathode or anode; and 4) the integrative configuration (Figure 2). Based on the progress made so far, a perspective on existing issues and future directions is presented. Particularly, personal insights into the



Hong-Jie Peng gained his B.Eng. from the Department of Chemical Engineering at Tsinghua University in 2013. He is currently a Ph.D. candidate at Tsinghua University. His research interests focus on nanocarbon, advanced energy storage/conversion, lithium–sulfur (Li–S) batteries, and catalysis.



Jia-Qi Huang is a professor in Advanced Research Institute for Multidisciplinary Science at Beijing Institute of Technology. He received his Ph.D. degree in Department of Chemical Engineering from Tsinghua University in 2012. His research interests cover the synthesis approaches and application of nanomaterials for rechargeable batteries.



Qiang Zhang received his bachelor and Ph.D. degree from Tsinghua University in 2004 and 2009, respectively. After a stay at Case Western Reserve University, USA, and Fritz Haber Institute of the Max Planck Society, Germany, he was appointed as an associate professor at Tsinghua University in 2011. His interests focuses on energy materials, and includes Li–S batteries, Li metal anodes, 3D graphene, and electrocatalysts.

unaddressed problems induced by high E/S ratio and electrolyte depletion, as well as potential strategies, are provided.

2. Cathode

The most commonly used cathode material in Li–S batteries is elemental sulfur, among which cyclo-S₈ is thermodynamically the most stable allotrope under ambient conditions.^[34] One of the major obstacles to utilize elemental sulfur as electrochemically active materials is the inherently low electronic conductivity ($5 \times 10^{-30} \text{ S cm}^{-1}$ at $25 \text{ }^\circ\text{C}$).^[35] Therefore, the direct solid–solid conversion between sulfur and lithium sulfide (Li₂S) at room temperature is strictly impeded by the conductivity

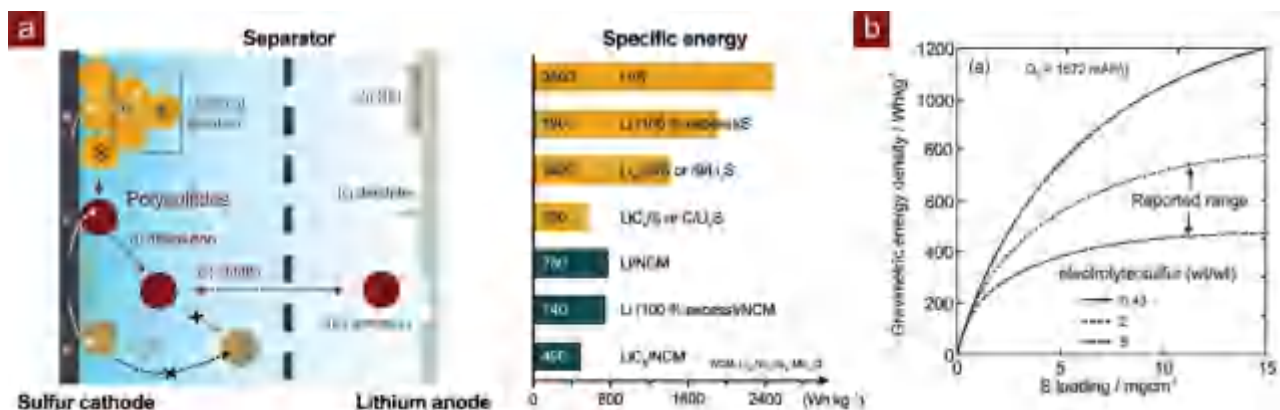


Figure 1. a) Schematic of a typical Li-S battery and specific energies of various rechargeable battery systems. b) Specific energy as a function of the sulfur loading for various ratios of electrolyte mass to sulfur mass. Reproduced with permission.^[25] Copyright 2015, Wiley-VCH.

issue. To enable this kinetically sluggish reaction, a series of soluble intermediates, namely polysulfides, are introduced in the overall reaction scheme. In general, polysulfides are in the form of sulfur chains with two terminal lithium ions (Li_2S_n , $n = 3-8$). The solubility and mobility in organic electrolytes make it easy for active materials to access both electrons from the solid surface and ions from the solution. Polysulfides, naturally playing the role of redox mediator, enable viable Li-S redox reactions.

Lithiated sulfur, either polysulfides or $\text{Li}_2\text{S}_2/\text{Li}_2\text{S}$, is also under intensive investigation as starting electrode materials.^[6,9,36] Their electrochemical characteristics are literally the same as those of cyclo- S_8 , especially after the first cycle. Some unique sulfur allotropes, such as short sulfur chains (S_2-S_4) physically confined in porous substrates,^[37,38] and chemically

covalent-bonded organosulfides (e.g., pyrolyzed polyacrylonitrile (pPAN)/sulfur composite (pPAN@S)^[39-41] and carbyne polysulfides)^[42] exhibit a distinctly different electrochemistry from cyclo- S_8 . Owing to the ultra-dispersion of sulfur atoms at molecular level, in combination with the polysulfide-insoluble carbonate electrolytes, polysulfide formation is unexpected. Therefore, in the following part, we will primarily discuss the design principles for elemental sulfur cathodes based on cyclo- S_8 , polysulfides, and Li_2S , as well as their composites. The other sulfur allotropes, which are compatible with the carbonate electrolytes and possess unique electrochemistry, will be discussed later.

In this section, we present a hierarchical overview of design principles and approaches toward high-sulfur-loading cathodes. The design of sulfur cathodes, especially those based on typical sulfur-polysulfides- Li_2S reaction scheme, is divided into three hierarchies: 1) interface engineering, 2) particle design, and 3) electrode architecture. Some design principles, particularly discussed in the latter two parts, are also general for high-loading electrodes based on unique sulfur allotropes such as S_2-S_4 chains and covalent-bonded sulfur.

2.1. Interface Engineering

Introducing polysulfides into the whole reaction scheme of Li-S redox paves the way toward viable Li-S batteries operated at room temperature. On one hand, the dissolution and diffusion of polysulfides provide the naturally existed redox mediators to make the insulating sulfur/ Li_2S electrochemically active. On the other hand, the shuttle effect, induced by the diffusion of polysulfides across the separator and their internal redox with both sulfur cathodes and lithium anodes, however, renders several technical obstacles, including capacity fading, low efficiency, and self-discharge.^[43] Moreover, the repeated dissolution and re-deposition of sulfur result in drastic structural change, which is more serious than the hypothetical volume expansion/shrinkage during solid-solid conversion between sulfur and Li_2S ($\approx 70\%$).^[44] Therefore, to manipulate the dissolution, diffusion, and redox reactions of polysulfides at the electrode/electrolyte interface is becoming the kernel of advanced



Figure 2. Schematic of the hierarchical design principle for high-loading Li-S battery.

electrode design.^[45] Especially in the case of high-loading Li–S batteries, the shuttle effect will be more serious as the polysulfide crossover is multiplied. In addition, the reaction rates should simultaneously be enhanced to meet the high areal current densities. All of these requirements demand for mechanistic understanding and rational engineering of the interfaces between active materials, conductive host, and electrolyte.

Since 2009, designing conductive nanoporous host materials for sulfur-based cathodes has been the most primary approach to enhance Li–S batteries.^[46] Nanocarbon or nanoporous carbon, such as one-dimensional (1D) carbon nanotubes (CNTs)/carbon nanofibers (CNFs),^[47,48] two-dimensional (2D) graphene/carbon nanosheets,^[49,50] and three-dimensional (3D) porous carbon,^[51,52] as well as their hybrids,^[53] have gained the first attention to serve as sulfur hosts due to their superior electrical conductivity, high surface area, tunable porous structure, and excellent chemical/electrochemical stability. Despite that considerable efforts have been devoted in nanocarbon hosts and huge progress has been made in improving capacity, cycling stability, and rate performance of Li–S batteries so far,^[54,55] most of reported carbon/sulfur composite cathodes possessed areal sulfur loadings of <2 mg cm⁻² or even lower. As the sulfur loading increases, routine carbon/sulfur composite cathodes still suffer from substantial dissolution of polysulfides and rapid capacity fading. Alternative hosting materials are in urgent demand, especially aiming at high-areal-capacity Li–S batteries with acceptable specific energy and cycling stability.

Recent progress in in situ and in operando characterization techniques,^[56] including Raman spectroscopy,^[57] X-ray diffraction,^[58] X-ray adsorption spectroscopy/X-ray adsorption near-edge spectroscopy (XANES),^[59,60] X-ray fluorescence microscopy,^[61] nuclear magnetic resonance,^[62] and ultraviolet-visible light adsorption spectroscopy,^[63,64] significantly accelerated the mechanistic understanding of Li–S redox chemistry in working cells. Particularly, crucial steps in Li–S redox reactions that involve polysulfides have been partially disclosed by speciation of various polysulfides during charging/discharging. For example, Cuisinier et al. developed an operando XANES technique to monitor sulfur speciation in a working Li–S cell as a function of degree of discharge/charge, indicating the disproportionation pathway for solution (polysulfides)-to-solid phase transfer and confirming the delayed formation of Li₂S (until >60% of degree of discharge) from a supersaturated state (Figure 3a).^[59] By combining in situ or operando characterizations and physical modeling, a bunch of mechanisms have been proposed and summarized in a comprehensive review.^[65] Hypothetically, the competition between electrochemical reactions (e.g., electrochemical reduction on the surface) and chemical reactions (e.g., disproportionation in solution) has been widely accepted to exist, and it is also correlated to the nature of key intermediates, or, more specifically, whether they are anions (e.g., S₄²⁻) or radicals (e.g., S₃^{•-}) (Figure 3b).

The detailed charge/discharge mechanisms of Li–S batteries still remain exclusive. However, learning from the analogous system of Li–O₂ battery, it has been commonly accepted that electrolyte solvents,^[66] anions,^[67] and current rates^[68] affect the ionic strength of Li⁺ complexes and relative stability of various intermediates. Consequently, these differences determine the detailed multielectron reaction mechanism in a working cell.

These insights have been implemented in Li–S batteries through some mechanistic works.^[64,69,70] Indicatively, the novel design of sulfur host materials becomes more and more appealing as it shows tremendous potential for tuning the Li–S redox reactions. The intrinsic sluggish conversion of polysulfides on a nonpolar surface, as well as substantial loss of active materials in bulk electrolyte, is attributed to the weak interaction between polar polysulfides and nonpolar carbon materials.^[71,72] Therefore, adopting polar and conductive host materials in sulfur composite cathodes is becoming the most rapidly growing area for Li–S battery research.^[73] These polar and conductive hosts include heteroatom (O, N, and S, etc.)-incorporated conjugated polymer,^[74,75] heteroatom mono-/dual-doped carbon,^[16,22,76] transition metal oxides,^[77–79] transition metal sulfides,^[17,80–82] transition metal carbides/nitrides,^[71,83] and metal–organic frameworks (MOFs)/MOF-derived composites.^[84] Normally, the replacement of carbon hosts by these materials facilitate the chemical interactions between polysulfide intermediates and conductive surface. Very recently, our group revealed that both suitable polarity and intrinsic electrical conductivity were crucial for Li–S redox reactions regarding the inevitable adsorption and charge-transfer processes during discharge (Figure 3c).^[71] Polar conductor possessed superb capability to enhance the surface electrochemical kinetics and solution–solid phase transfer.

Some review articles have systematically summarized the strategies and design principles of polar host materials for advanced sulfur cathodes.^[45,73,85] In this review, overlapped content will not be discussed in details. Instead, applications of these novel polar host materials will be stated and referred in following parts separately. The purpose of this section is to highlight the role of electrolyte/cathode interfaces, at which transport and reaction behaviors of polysulfides determine the battery performance. The use of polar and conductive host materials, at least, will endow high-loading sulfur cathodes with three remarkable attributes: 1) superior retention of active materials through strong chemisorption of polysulfides, 2) facile control of solid deposits (e.g., Li₂S) in spatial and size uniformity to prevent their detachments and redistribution in electrically insulating region, and 3) kinetic modulation of electrochemical surface redox reactions to synergistically suppress undesirable chemical disproportionation, lower discharging/charging overpotentials, and reduce voltage hysteresis. The last trait also implies the possibility to operate an Li–S battery with a low E/S mass ratio because the formation of Li₂S on polar hosts is regulated to early stage of discharge through a surface-dominant reaction pathway, while dissolution of polysulfides in electrolyte is diminished heavily (Figure 3d).^[78,79] The prior formation of solid deposits (e.g., Li₂S) has also been observed using electron microscopy.^[17] It is crucial for building high-energy-density Li–S batteries, especially with a high areal loading of active materials.

Section Summary (2.1.): Aiming at high-sulfur-loading Li–S batteries, interface engineering is not necessarily needed. However, deepening the understanding of the solid–solution–solid redox reaction mechanisms and hereby exploring innovative cathode substrates are of incredible importance for the development of Li–S chemistry and devices. In fact, inspiration has been drawn from the aforementioned engineered host–guest (i.e., sulfur species) interfaces and a large number of polar host

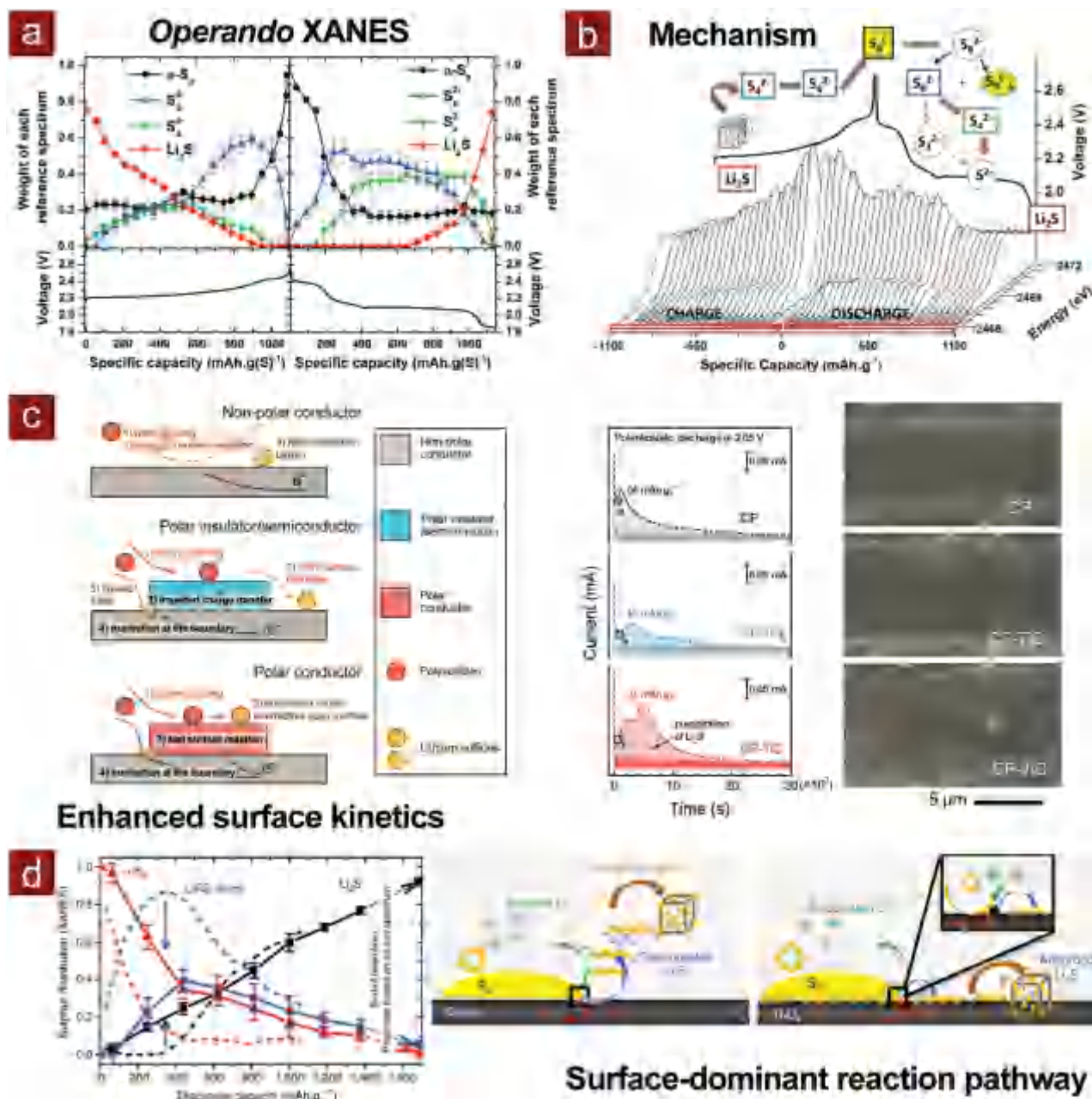


Figure 3. Interface engineering for sulfur cathodes. a) Evolution of operando sulfur K-edge XANES upon electrochemical cycling based on linear combination analysis (based on four reference compounds: α -S₈, S₆²⁻, S₄²⁻, and Li₂S) shown upon charge and discharge of a conventional carbon/sulfur cathode at C/10. Reproduced with permission.^[59] Copyright 2013, American Chemical Society. b) Hypothetic Li-S mechanism based on operando XANES. Reproduced with permission.^[59] Copyright 2013, American Chemical Society. c) Schematic of the working mechanism of the polar conductor to enhance the surface kinetics and potentiostatic nucleation/growth of Li₂S on various hosts, as well as the morphologies of Li₂S deposits. Reproduced with permission.^[71] Copyright 2016, Wiley-VCH. d) Comparison in the distribution of sulfur species (determined by operando XANES) between metallic polar host (Ti₄O₇)/sulfur (solid lines + symbols) and nonpolar carbon/sulfur (dashed lines), as well as diagram illustrating surface-mediated reduction of Li₂S from polysulfides on metallic polar host. Reproduced with permission.^[79] Copyright 2014, Nature Publishing Group.

materials have been mechanically employed to realize other concepts at particle or electrode level. Since the global performance is controlled by factors at each dimensional hierarchy ranging from nanoscale (interface), to mesoscale (particle), and macroscale (electrode), it is quite necessary to understand and highlight the advancements in interface engineering primarily.

2.2. Particle Design

Owing to the transport limitation of both electron and ion in Li-S batteries, nanomaterials are primarily preferred because they decrease the characteristic diffusion length of charge carriers, consequently lowering kinetic barriers.^[86] In addition,

electrochemically active surface is enlarged to provide abundant reaction sites. The application of nanomaterials in rechargeable batteries, however, is also strongly hindered by their small dimensions. The direct use of nanomaterials such as nano-carbon and sulfur nanoparticles for constructing a compact electrode raise several fatal problems:

- (1) A large amount of sulfur is exposed to the electrolyte without control, which aggravates the shuttle effect.
- (2) Substantial uptake of electrolyte is normally required to wet sulfur cathodes with a high porosity. The increased E/S mass ratio cuts the cell specific energy down.
- (3) Macroscopic anisotropy, induced by randomly packed nanomaterials, disturbs spatial distribution of electrons, ions, and heat within the whole electrode, resulting in non-uniform reactions and transport behaviors, or even local deactivation of active mass/volume.
- (4) Nanomaterials normally possess a low packing density, which decreases the volumetric energy density.^[87]

To utilize nanomaterials and exert their advantages efficiently, while simultaneously to circumvent the above problems, it becomes straightforward and smart to build micron-sized secondary particles that are composed of nanomaterials.^[88] On one hand, advantages of nanomaterials in reducing transporting resistance can still be exerted in each secondary particle. On the other hand, it is much easier for micron-sized secondary particles to be packed compactly than nanoparticles.^[89] Closer packing benefits a higher density and macroscopic uniformity of various distribution fields of electrons, ions, heat, or even mobile polysulfide intermediates. For Li–S batteries, existing approaches or concepts toward rational particle design can be broadly divided into three categories: 1) binder-assisted assembly, 2) self-assembly, and 3) core/shell or yolk/shell particles.

2.2.1. Binder-Assisted Assembly

Though accounting for only 2–10% weight percentage in electrodes, binder is a crucial component for rechargeable batteries, primarily affecting the cycling performance.^[90,91] From a conventional perspective, the function of binder in LIBs, where only solid–solid phase transfer occurs during electrochemical ion intercalation/deintercalation or alloying/dealloying, is to glue

solid-state active materials to conductive agents, and to attach as-obtained composite particles to current collectors. Especially for thick electrodes with a high loading of active materials, the role of binder becomes more critical as the number of particle-to-particle junctions inevitably increases within thicker electrodes. Therefore, an ideal binder should offer strong bonding strength to active materials and conductive agents, low resistance, and satisfactory physical/chemical stability.

For Li–S batteries, however, some attributes should be further possessed by the binder in addition to the aforementioned requirements. First, owing to the dissolution and diffusion of polysulfides, the active phase in Li–S batteries is more than simply in the solid state. Therefore, appropriate affinities to polysulfides are usually needed to maintain the electrical contact between liquid active phases and conductive agents. Second, the dissolution of polysulfides, strictly speaking, cannot be completely constrained. Initial solid sulfur/Li₂S particles are unable to remain unchanged. Thus, rather than directly bonding solid sulfur/Li₂S to conductive agents, assisting to construct a continuous conducting skeleton for solid sulfur/Li₂S being electrodeposited from soluble polysulfides is necessitated in operating unique sulfur (solid)–polysulfides (solution)–Li₂S (solid) conversion. Third, the binder should be highly robust and durable to withstand huge volume change during complicated phase transfer. In addition, an aqueous binder is preferred as it eases the fabrication process, reduces the emission of volatile organic compounds, and lowers the cost.^[91] Simultaneously, the interfacial and mechanical properties of the binder should be tailored to enable electrodes with compact structure, strong adhesion on current collectors, and facile wetting by electrolytes. In general, the functions, as well as corresponding desired properties, of the binder are broadly divided and discussed at two hierarchies (Table 1).

In this section, binder materials used for constructing micron-sized secondary particles will be reviewed first; while at electrode level, the function of the binder will be discussed in (2.3.1.). Poly(vinylidene fluoride) (PVDF) is the most widely utilized binder in LIBs and Li–S batteries due to its good electrochemical stability and stickiness. However, as we discussed above, the binder for sulfur/Li₂S cathodes necessitates a paradigm shift from PVDF to alternative materials because the weak binding of PVDF to polar sulfur species renders ineffective retention of active mass in cathodes.^[92] Moreover, organic solvents are usually required to dissolve PVDF, which are detrimental to the environment.

Table 1. Functions and desirable properties of binder at particle/electrode level.

	At particle level	At electrode level
Functions	<ol style="list-style-type: none"> a) Glue conducting sulfur hosts or glue non-conducting sulfur hosts with conductive agents b) Adsorb polysulfides to suppress their dissolution in bulk electrolyte c) Buffer volume change during solid–solution–solid conversion 	<ol style="list-style-type: none"> a) Remain the macroscopic compactness b) Adhere the electrode layer on current collectors firmly c) Lower inner resistance d) Allow a low-cost and environmentally friendly process
Properties	<ol style="list-style-type: none"> a) Suitable binding to both hosts and polysulfides b) Short-range flexibility to withstand volume change 	<ol style="list-style-type: none"> a) Anti-swelling and long-range rigidity b) Moderate stickiness c) Long-range electrical conductivity d) Aqueous solubility

To gain a theoretical perspective for binder design from first-principle calculations, Seh and Zhang et al. screened different molecular adsorbents for Li_2S and polysulfides (modeled as Li-S clusters) based on vinyl polymer $-(\text{CH}_2-\text{CHR})_n-$ with $-\text{R}-$ as substitutional binding centers.^[93] They found that functional groups containing O and N heteroatoms exhibited substantial increase in binding energies to Li_2S . Among these functional groups, carbonyl group ($>\text{C}=\text{O}$) and its derivatives (ester, ketone, and amide) possessed highest binding energies while amine ($-\text{NH}_2$), imine ($=\text{NH}$), and ether ($-\text{O}-$) also held considerable enhancement in binding energies to Li_2S by at least 0.5 eV. Accordingly, the origin for polysulfide adsorption by polymeric binder is attributed to the interaction between heteroatoms and Li^+ in polysulfides, as well as in Li_2S . This understanding paves the way to develop a high-performance binder for high-loading Li-S batteries.

Synthetic polymers doped with O or N emerged as a variety of binders being widely used in Li-S batteries. Lacey et al. systematically investigated the effect of poly(ethylene oxide) (PEO)/poly(ethylene glycol) (PEG) to serve as electrolyte additives, coating layer, and binder with the increase in molecular weight.^[94] PEO/PEG with repeated $-\text{O}-$ ether groups can intrinsically stabilize and solubilize polysulfides in the polymer phase via Li^+-O coordination, thereby minimizing the dissolution of polysulfides in bulk electrolyte and improving the cycling stability of Li-S batteries with a sulfur loading of 2.5 mg cm^{-2} . N-containing polymer was also proved to be efficient in stabilizing Li-S batteries. Jung and Kim explored a mixed binder system of polyvinyl pyrrolidone (PVP) and polyethyleneimine (PEI) for Li-S batteries with a sulfur loading of 2.4 mg cm^{-2} .^[95] The addition of 50% PEI in the mixed binder simultaneously enhanced the viscosity and insolubility. Very recently, Yan and Xiong's group developed a multifunctional polar binder based on hexamethylene diisocyanate-crosslinked PEI for high-loading sulfur cathodes.^[96] High areal capacity of 7.9 mA h cm^{-2} and excellent cycling stability were enabled by modified PEI binder. Zhang et al. explored a kind of cationic polyelectrolyte, poly(acrylamide-co-diallyldimethylammonium chloride) (PAMAC), which was water-soluble and had preferable amide/ammonium groups to bind polysulfides.^[97] Using PAMAC as binder in a sulfur/carbon black composite cathode, they obtained a reversible discharge capacity of 652 mA h g^{-1} after more than 100 cycles, which was $\approx 70\%$ higher than controlled cells using PEO binder. Considering the high sulfur content (80 wt% in the composite and 68 wt% in the cathode) and an average sulfur loading of 3.0 mg cm^{-2} , these results unambiguously indicated the unique role of binder in high-loading Li-S batteries.

Considering the relatively high cost of synthetic polymer, polymeric materials derived from biomass were developed as low-cost, naturally abundant substitutes to PVDF. Huang and Wang's groups collaborated to exploit the possibility of applying gelatin, which is a hydrolyzed form of collagen with enriched ionizable groups such as $-\text{COO}^-$ and $-\text{NH}_3^+$, in Li-S batteries, demonstrating enhanced cyclabilities.^[98] To enhance the performance of PAN/S composite cathodes, Wang et al. also modified β -cyclodextrin ($\beta\text{-CD}$) by partially oxidizing it into carbonyl- $\beta\text{-CD}$, which served as an aqueous binder with superior solubility in water, strong bonding strength, and moderate

viscosity.^[99] Nevertheless, the typical sulfur loading amounts were lower than 2.0 mg cm^{-2} because the size of secondary particle was mainly less than $1 \mu\text{m}$, which increased the number of particle-to-particle junctions.

Rationally assembling functional polymeric binder with sulfur composites into micron-sized particles will be more suitable for thick electrodes. To do that, Zhou et al. synthesized amylopectin wrapped graphene oxide/sulfur composites (GO-S-Amy) with particle size larger than $2 \mu\text{m}$ (Figure 4a).^[100] The structure of GO-S-Amy composite particle was stabilized through hydrogen bonding between GO and amylopectin, both of which are rich in hydroxyl ($-\text{OH}$) and carboxyl ($-\text{COOH}$) groups. Simultaneously, polysulfides were also chemically confined within GO-Amy skeletons. At sulfur loadings of 2.0 and 6.0 mg cm^{-2} , high discharge capacities of ≈ 1200 and $\approx 800 \text{ mA h g}^{-1}$ (2.4 and 4.8 mA h cm^{-2}) were obtained at a current density of $C/8$, respectively. To gain more superb adsorptivity toward polysulfides, Zeng et al. intentionally introduced quaternary ammonium cations into $\beta\text{-CD}$, obtaining a hyperbranched cationic $\beta\text{-CDp-N}^+$ polymeric network to connect and wrap micron-sized sulfur/carbon black blends with extremely high sulfur content of 90 wt% (Figure 4b).^[101] In the whole cathode, the sulfur content was 63 wt%. $\beta\text{-CDp-N}^+$ provided multifunctional advantages, including good durability to volume change, enhanced bonding strength, and immobilization of polysulfides. Therefore, a high areal capacity of 4.4 mA h cm^{-2} after 45 cycles was enabled by $\beta\text{-CDp-N}^+$ binder for cathodes with 5.5 mg cm^{-2} loading of sulfur, in contrast to PVDF that only allowed a low capacity of 0.9 mA h cm^{-2} . More importantly, a low electrolyte amount of $7 \mu\text{L mg}_\text{S}^{-2}$ was applied since $\beta\text{-CDp-N}^+$ binder constructed continuous multidimensional networks, providing efficient accessibility of active materials to the electrolyte.

Very recently, Bhattacharya and Xiao et al. presented a work in which commercial polyamidoamine (PAMAM) dendrimers were explored as a physically and chemically tailorable prototype of spherical binder (Figure 4c).^[102] On one hand, PAMAM is structurally self-branched with interior porosities of 2 nm, which allow facile wetting of sulfur by electrolytes and simultaneously trap polysulfides within branches. On the other hand, PAMPAM dendrimers possess highly exposed surface functional groups to offer multiple binding sites, and these groups can be tuned by grafting different linear polymeric branches onto the dendrimer. They demonstrated that simply mixing PAMAM dendrimers and carbon/sulfur composites in aqueous solvents rendered secondary composite particles with size of $>5 \mu\text{m}$, and sufficient binding was also induced. The enhancement in battery performance by various PAMAM dendrimers was therefore remarkable. With the assist of 4-carboxymethylpyrrolidone-terminated PAMAM (G4CMP) binder, carbon/sulfur cathodes with a sulfur loading of 4.38 mg cm^{-2} delivered a high discharge capacity of $4.56 \text{ mA h cm}^{-2}$ (1045 mA h g^{-1}) at $C/20$ and maintained 98% of initial capacity after cycling at $C/5$ for 100 cycles. Since the sulfur cathode was non-engineered and PAMAM dendrimers were commercially available, this approach held great promise for applicable Li-S batteries.

The concept of binder-assisted particle assembly also enlightened some other unusual applications such as primary (or non-rechargeable) Li-S batteries. For example, Ma et al. built

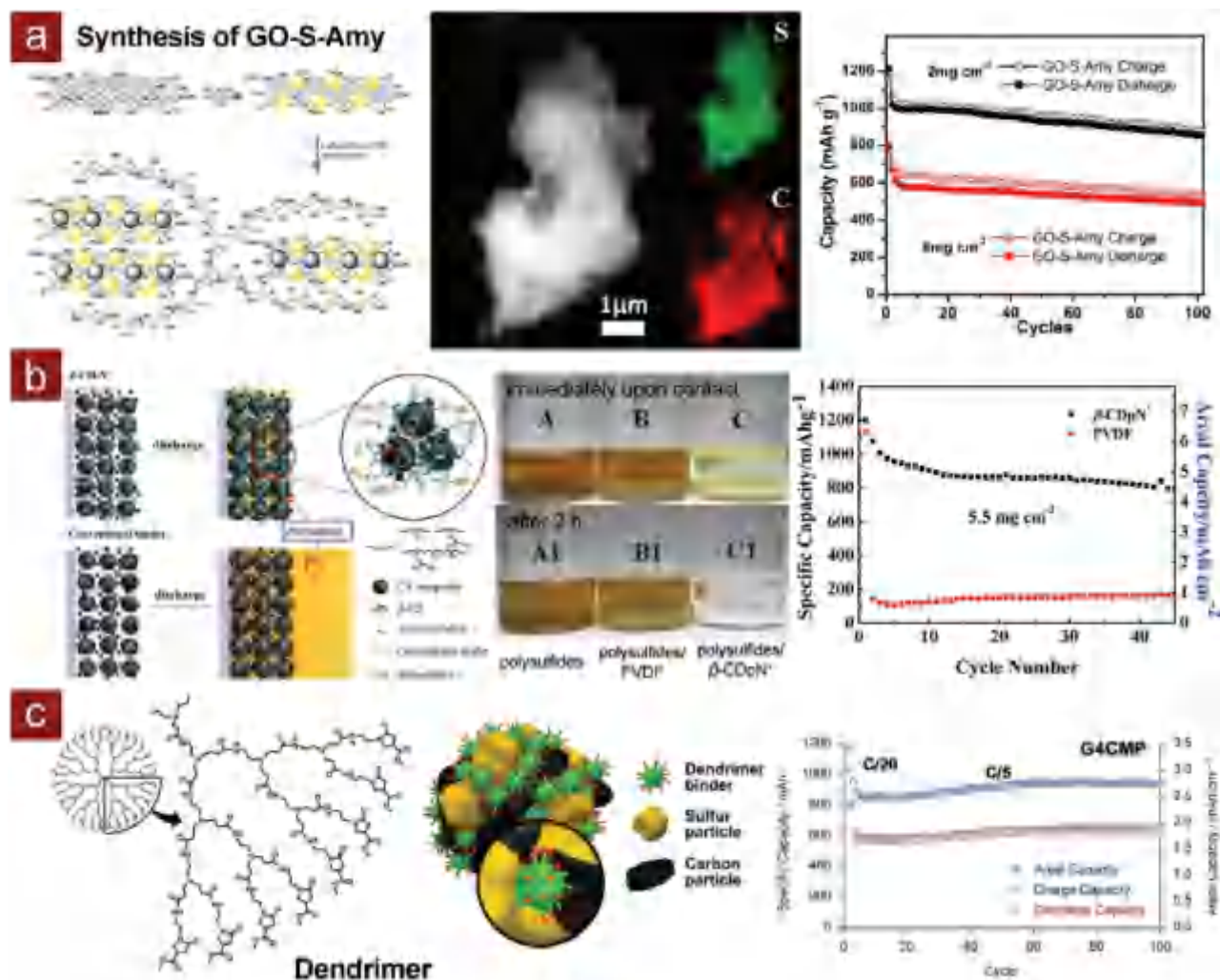


Figure 4. Binder-assisted assembly of cathode microparticles. a) Left: schematic of two-step synthesis route for a GO-S-Amy composite, with yellow balls representing sulfur and black balls representing carbon black; Middle: scanning transmission electron microscopy (STEM) dark field image of GO-S-Amy composite after the 50th discharge in the cell and corresponding elemental mapping for sulfur and carbon; Right: cycling performance of GO-S-Amy with different sulfur loadings (at C/8). Reproduced with permission.^[100] Copyright 2013, American Chemical Society. b) Left: schematics of cathode configurations with the new binder β -CDp-N⁺ and the conventional binder; Middle: visual discrimination of the interactions of (A, A1) polysulfide-containing electrolyte with (B, B1) PVDF and (C, C1) β -CDp-N⁺ immediately upon contact (A–C) and after 2 h (A1–C1); Right: cycle performance of the β -CDp-N⁺ cathode and the PVDF cathode. Reproduced with permission.^[101] Copyright 2015, American Chemical Society. c) Left: schematic of a generation dendrimer and of dendrimer–carbon–sulfur interactions within the composite particle; Right: cycling performance of G4CMP dendrimer binder-based Li–S cells. Reproduced with permission.^[102] Copyright 2016, Elsevier.

a cauliflower-like structured carbon/sulfur cathode by gluing carbon blacks and sulfur into hierarchical agglomerates with the assist of gelatin binder.^[103] The size of secondary particles was 1–2 μm , benefiting a high tap density of the whole electrode. At high sulfur loadings of 6, 10, and 14 mg cm^{-2} , high capacities over 1200 mA h g^{-1} were obtained. Though as-fabricated Li–S batteries were non-rechargeable, this method can be readily implemented in high-loading secondary Li–S batteries.

Subsection Summary (2.2.1.): At particle level, binder used to construct secondary energy particles for Li–S batteries must be capable of stabilizing the whole architecture of each microparticle both mechanically and chemically. That demands the binder for not only the intrinsic gluing strength but also the interfacial binding affinities to other building blocks. Besides,

it is highly anticipated that rendering the binder with suitable adsorption to polysulfides will create more opportunities for restraining the dissolution within the particle. Through rationally exerting polymeric chemistry and materials chemistry to tailor the polymeric backbone, intermolecular interaction, and macroscopic aggregation of the binder, its multifunctional role will be further illuminated in the future.

2.2.2. Self-Assembly

Though binder impacts battery performance significantly, most of binder materials are electrochemically inactive, accounting for additional weight. Besides, the swelling of binder is

normally inevitable, which is detrimental to maintaining porosity, compactness, and electrical contact of electrodes. Therefore, reducing the amount of binder while not degrading cell performance is highly desirable. In this regard, self-assembly strategies for constructing secondary particles hold great promise because a binder is only used to connect secondary particles. Therefore, a small weight percentage of binder in the whole electrode is needed. Without the assist of a binder, the interaction between building blocks within each assembly should be engineered to be comparable to the gluing strength. Additionally, aforementioned functions of binder, including sufficient binding to polysulfides/Li₂S and buffering effect on volume change, ought to be enabled within these self-assembled particles. Combinatorial materials chemistry, as well as preferable industrial techniques, were exploited and manifested as several approaches.

One approach is direct or in situ co-assembly of sulfur and conductive hosting scaffolds, which mainly involves dispersion and assembly in a solution and subsequent collection. In this way, various microstructured carbon/sulfur assemblies, such as sulfur microparticles wrapped by carbon black,^[104] graphene,^[49] CNT,^[105] or polypyrrole (PPY),^[106] have been obtained. Wang et al. reported a one-pot synthesis of unique micrometer bipyramidal sulfur particles enclosed with multiwalled CNTs through mixing aqueous dispersion of CNTs and sulfur-saturated tetrahydrofuran.^[105] The as-obtained bipyramidal sulfur particles, homogeneously wrapped by CNT networks, had an axial diameter of ≈ 13 μm and a length of ≈ 20 μm (Figure 5a). The intimate contact between sulfur and CNTs allowed sufficient supply of electron, resulting in very high initial capacity of 1600 mA h g⁻¹ at C/20 with a sulfur loading of ≈ 2 mg cm⁻². To improve the collecting efficiency, a spray-pyrolysis method, a well-known industry-oriented technique, was developed by Wang and colleagues, to produce ternary porous sulfur/dual-carbon architectures continuously (Figure 5b).^[107] The as-obtained porous sulfur particles had a diameter of 15–20 μm . Nevertheless, it is still short of demonstration on sulfur cathodes with an areal sulfur loading of >3.0 mg cm⁻². In addition, electrochemical performance, especially the cycling stability, should be further promoted. One possible reason for the degraded performance could be attributed to the presence of sulfur during co-assembly. Though sulfur and other conductive agents were assembled intimately before cycling, sulfur suffered from gradual dissolution during subsequent electrochemical cycling, leading to loose connection between conductive agents or even structural collapse. As a result, both electron/ion channels were devastated.

To circumvent the above issue, constructing microstructured scaffolds from nanoscale building blocks and then impregnating sulfur into this scaffold to obtain composite particles are quite promising. So long as sulfur does not participate into assembly, the structural stability of scaffolds is mainly determined by the interactions between other electrochemical inactive components. Consequently, dissolution and re-precipitation during electrochemical reactions are expected to hardly impact on the backbone of microstructured composite particles. To realize such a concept, Wang's group developed a synthetic method towards porous carbon/sulfur composite microspheres. Uniform spherical morphologies, a precise control of

particle size distribution within several tens of micrometers, and versatile regulation of hosting materials were achieved (Figure 5c).^[108–110] Generally, this synthetic method involved emulsion polymerization to control the shape of carbon precursors, and evaporation-induced self-assembly (EISA) to enable uniform dispersion of various pore templates, as well as other additives, such as CNT, in the polymer matrix. During EISA and carbonization, all the components were closely packed into highly porous and conductive microspheres with excellent mechanical integrity. By alternating the pore templates and additives, various microspheres could be obtained. For example, porous spherical carbon (PSC)–CNT microspheres, possessing a median diameter of 33 μm , high Brunauer–Emmett–Teller (BET) surface area of 963 m² g⁻¹, and large pore volume of 2.10 cm³ g⁻¹, were used to hold 75 wt% sulfur in nanosized pores, resulting in a tap density (0.80 g cm⁻³) as twice higher as that of routine carbon/sulfur blends.^[108] At a sulfur loading of 5 mg cm⁻², the composite cathode delivered high capacity of ≈ 6 mA h cm⁻² at a current density of 0.42 mA cm⁻² and retained $\approx 87\%$ of initial capacity after cycled at 2.8 mA cm⁻² for 200 cycles. To further enhance the electrochemical performance, Song et al. further synthesized CNT-interpenetrated mesoporous N-doped carbon spheres (MNCS/CNT) with a mean particle diameter of 24 μm by altering carbon precursors into N-rich poly(melamine-co-formaldehyde) (Figure 5d).^[109] Doped N atoms have been demonstrated as highly efficient chemisorptive sites to immobilize polysulfides, thereby significantly promoting the cycling stability. Consequently, MNCS/CNT scaffolds enabled extraordinary cycling performance at a sulfur loading of 5 mg cm⁻², indicating high initial capacity of 1438 mA h g⁻¹ at 0.84 mA cm⁻² and ≈ 1200 mA h g⁻¹ (≈ 6 mA h cm⁻²) after 200 cycles at 1.68 mA cm⁻² without obvious capacity fading. Such a superior performance was attributed to rational integration of polysulfide chemisorption of N-doped carbon, high electrical conductivity of CNT, and structural rigidity of microspheres.

Compared to multistep synthetic routes, more readily scaled-up techniques are preferred in continuous and mass production. As indicated above, spray-pyrolysis/drying method has been widely employed in battery technologies due to its simplicity, robustness, rapidness, and continuous operation,^[111] and has also shed a light on Li–S batteries. For example, Jung et al. fabricated micrometer hierarchical porous carbon (HPC) spheres by one-pot high-throughput spray pyrolysis of sucrose/sodium carbonate precursors.^[112] With a sulfur loading of 2.5 mg cm⁻², HPC-sulfur composite cathode remained more than 700 mA h g⁻¹ at a relatively large current density of 2 A g⁻¹ (5 mA cm⁻²). Long's group successfully employed spray drying to synthesize Nb₂O₅-nanocrystal-embedded mesoporous carbon microspheres, enabling kinetically enhancement of polysulfide redox reactions.^[113] Similar spray-drying method was employed for large-scale production of CNT porous microspheres for commercial aqueous CNT dispersion, yielding micron-sized spherical composite particles after impregnation of 70 wt% sulfur.^[114] Discharge capacities of 858 and 806 mA h g⁻¹ after 100 cycles were obtained at current rates of C/5 and C/2, respectively, corresponding to a capacity retention of 87–88%. The excellent rate capabilities of microstructured particles indicated that the increase in particle diameter and corresponding

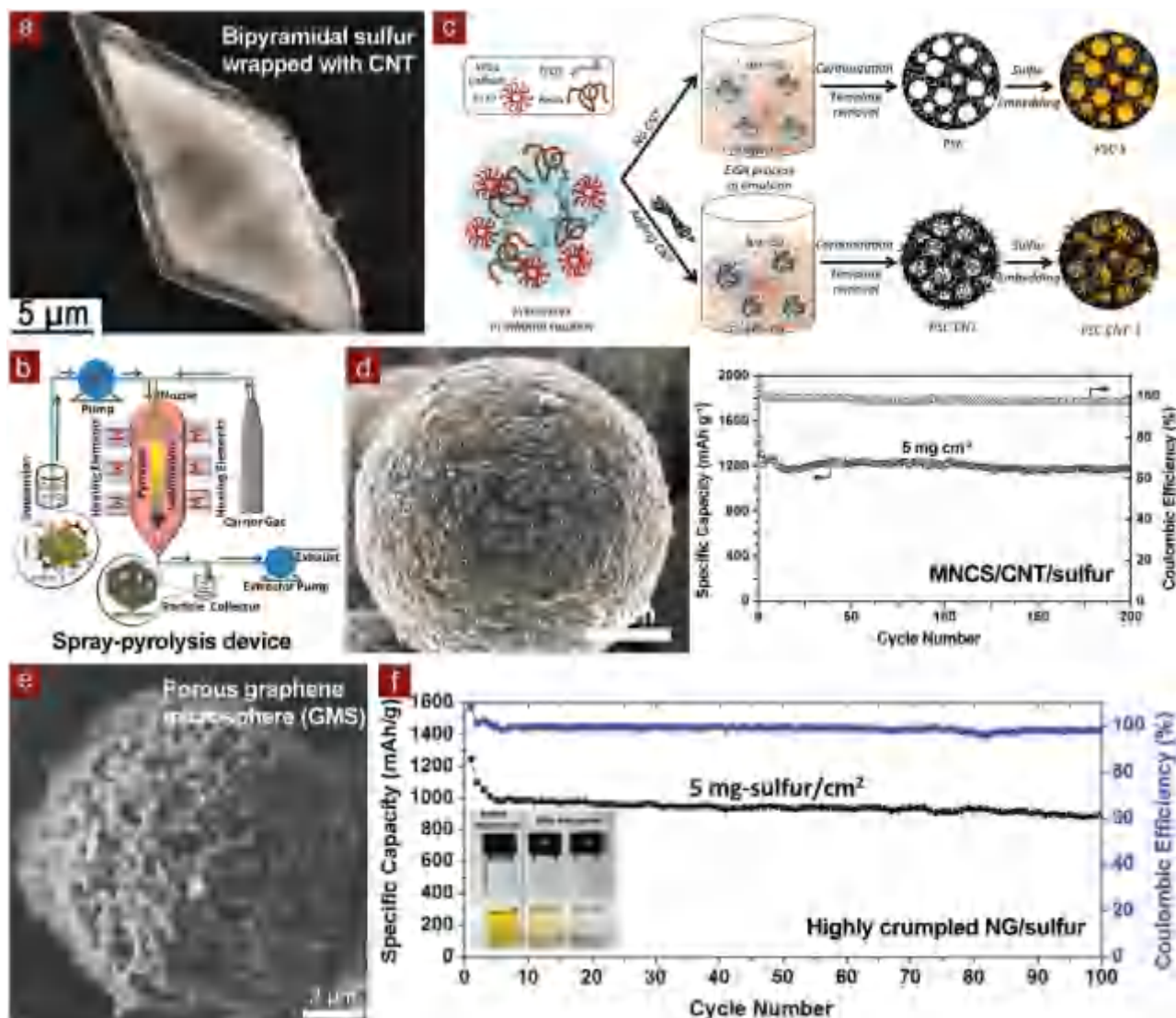


Figure 5. Self-assembly of cathode microparticles. a) Scanning electron microscopy (SEM) images of CNT-wrapped bipyramidal sulfur microparticles. Reproduced with permission.^[105] Copyright 2014, Wiley-VCH. b) Schematic of spray-pyrolysis/sublimation device. Reproduced with permission.^[107] Copyright 2016, American Chemical Society. c) Schematic of the synthesis of porous spherical carbon (PSC)–sulfur and PSC–CNT–sulfur composite microparticles using a combination of the emulsion polymerization process and the EISA method. Reproduced with permission.^[108] Copyright 2013, American Chemical Society. d) SEM image of MNCS/CNT composite microparticle and cycling performance of MNCS/CNT/sulfur at 1.68 mA cm^{-2} . Reproduced with permission.^[109] Copyright 2015, Wiley-VCH. e) SEM image of GMS. Reproduced with permission.^[116] Copyright 2015, Elsevier. f) Cycling performance of highly crumpled NG/sulfur composite at 1.3 mA cm^{-2} and (inset) photograph of the polysulfide solution after exposure to the different adsorbers: (I) undoped graphene, (II) highly crumpled NG. Reproduced with permission.^[117] Copyright 2016, American Chemical Society.

decrease in number of inter-particle junctions significantly lower the inner resistance of thick electrodes.

Different from co-assembly strategies whether sulfur is involved or not, direct use of self-organized micron-sized scaffolds to accommodate sulfur represents another route toward microstructured sulfur composite particles. Our group has employed aligned CNTs as sulfur scaffolds to accommodate 90 wt% sulfur. Four-times higher tap density of 1.98 g cm^{-3} than that of 54 wt% sulfur/aligned CNT composites was obtained, enabling high volumetric capacity of $1116 \text{ mA h cm}^{-3}$.^[14] Densified graphene/sulfur microparticles were also demonstrated for Li–S batteries with high volumetric specific energies.^[115]

Nevertheless, sulfur loading amounts in these works were limited to lower than 1.5 mg cm^{-2} . The main challenge is to tailor the internal porosity and interfacial properties of microparticles for better wetting by electrolytes and smooth ion diffusion across the thick electrode. To do so, our group reported the templated chemical vapor deposition (CVD) method to grow porous graphene microspheres (GMSs) on spherical oxide assemblies, which was produced by spray drying. GMSs successfully inherited the microspherical morphology of oxide templates with size of $11 \mu\text{m}$, while the internal porosity was induced by removing template building blocks (Figure 5e).^[116] As a result of smaller contact resistance at a micrometer range,

GMS-sulfur composites exhibited superb rate capability with a sulfur loading of 2.5 mg cm^{-2} . For synthesis of micrometer graphene-based assemblies, Song et al. reported a simple annealing method to fabricate highly crumpled N-doped graphene (NG) from GO/cyanamide precursors (Figure 5f).^[117] Self-organization of NG sheets during annealing resulted in huge assemblies of NG with size of $>5 \mu\text{m}$, which benefited a compact electrode. NG-sulfur composites with 80 wt% of sulfur was proved to be cycled stably with a capacity higher than 800 mA h g^{-1} even when the sulfur loading was as high as 5 mg cm^{-2} . Other self-organized hosts, such as 3D N-enriched CNT-graphene hybrid microtubes (2.2 mA h cm^{-2} at 2.0 C, 4.2 mg cm^{-2} sulfur),^[118] 3D cobalt nanoparticle-embedded graphene nanosheet-CNT (3.0 mA h cm^{-2} at C/10, 4.7 mg cm^{-2} sulfur),^[119] conjugated polymer-derived graphitic HPC (4.2 mA h cm^{-2} at C/5, 3.2 mg cm^{-2} sulfur),^[120] HPC/graphene aerogel (4.5 mA h cm^{-2} at C/10, 4.0 mg cm^{-2} sulfur),^[121] ionic liquid-derived N-enriched HPC (5.8 mA h cm^{-2} at C/50, 4.0 mg cm^{-2} sulfur),^[122] and graphene-like Co_9S_8 microstructured assemblies (4.3 mA h cm^{-2} at C/10, 4.5 mg cm^{-2} sulfur)^[81] also demonstrated superior electrochemical performance in high-loading Li-S batteries.

Subsection Summary (2.2.2.): In general, the self-assembly strategy toward high-performance microparticles basically necessitates some crucial prerequisites to fully exert the merits of engineered microparticles:

- (1) Since it is important for remaining the structural integrity of microparticles, the interactions between each building blocks should be regulated for agglutinating them into mechanically rigid frameworks. The interactions can be broadly divided into strong van der Waals interactions between large-surface-area nanomaterials (e.g., CNT and graphene), hydrogen bonding, and covalent bonding (e.g., C-C bond in self-organized carbon).
- (2) Internal porosity within microparticles ought to be controlled; otherwise too narrow and tortuous pores retard Li^+ ion transport, while too wide and open pores facilitate the outward diffusion of polysulfides. In addition to exotic porogens or templates, controlled vapor volatilization or gas evolution during assembly are expected to induce desired internal porosities.
- (3) To prevent outward diffusion of polysulfides while to ease the electrolyte wetting, necessary lyophilic modification on building blocks could be introduced or alternatively, building blocks with unique interfacial properties (e.g., NG and other N-doped carbon) should be applied.
- (4) All of the materials for granulation ought to be easily processed, demanding suitable dispersibility, solubility, viscosity, volatility, flowability, thermal/chemical stability, and so on.

2.2.3. Core/Shell Particles

The concept of core/shell or yolk/shell particles has been explored for a long time in LIB applications. For example, carbon coating for insertion-type cathode materials has widely been utilized in LIB industry.^[123] Yolk/shell design was proved to be very efficient to accommodate electrode materials with

huge volume expansion (e.g., silicon,^[124] tin,^[125] aluminum,^[126] etc.) and improve their cycling stability. For Li-S batteries, core/shell^[127,128] or yolk/shell^[18,129] nanostructures have also been conceptually substantiated to encapsulate either sulfur or Li_2S nanoparticle. For example, Cui's group pioneered the concept of yolk/shell TiO_2 -encapsulated sulfur particles, firstly extending the cycling life of Li-S batteries to 1000 cycles with remarkably low capacity fading rate of 0.033% per cycle.^[18] Many other encapsulating materials, including carbon,^[127,130] polymer,^[75,128,131] and inorganics,^[132] have been employed to segregate and protect sulfur nanoparticles. Nevertheless, most of these examples were limited below 2 mg cm^{-2} loading of sulfur, which was attributed to the intrinsic drawbacks of nanoparticles for being integrated in a high-loading, thick electrode.

Learning from core/shell or yolk/shell nanoparticles, architecturing shelled particles at a micrometer scale will fully exert the merits of both microparticle cores and engineered shell materials. On one hand, microparticle cores can be prepared through either binder assistance or self-assembly as indicated in (2.2.1.) and (2.2.2.); whereas the binding strength between each building block, as well as to polysulfides, can be compromised to some extent. For example, low-cost carbon black/sulfur blends, being prepared through simple ball milling, are able to serve as the micron-sized core. On the other hand, necessary functions or properties, such as structural integrity, mechanical robustness, shuttle inhibition, and redox promotion, can be realized and optimized by engineering suitable shell materials and adjusting shell structures. In this way, the 'core' and the 'shell' can be designed separately, broadening the choices of nanomaterials, lowering the synthetic complexity, and making the concepts easier to understand. Analogous to pomegranate-inspired design for silicon anodes,^[133] Yushin and colleagues proposed a hierarchical particle-shell architecture to mitigate the failure of large-volume-change electrode materials (e.g., Li_2S) and numerically modeled the significant reduction of stress enabled by increasing hierarchies of particle's shelling (Figure 6a).^[134] This work provided a theoretical insight into hierarchical design for core/multishell particles; however, to completely seal vulnerable Li_2S from electrolytes, impermeable graphitic shells were constructed, which limited secondary particle size to below 200 nm to remain acceptable Li^+ diffusivity within short length. Therefore, the structures and properties of particle's shelling ought to be deliberately engineered to fully exert the advantages of core/shell and yolk/shell microparticles.

Owing to the conductive nature, carbonaceous materials are still the first choice to encapsulate microparticles and offer good electrical contact. For instance, Lv et al. reported a synthesis of integrated Ketjen Black (IKB) secondary particles with amorphous carbon coated on and infiltrated in (Figure 6b).^[135] Citric acid and ethylene glycol were successively introduced to glue and crosslink KB and to offer carbon sources for the formation of amorphous carbon. Integrated aggregates with size of several-tens of micrometers were obtained. The IKB/sulfur composite cathode (4.7 mg cm^{-2} sulfur) exhibited a high discharge capacity of $\approx 1200 \text{ mA h g}^{-1}$ at C/20. During cycling at C/5, a capacity of 900 mA h g^{-1} slightly decreased to above 700 mA h g^{-1} after 90 cycles. Note that all materials were commercially available and no specific design was employed for the whole electrode. Thus, this work was remarkable and

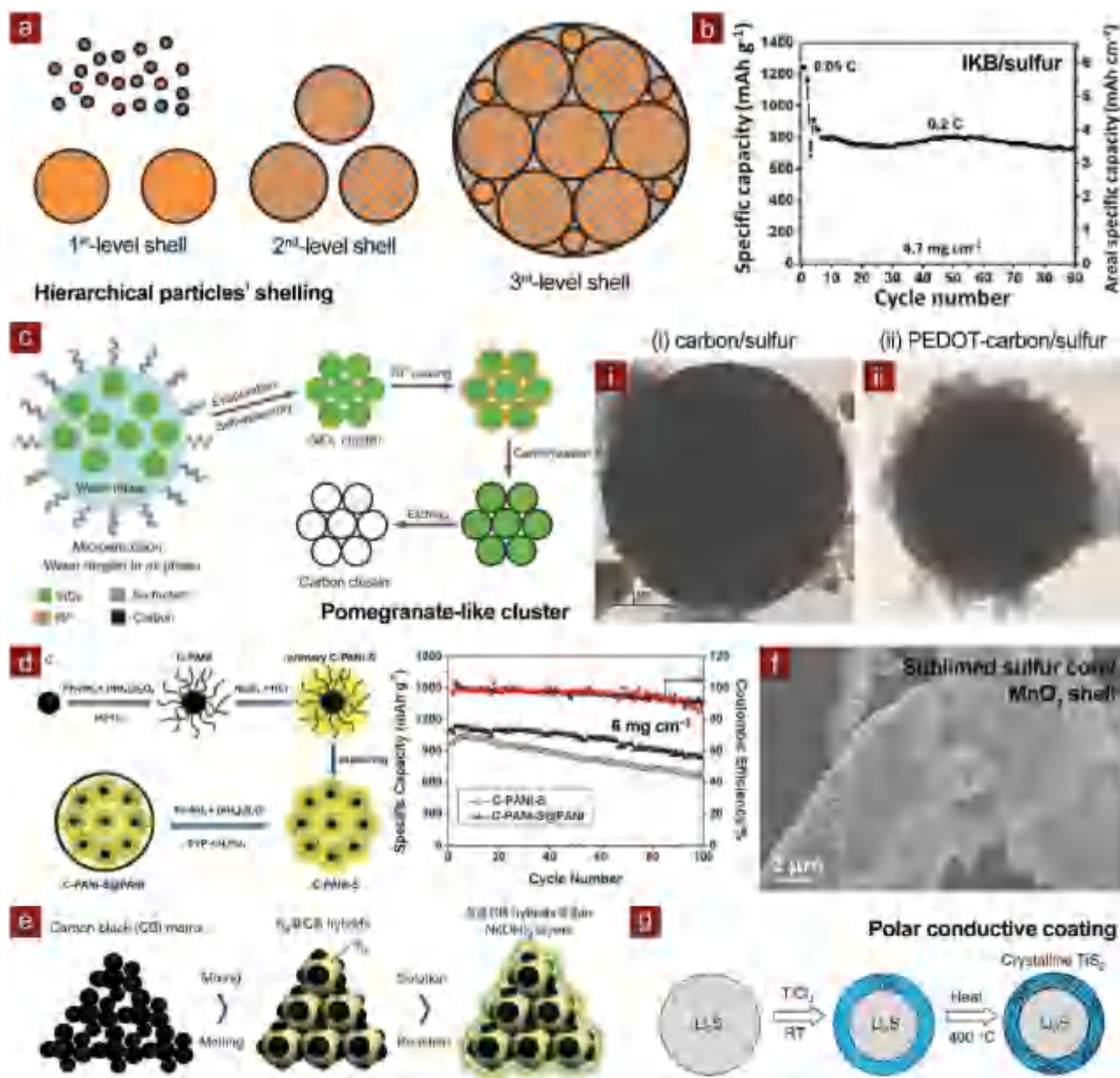


Figure 6. Core/shell structured cathode microparticles. a) Schematic of hierarchical particles' shelling for enhanced mechanical stability of volume-changing active materials, such as Li₂S. Three levels of enclosing hierarchy mitigate the failure of inner shell sequentially. Reproduced with permission.^[134] Copyright 2015, Wiley-VCH. b) Cycling performance of thick IKB/sulfur electrode. Reproduced with permission.^[135] Copyright 2015, Wiley-VCH. c) Schematic of the fabrication process of pomegranate-like carbon clusters and transmission electron microscopy (TEM) images of (i) carbon/sulfur cluster and (ii) PEDOT-carbon/sulfur cluster. Reproduced with permission.^[138] Copyright 2015, Wiley-VCH. d) Schematic of the synthesis of the C-PANI-S@PANI composite and cycling performance at C/5. Reproduced with permission.^[139] Copyright 2013, Royal Society of Chemistry. e) Schematic of the fabrication of sulfur/carbon black@NNH hybrids. Reproduced with permission.^[143] Copyright 2015, Nature Publishing Group. f) SEM image of sublimed sulfur particle core/MnO₂ shell microparticles. Reproduced with permission.^[144] Copyright 2016, American Chemical Society. g) Schematic of the synthesis process of Li₂S@TiS₂ core/shell nanostructures. Reproduced with permission.^[146] Copyright 2014, Nature Publishing Group.

strengthened the effectiveness of designing core/shell micron-sized secondary particles. Similar core/shell design of carbon/sulfur composites with carbonaceous outer coating was also explored.^[136]

Conductive polymer is another class of intriguing shelling materials for composite microparticles because of the structural flexibility, conformal adaptability, ion permeability, and

tailorable chemisorptivity. Ga's group reported polyaniline (PANI)-coated carbon/sulfur blends as irregular micron-sized aggregates with enhanced electrochemical performance.^[137] Nevertheless, the lack in design of internal core particles prohibited further demonstration of core/conductive polymer shell structures in high-sulfur-loading Li-S batteries. Towards rational design of core/shell hierarchies, Li et al. firstly explored

a pomegranate-inspired design of conductive polymer poly(3,4-ethylenedioxythiophene) (PEDOT)-coated carbon cluster–sulfur cathode (PEDOT-C/S), in which sulfur nanoparticles were segregated in nanosized primary hollow carbon particles with sufficient empty space to withstand volume expansion; while primary nanoparticles densely packed into micron-sized secondary clusters and coated by PEDOT, synergistically stabilizing interparticle contact and minimizing sulfur exposure to electrolyte (Figure 6c).^[138] As a result of such holistic advantages in hierarchical micro-/nanostructures, PEDOT-C/S cathodes, with a moderate sulfur loading of ≈ 2 mg cm⁻², exhibited superior capacity retention of 70% after 300 cycles at C/2 (1.67 mA cm⁻²) and outstanding high-rate capacity of 733 mA h g⁻¹ at 3.0 C (10.0 mA cm⁻²). Wang et al. reported a multicore/shell structured composite particle based on PANI to enable stable operation of high-sulfur-loading cathode (Figure 6d).^[139] Different from the previous work,^[137,140] they firstly grafted PANI onto carbon black to obtain branched conductive networks and then further coated secondary particles with an extra PANI shell. At a sulfur loading of 6 mg cm⁻², a high initial capacity of 1101 mA h g⁻¹ (6.6 mA h cm⁻²) was attained and remained 76% after 100 cycles at C/5. By altering polymeric shell materials to poly(styrene sulfonate) (PSS),^[141] PEDOT:PSS,^[142] and so on, different core/shell structured composite cathodes were proposed to facilitate high-sulfur-loading Li–S batteries.

Compared to carbon and polymer, inorganic shelling materials possessed more superb chemisorption to Li₂S/polysulfides to enhance interfacial redox reactions and retard outward diffusion of polysulfides. Yu and Huang's group reported the encapsulation of large carbon black/sulfur aggregates of ≈ 20 μ m by thin-layered nickel nitrate hydroxides (Ni₃(NO₃)₂(OH)₄, denoted as NNH) with thickness of ≈ 7 nm (Figure 6e).^[143] During electrochemical cycling, NNH not only served as a durable physical shell but also irreversibly reacted with Li⁺ to form (Li, Ni)-mixed hydroxide layers with good Li⁺ accessibility and abundant polar anchoring sites for polysulfide immobilization. As a result of such a smart core/shell design, as-obtained sulfur/carbon black@NNH hybrid electrode achieved drastic improvements in capacity retention, which was $\approx 500\%$ higher than bare sulfur/carbon black. Enlightened by their previous exploration of MnO₂ as an efficient mediator based on surface (poly)thiosulfate redox,^[78] Liang and Nazar further presented an in situ reactive-assembly method to fabricate micron-sized sublimed sulfur particle core/MnO₂ shell materials based on the aqueous reaction between KMnO₄ and sulfur (Figure 6f).^[144] At a sulfur loading of 4.1 mg cm⁻², this material demonstrated an initial capacity of 780 mA h g⁻¹ and a fade rate of 0.048% per cycle at C/5. Besides, 800-cycle long lifespan has been achieved, indicating the effectiveness of inorganic materials with extraordinary binding to soluble intermediates. Analogously, they also reported the stable operation of micron-sized VO_x hollow sphere/sulfur composites (2.5 mg cm⁻² sulfur) in a selected voltage range to exert surface-redox mechanism.^[145]

Despite the extended cyclic life enabled by upgraded chemisorption to polysulfides, capacities of inorganic-shelling microparticles were normally limited to <1000 mA h g⁻¹ even at small current densities, which were probably owing to the poor electrical conductivities of inorganic shell materials. To address this issue, Seh et al. reported a series of 2D layered

transition metal disulfides (MS₂) such as TiS₂, ZrS₂, and VS₂ to encapsulate Li₂S electrodes by in situ reacting commercial Li₂S powders with metal tetrachloride precursors (Figure 6g).^[146] These compounds possessed high conductivities comparable to carbon and polar M–S groups to interact with Li₂S/polysulfides, thus significantly facilitated the electrochemical performance. At a high Li₂S loading of >4.8 mg cm⁻², capacities of >540 mA h g_{Li₂S}⁻¹ (780 mA h g_S⁻¹) were normally obtained and increased as the electrical conductivity of 2D layered MS₂ increased. Since the core material was commercial Li₂S powder, restraining the core size at submicrometer scale, there would be opportunities to further enlarge the size of particles and rate performance by engineering the interior particle architectures.

Subsection Summary (2.2.3.): Compared to binder-assisted assembled and self-assembled microparticles, core/shell or yolk/shell particles possess major merits in protecting sulfur from losing and stabilizing structural integrity. The structure and properties of shelling materials play a vital role in the performance of microstructured particles. Advantages and disadvantages of various shell materials are summarized (Table 2).

In the future, multishell design or hybrid shell materials with mixed ion/electron conductivity and polar affinities is a promising route to enhance core/shell microparticles for high-sulfur-loading Li–S batteries.

Section Summary (2.2.): Delicate particle design possesses multiple advantages in addressing the inherent flaws of utilizing nanomaterials in applicable large energy storage cells. Either binder-assisted assembly, or self-assembly is an efficient way to build high-performance energy particles. Protecting the microstructured assembly by a tactically engineered shell further optimize the electrochemical performance and structural stability. A huge range of materials for particle design has been summarized, including carbon, polymer, and inorganic compounds. Up to date, polymer and inorganics with superior binding properties to polar sulfur species of polysulfides/Li₂S usually exhibit better electrochemical performance than that of nonpolar carbon. However, it is also noteworthy that extra conductive agents still constitute a certain fraction of the electrode to offer sufficient electron conduction. Efficient hybridization strategies ought to fully exert the merits of each simple constituent, or else it would be imperative to explore materials that are both polar and highly conductive.

From an industrial perspective, there are still remaining issues and difficulties in synthesizing, storing, freighting, and applying these secondary nanocomposites. The synthetic method must be easy and cost-effective for bulk and continuous production. The as-produced secondary composite particles should hold a narrow size distribution and a uniform shape, which guarantee the product conformity between different batches. The storage of these secondary composite particles also has several latent difficulties. For example, the mechanical and rheological properties of polymer strongly depends on the temperature. Therefore, storing these secondary nanocomposites made of polymer may easily lead to embrittlement or inteneration at unusual temperature. Humidity could be another factor to trigger the degradation of secondary particles upon storage because water moisture may induce the swelling of hydrophilic polymer or deliquescence of some hygroscopic compounds. Basically, thermal, light, electrical, magnetic, and moisture

Table 2. Advantages and disadvantages of various shell materials for core/shell particles.

	Advantages	Disadvantages
Impermeable carbon (nonporous carbon)	<ul style="list-style-type: none"> a) Superior electrical conductivity b) Mechanical strength c) Complete isolation of sulfur/Li₂S from electrolytes d) Electrochemical/thermal stability 	<ul style="list-style-type: none"> a) Slow Li⁺ diffusion through graphitic interlayers or carbon turbostratic defects b) Limited shell thickness and particle diameter
Permeable carbon (porous carbon)	<ul style="list-style-type: none"> a) Superior electrical conductivity b) Mechanical strength c) Large flux of Li⁺ ions through electrolyte permeation d) Electrochemical/thermal stability 	<ul style="list-style-type: none"> a) Thermodynamically possible outward diffusion of polysulfides through pores within the shell b) Poor affinity to polysulfides
Polymer	<ul style="list-style-type: none"> a) Structural conformality b) Mechanical flexibility c) Ion permeability d) Polysulfide impermeability e) Tunable binding to polysulfides 	<ul style="list-style-type: none"> a) Moderate electrical conductivity b) Inferior electrochemical/thermal stability c) Undesirable modulus/hardness
Inorganics	<ul style="list-style-type: none"> a) Superb chemisorption to polysulfides b) Tunable Li⁺ transport properties through either pores or lattices 	<ul style="list-style-type: none"> a) Poor electrical conductivity (except for a few cases) b) Inflexibility and brittleness c) Parasitic reactions (e.g., lithiation)

sensitivities of the secondary nanocomposites are worth being considered. Moreover, during the slurry preparation, electrode fabrication, and cell assembly, these secondary particles must be able to withstand the various deformative stresses induced by stirring, flowing, evaporating, and pressing. Hence good mechanical stability is a kernel feature. We believe that there will be fruitful opportunities co-existed with the aforementioned issues, which are anticipating effective solutions.

2.3. Electrode Architecture

The third hierarchy is at electrode level, to which the actual performance of one electrochemical cell is directly correlated. All the desired attributes, discussed above for the first two hierarchies at interface and particle cells, have to be well integrated in a rationally designed electrode architecture. Especially for high-sulfur-loading Li-S batteries, the increase in the thickness of sulfur cathode makes a great challenge to dealing with the transport issues across macroscopic dimensions. On one hand, according to the essence of electrochemical reactions, the kernel function of an architected electrode is to build efficient electron/ion transporting channels and maintain them during long-term operations. More than that, mechanically and chemically stable and durable scaffolds within the thick electrode are usually preferred because these electron/ion channels are mostly constructed from the connections among energy particles and scaffolds. During the electrode fabrication, tricontinuous electron/ion/mechanical networks are formed and their structure can be adjusted by parameterizing and technologizing each procedure. On the other hand, the current collector, on which the electrode layer attaches, is another important component in the battery as all electrons flow out and in through the

boundary between it and the electrode layer.^[147] And electrode architectures can be easily regulated by tuning materials, surface roughness, and shape of current collectors.

In a typical process for fabricating sulfur electrode, several steps are normally involved: 1) preparing sulfur composites; 2) mixing sulfur composites, conductive agents, and binder in solvents to form electrode slurry; 3) coating slurry on current collectors, routinely 2D metal foils such as aluminum (Al) foils; 4) evaporating the solvent to dry the coated electrode. Therefore, existing strategies for fabricating advanced electrodes mainly focus on modifying each step to meet the practical demands for high sulfur loadings. Al foil, the most common current collector for cathode materials of both LIBs and Li-S batteries, is limited by its insufficient electrical contact area owing to the planar structure.^[148] Therefore, the most straightforward approach is to alter the current collector into 3D structures. According to current collectors and fabrication techniques employed for sulfur cathodes, we generally categorized the strategic hierarchy into: 1) 2D coated electrodes, 2) 3D assembled electrodes, and 3) 3D infiltrated electrodes.

2.3.1. 2D Coated Electrodes

2D coated electrodes are normally coated on metal foils by blade coating. Most typically employed 2D current collectors are Al foils owing to the advantages of low cost, good electrical conductivity, rolling processibility, and mature industrial plants for large-scale fabrication. However, owing to the geometrical limitations, 2D current collectors are incapable of directing the formation of internal electron/ion channels within the electrode layer. The mechanical support is also insufficient when the electrode layer is thick. Therefore, tailoring the structure of

thick electrode layer becomes primarily important and urgent. The conductivity, internal hierarchical porosity, mechanical stability, and adhesion strength on the 2D current collector ought to be deliberately controlled during fabrication processes.

One issue for thick sulfur electrodes is the difficulty in infiltrating electrolytes in and allowing Li^+ ions react with the interior sulfur. The capillary pressure provided by the surface interaction is the driving force, which, however, drops significantly with the increasing thickness. Typically, in routine electrode fabrication, pores are mainly generated through solvent evaporation. Nevertheless, stresses induced by the differences in interfacial tensions between solid/liquid interfaces and

solid/gas interfaces inevitably results in collapse of interparticle pores. To fully utilize the reactive interfaces and reduce transport barriers of Li^+ ions, creating more persistent porous structure is one simple and effective approach. For example, Ma et al. employed ammonium bicarbonate (NH_4HCO_3) as the porogen in the slurry consisted of spray-drying carbon/CNT microspheres and binder (Figure 7a).^[149] NH_4HCO_3 decomposed at 60 °C in vacuum during electrode drying, releasing gaseous products and leaving the electrode a hierarchical porous structure. The as-obtained sulfur cathode with a sulfur loading of 2.5 mg cm^{-2} exhibited a capacity of 1133 mA h g^{-1} at C/2 and maintained 77% of the initial capacity after 250 cycles,

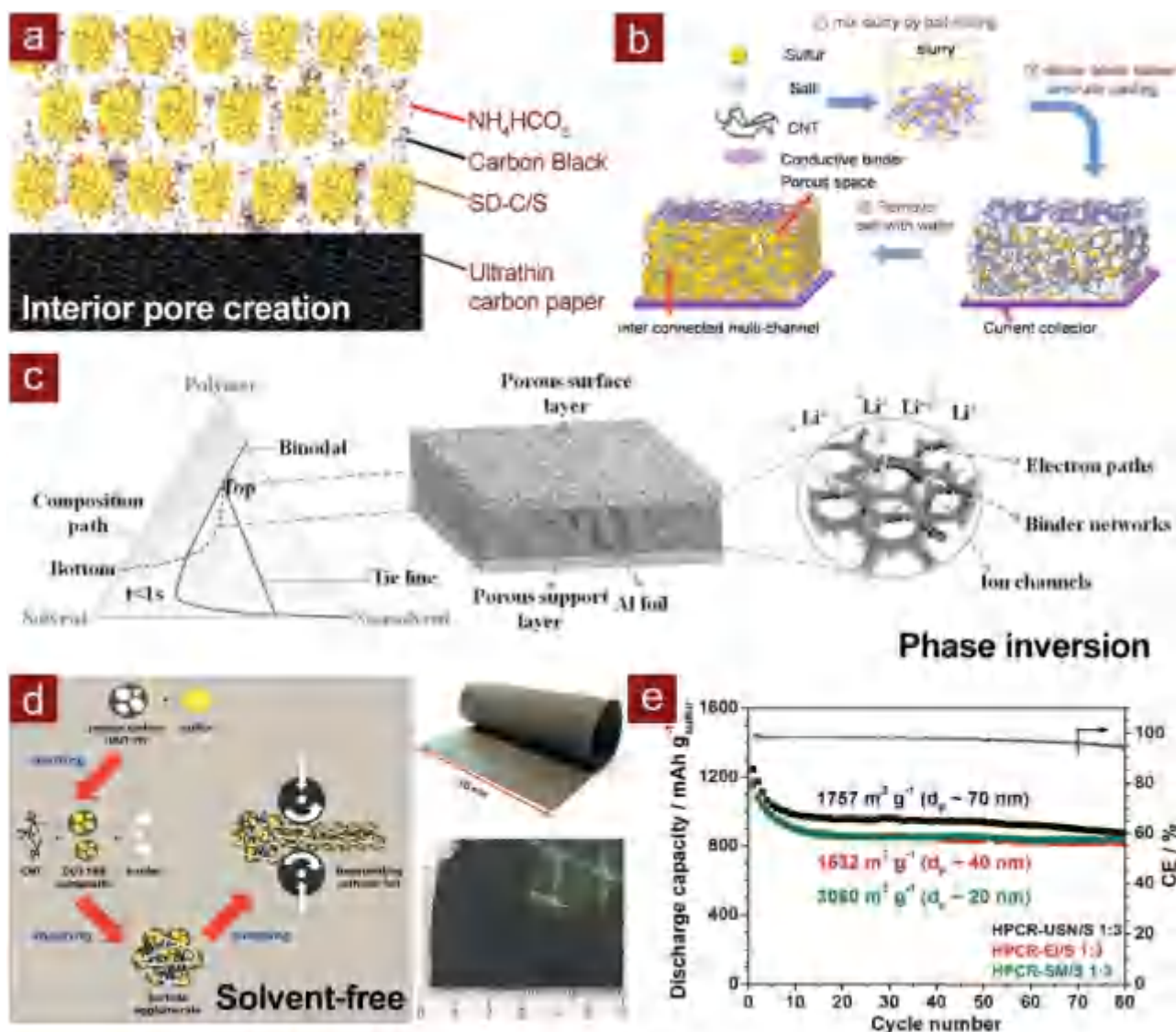


Figure 7. Fabrication method for 2D coated electrodes. a) Schematic of fabrication of polyporous cathode through NH_4HCO_3 decomposition. Reproduced with permission.^[149] Copyright 2015, Wiley-VCH. b) Schematic of the porous ant-nest structured cathode templated from the dissolution of NaCl crystals. Reproduced with permission.^[150] Copyright 2016, American Chemical Society. c) The formation mechanism of phase inversion electrodes and internal ion/electron transport, including ternary phase diagram of instantaneous phase inversion, the electrode structure, and internal ion/electron transport. Reproduced with permission.^[151] Copyright 2016, Wiley-VCH. d) Schematic of the solvent-free processing approach and photographs of as-obtained free-standing cathode foil and the lamination of cathode on a carbon-coated Al current collector. Reproduced with permission.^[152] Copyright 2013, Royal Society of Chemistry. e) Cycling performance of DUT-106 (templated from various ZnO nanoparticles)/sulfur composites based on the solvent-free procedure. Reproduced with permission.^[154] Copyright 2015, Wiley-VCH.

remarkably higher than the control cathode without being added NH_4HCO_3 . Inspired from natural ant-nest structure, Ai et al. proposed a biomimetic electrode structure by employing sodium chloride (NaCl) as a cost-effective sacrificial template to induce interconnected multichannels within CNT/sulfur composite electrodes (Figure 7b).^[150] At a sulfur loading of 3.0 mg cm^{-2} , the as-obtained CNT-nest-S cathode delivered capacities of 1124 and 909 mA h g^{-1} at C/10 and C/3, respectively. After cycles, the interconnected porous structure templated from NaCl could be remained to accommodate a large amount of solid products.

Except for the aforementioned strategies by introducing additional porogens or templates, parameters for the evaporation procedure, including solvents, temperature, and duration, can also be modulated to adjust the as-generated pore structures. Nevertheless, these necessitate complicated parameterization. Alternative approaches that are industrially viable might give rise to new opportunities. Zhang's group developed a universal method to fabricate high-performance porous electrodes based on the understanding of phase inversion, which is one of the most popular membrane manufacturing methods.^[151] By simply immersing slurry-coated current collectors into a water or nonaqueous coagulation bath, the phase inversion process was immediately triggered. Driven by the thermodynamic equilibrium of nonsolvent (e.g., water or alcohol)–polymer (e.g., PVDF)–slurry solvent (e.g., *N*-methyl-pyrrolidone (NMP)) triphase systems and the exchange between nonsolvent and solvent, polymer-rich phase containing binder and active materials, and solvent-rich phase were spontaneously separated with the former being solidified into electrode skeletons, while the latter being removed to form pores (Figure 7c). Through this method, they obtained tricontinuous electron/ion/binder networks within high-loading electrodes, which exhibited higher porosity and larger electrolyte uptake than routinely dried electrodes. Such kind of electrodes were further employed in Li–S pouch-cell batteries with sulfur loadings of 4 and 7 mg cm^{-2} . Capacities of 995 and 951 mA h g^{-1} were attained at two sulfur loadings, corresponding to areal capacities of 3.98 and $6.66 \text{ mA h cm}^{-2}$, respectively. This work firstly introduces membrane manufacturing technologies to the fabrication of battery electrodes, shedding a light on interdisciplinary cooperation for energy storage.

Although enriched porosity within thick electrodes significantly facilitates the Li^+ -ion transport through lengthened pathways, the electrolyte uptake for wetting the electrode will be enlarged as well, which inevitably decreases the E/S ratio and is detrimental to the specific energy. If the evaporation or drying procedure can be optimized or even replaced, internal porosity and packing density of an electrode might be balanced through other controls. Kaskel's group developed a solvent-free method to fabricate high-sulfur-loading cathodes based on various porous carbon/sulfur composites (Figure 7d).^[152] In a typical process, porous carbon/sulfur composites, conductive agents (e.g., carbon blacks or CNTs), and polytetrafluoroethylene (PTFE) binder were intensively grinded to homogenize mixed powders and fibrillate PTFE through shearing forces. As-obtained agglomerates were rolled out at $150 \text{ }^\circ\text{C}$ to obtain mechanically stable cathode foil, which subsequently was laminated on carbon-coated Al current collectors. Normally the sulfur loading

was around $3\text{--}5 \text{ mg cm}^{-2}$ and after 80–100 cycles at C/10, capacities of $\approx 800\text{--}900 \text{ mA h g}_S^{-1}$ ($\approx 500\text{--}600 \text{ mA h g}_{\text{electrode}}^{-1}$) were sustained, and the exact values depended on the pore volume and surface area of employed porous carbon hosts.^[152–154] Among them, hierarchical porous carbon DUT-106, templated from versatile ZnO nanoparticles, exhibited the best electrochemical performance (Figure 7e).^[154] Their solvent-free method for fabricating high-loading sulfur electrodes shows great potential for its versatility and industrially viable procedures.

Binder, as we discussed in (2.2.1), is another dominant component to determine the electrochemical performance. Different from the case at particle level, properties of binder materials need to satisfy some unique functions, including 1) long-range rigidity to remain the macroscopic compactness, 2) moderate stickiness for good adhesion but allowing acceptable processibility of binder solution, and 3) anti-swelling properties to lower inner resistance. In addition, aqueous binder is preferable as water is a green nontoxic solvent with low boiling point compared to organic solvents such as NMP, which makes the fabrication processes environmentally friendly, cost-effective, and energy saving. Conventional aqueous binder materials include PEO,^[94] PTFE,^[152] styrene butadiene rubber (SBR)/carboxymethyl cellulose (CMC),^[155] poly(acrylic acid) (PAA),^[52,156] polyacrylonitrile (PAN),^[157] alginate,^[158] and gelatin.^[98] Among them, SBR/CMC has advantages inherited from the hybrid polymeric systems. SBR is a typical elastomer with remarkably larger elongation than PVDF to withstand the volumetric change; while CMC, serving as the thickening agent, has rigid frameworks to prevent agglomeration of electrode particles, and is rich in hydrophilic functional groups such as $-\text{OH}$ and $-\text{COO}^-$ to retard diffusion of polysulfides. Therefore, SBR/CMC and its derivatives are the most widely employed binder systems in high-loading Li–S batteries.

To further enhance the mechanical properties of thick electrodes, crosslinking has been proposed as an effective and efficient strategy to build macroscopically-rigid while microscopically-elastic binder skeletons. Wang et al. explored the concept of interface chemistry-guided networks by crosslinking PAA binder with polydopamine (PD)-coated sulfur and carboxylic CNTs through covalent amide bonds (Figure 8a).^[159] Firmly integrated sulfur electrodes were obtained, showing little volumetric change after cycling. As a result, stable operation of Li–S batteries for 500 cycles at a current density 1.0 A g^{-1} was achieved. Despite the relatively low sulfur loading, it, for the first time, indicated the key role of crosslinking. Similar strategy was proposed by Pang et al., who integrated the merits of chemisorptive nitrogen-doped graphene/graphitic C_3N_4 (NG-CN) hybrid sulfur hosts, self-assembled NG-CN/S microparticles, and in situ crosslinked architectures together (Figure 8b).^[160] Through the esterification between $-\text{OH}$ in CMC and $-\text{COOH}$ in citric acid, electrodes with a high sulfur loading up to 14.9 mg cm^{-2} were fabricated without any visible cracks, in contrast to the PVDF-based thick electrode (Figure 8c). The maximum areal capacity was $14.7 \text{ mA h cm}^{-2}$. Note that such a holistic approach also decreased the amount of electrolyte employed. A low E/S ratio $3.5 \text{ } \mu\text{L mg}^{-1}$ was enabled (Figure 8d). Nevertheless, Nazar and co-workers also suggested that further decrease in E/S ratio might be more appropriately accomplished and investigated in pouch-cell prototypes.

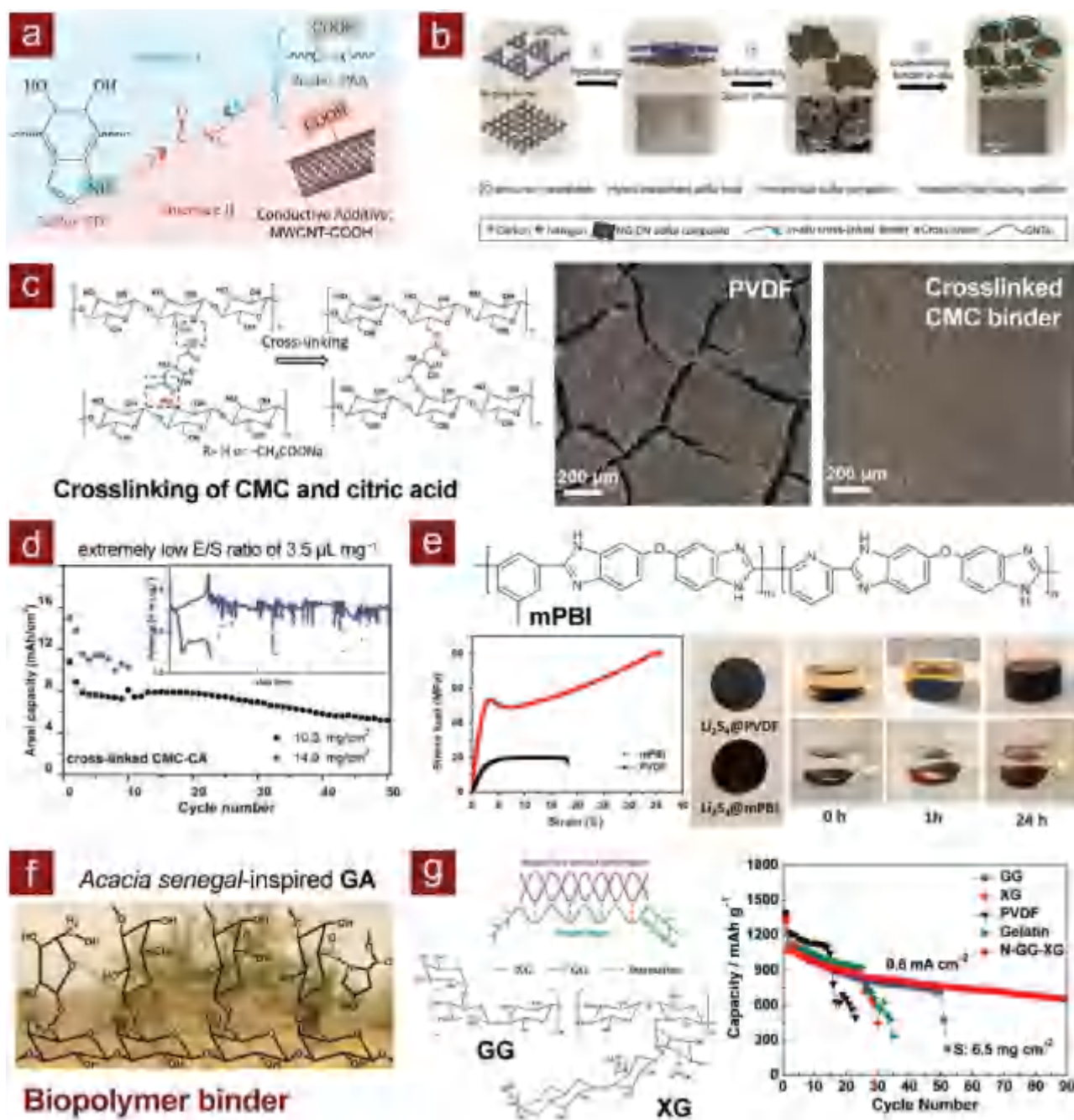


Figure 8. Advanced binder for 2D coated electrodes. a) Schematic of the formation of amide bond between PD and PAA (named as interface I) and PD and CNT-COOH (named as interface II). Reproduced with permission.^[159] Copyright 2013, American Chemical Society. Schematic of b) the concept of coupling hierarchical sulfur composite based on a hybrid host with in situ cross-linked binder to fabricate stable high-loading cathodes and c) of the cross-linking based on the esterification of the -OH groups in CMC and the -COOH groups in citric acid (CA), SEM images of thick sulfur electrodes using PVDF and crosslinked CMC-CA binder, d) the cycling stability of NG-CN/CMC-CA cathodes with sulfur loadings of 10.2 and 14.9 mg cm^{-2} at 1.0 mA cm^{-2} , and (inset) the voltage profiles of the 14.9 mg cm^{-2} electrode at 11^{th} cycle. Reproduced with permission.^[160] Copyright 2017, Wiley-VCH. e) Molecular structure of mPBI (prepared through the copolymerization of 3,3,4,4-tetraaminodiphenyl ether and 2,6-pyridinedicarboxylic acid), stress-strain curves of the mPBI film, visual observation of the Li_2S_4 @PVDF and Li_2S_4 @mPBI films and their dissolution behaviors in electrolyte solution. Reproduced with permission.^[161] Copyright 2016, Nature Publishing Group. f) Molecular structure of GA with the background of *Acacia senegal*. Reproduced with permission.^[163] Copyright 2015, Wiley-VCH. g) Molecular structures of GG and XG, Schematic of the intermolecular binding effect between GG and XG, and cycling performance of sulfur cathodes with different binders with a sulfur loading of 6.5 mg cm^{-2} at 0.8 mA cm^{-2} . Reproduced with permission.^[164] Copyright 2017, Royal Society of Chemistry.

The function of binder at the electrode scale is more than just mechanical stabilization. Chemical interaction between the binder and polysulfides is also highly preferable. Hence, Li et al. introduced modified polybenzimidazole (mPBI) as a binder, which withstood three times higher maximum stress load than PVDF and endowed sulfur cathodes with strong integrity, a high sulfur loading (7.2 mg cm^{-2}), and efficient polysulfide adsorption (Figure 8e).^[161] The corresponding Li–S batteries remained a high areal capacity of $5.21 \text{ mA h cm}^{-2}$ after 50 cycles at C/5. Moreover, mPBI can also serve as the coating layer on separators to suppress polysulfide crossover.

As reviewed in section (2.2.1.), bio-derived polymeric binder materials constitute an emerging class of alternatives to PVDF due to their natural abundance, low cost, excellent stiffness, and water solubility, which are especially interesting for large-scale deployment of high-loading electrodes composed of simple carbon/sulfur blends. Normally biopolymeric binder can be classified into polysaccharides or proteins. They contain abundant polar groups such as hydroxyl, carboxyl, and imide, which not only provide sufficient inter-/intramolecular adhesion but also adsorption of polysulfides. Various gummy biopolymers have been explored as the binder for high-loading Li–S batteries.^[162] For example, Zhang and Lin's group reported a bifunctional aqueous binder of gum arabic (GA), which was derived from *Acacia senegal*, for Li–S batteries with longevities (Figure 8f).^[163] GA is a complex mixture of polysaccharides and glycoproteins, containing abundant hydroxyl groups from saccharide units in both components and amide groups from polypeptide chains in glycoproteins. These functional groups, in combination with self-crosslinked networking structure, endowed GA with high friction coefficient for strong adhesion, low modulus, and hardness to tolerate volume change, and desirable affinities to sulfur through chemical bonds that formed during a thermal treatment. Even when the sulfur loading was increased to 4.4 mg cm^{-2} , a high areal capacity of $\approx 3 \text{ mA h cm}^{-2}$ was obtained after 50 cycles at C/5. Aiming at improving the comprehensive performance of binder, the same group further designed hybrid biopolymer binder of guar gum (GG) and xanthan gum (XG) with strengthened polymeric skeletons through intermolecular binding effects (Figure 8g).^[164] Each biopolymer had molecular-level flexibility while the rigidity was enhanced through intermolecular binding. Therefore, at a sulfur loading of 6.5 mg cm^{-2} , batteries employing hybrid GG/XG binder exhibited at least 100% longer lifespan than others adopting either routine PVDF and gelatin or GG and XG monobinder. By further increasing the sulfur loading to 19.8 mg cm^{-2} , an unprecedented areal capacity of $26.4 \text{ mA h cm}^{-2}$ was achieved, which have not been realized in binder studies before.

Subsection Summary (2.3.1.): In summary, the enhancement of 2D coated electrodes, on one hand, can be realized by rationalizing fabrication techniques such as slurry preparation, slurry coating, and electrode drying/densifying, or alternatively developing subversive schemes that are, however, suitable for industrial infrastructures. On the other hand, as a single component in the electrode, binder indisputably plays one of the most vital roles as it stabilize both particle assemblies (as discussed in (2.2.1.)) and electrode architectures. A comprehensive overview and future prospects will be given in the last conclusive part.

2.3.2. 3D Assembled Electrodes

Designing 3D free-standing electrode architectures, through either assembling various nanoscale building blocks into porous films,^[165,166] foams,^[167] papers,^[168,169] aerogels,^[121,170] or other macroscopic monoliths,^[171] or hybridizing active materials and functional additives on existing 3D skeletons,^[172,173] is the most widely explored strategy to fabricate high-sulfur-loading cathodes. These 3D assembled electrodes hold the prominent advantages in their interconnected porous structures, which, without the assist of a binder, naturally afford bicontinuous electron/ion transporting channels within macroscopic lengths across the thick electrode. The binder-free feature also reduces the extra weight of nonactive components. Additionally, by judiciously engineering the physical and chemical interactions between or within the 3D frameworks, mechanically stable architectures can be obtained to endure the drastic volume change and guarantee the structural stability of 3D assembled electrodes during long-term electrochemical cycling. In most cases, 3D assembled electrodes, especially those assembled from 1D nanomaterials such as CNTs and CNFs with large aspect ratios, have good flexibility or even foldability, stretchability, and twistability, to meet the demand for powering next-generation flexible electronic devices.^[174]

1D nanomaterials, especially CNTs and CNFs, constitute primary components for constructing high-performance 3D assembled electrodes due to their remarkable intrinsic properties including 1) high electrical conductivity along the *c*-axis, 2) less interfacial joints for charge transferring compared to networks consisted of carbon blacks, 3) self-woven morphology with a desirable macroporosity for electrolyte wetting and penetrating, 4) extraordinary strength and modulus to prevent mechanical failure, 5) large aspect ratio to guarantee global structural stability, and 6) light weight to enhance the specific energy on the basis of whole electrode/cell. Besides, the surface properties of CNTs and CNFs can be easily adjusted for controllable assembly into various macroscopic forms, such as thin films, foams, papers, and forests.

To date, a broad class of 3D assembled electrode based on 1D nanomaterials has been fabricated and evaluated as high-sulfur-loading electrodes. In 2011, Elazari et al. firstly employed commercial activated carbon fiber (ACF) clothes with abundant micropores of $< 2 \text{ nm}$ as nanoscale containers for sulfur, which was thermally impregnated into ACF at $155 \text{ }^\circ\text{C}$.^[175] With a sulfur loading of 6.5 mg cm^{-2} , ACF-sulfur binder-free electrodes exhibited a capacity of 800 mA h g^{-1} after 80 cycles at 0.98 mA cm^{-2} (Figure 9a). To simplify the sulfur loading process, Zhang dropped 20 wt% sulfur/carbon disulfide (CS_2) solution onto the ACF clothes and then evaporated CS_2 to obtain ACF-sulfur electrodes with a sulfur loading of 11.6 mg cm^{-2} (Figure 9b), resulting in a high areal capacity of $11.2 \text{ mA h cm}^{-2}$ (966 mA h g^{-1}) at 0.2 mA cm^{-2} .^[176] Owing to the simple fabrication and wide availability of CF/ACF clothes, other groups also demonstrated the capability of utilizing sulfur with sulfur loading amounts higher than 5 mg cm^{-2} .^[177] Nonetheless, CF or ACF are lack in efficiently constraining polysulfide dissolution and controlling the shuttle. Essential structural modulation or chemical modifications were thereby proposed. For example, Liu and co-workers employed coaxial graphene wrapping to

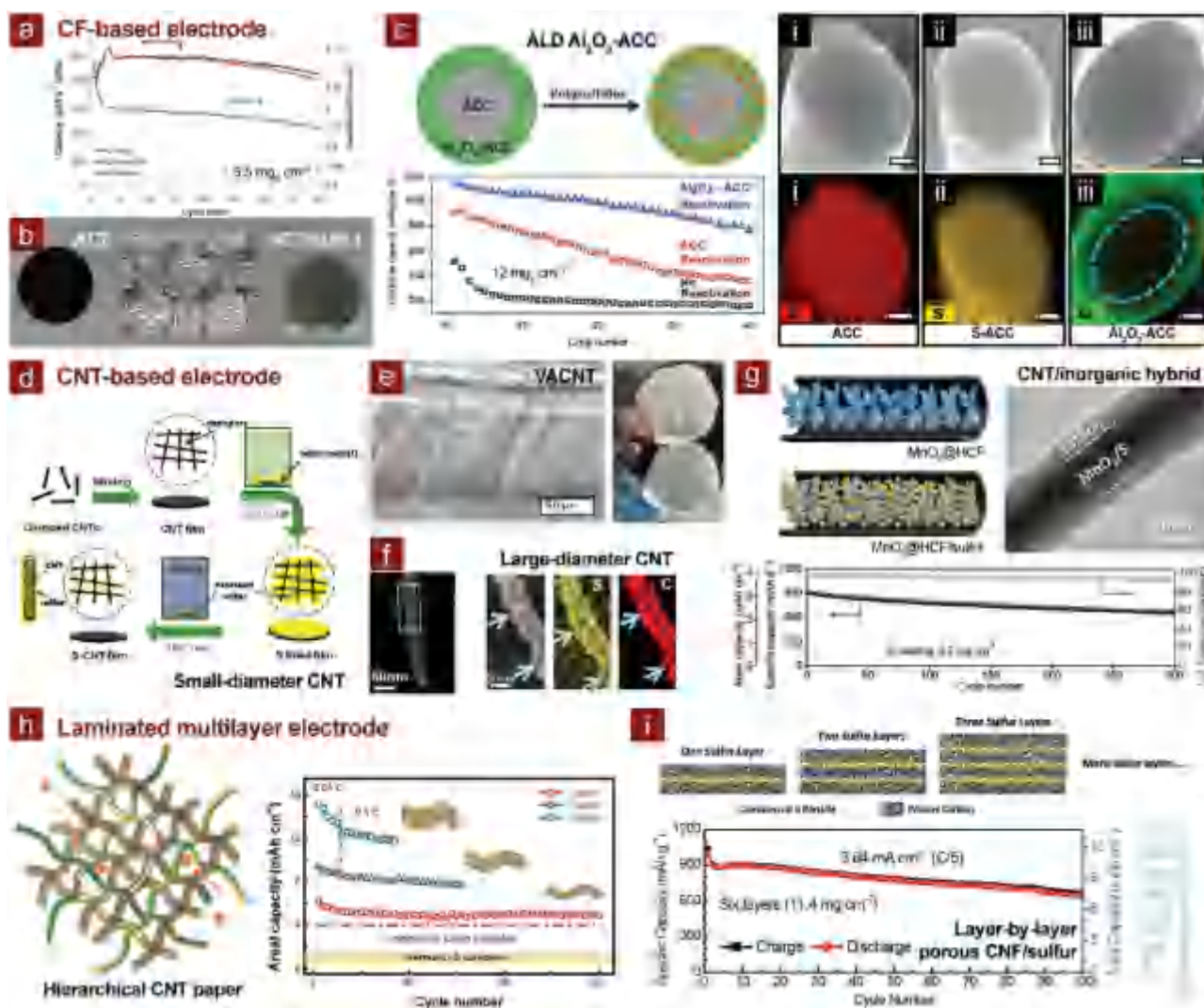


Figure 9. 3D assembled electrodes based on 1D CNT/CNF. a) Cycling performance of ACF/sulfur cloth at 0.98 mA cm^{-2} . Reproduced with permission.^[175] Copyright 2011, Wiley-VCH. b) Photographs and fine structure of ACF cloth (ACC) and ACF/sulfur. Reproduced with permission.^[176] Copyright 2013, Elsevier. c) Schematic, cycling performance (at 40 mA g^{-1}), SEM images, and corresponding elemental mapping of ALD- Al_2O_3 ACF-sulfur electrodes. Reproduced with permission.^[181] Copyright 2013, Elsevier. d) Schematic of the synthesis process for a sulfur-CNT film and its structure model. Reproduced with permission.^[165] Copyright 2013, American Chemical Society. e) Left: SEM image of VACNT grown on a metal foil. Reproduced with permission.^[171] Copyright 2012, Elsevier. Right: photograph of lithium metal anode and VACNT (grown on a gas diffusion layer)/sulfur cathode in separator pocket for pouch-cell assembly and evaluation. Reproduced with permission.^[185] Copyright 2013, Electrochemical Society. f) STEM image AAO-templated CNT/sulfur nanostructure and corresponding elemental mapping. Reproduced with permission.^[189] Copyright 2012, Royal Society of Chemistry. g) Schematic, SEM image, cycling performance (at C/2) of $\text{MnO}_2@HCF/sulfur$ composites. Reproduced with permission.^[190] Copyright 2015, Wiley-VCH. h) Schematic of hierarchical CNT paper and cycling performance lasagna-like laminated electrodes. Reproduced with permission.^[168] Copyright 2014, Wiley-VCH. i) Schematic of the layer-by-layer synthesis of multilayer porous CNF/sulfur electrodes and cycling performance of an electrode with six sulfur layers at C/5. Reproduced with permission.^[191] Copyright 2015, Wiley-VCH.

promote the cycling stability of the sulfur/CNF cathode with sulfur loadings of $2\text{--}3 \text{ mg cm}^{-2}$.^[178] Janek and Brezesinski's group developed a facile template method to synthesize free-standing fibrous N-doped carbon/sulfur cathodes on glass fiber templates.^[179] Tailorable sulfur loadings of 2.5 , 5.0 , and 8.5 mg cm^{-2} can be obtained with superior cycling stability. Zhou et al. fabricated N, O- modified CNF electrode, which was derived from low-cost zinc ethylene glycol/pyridine mixtures. Excellent electrochemical performance was achieved at sulfur loadings of 1.5 , 3 , and 4.5 mg cm^{-2} and capacities of

$>1000 \text{ mA h g}^{-1}$ were basically attained.^[180] Han et al. adopted atomic layer deposition (ALD) techniques to reactivate sulfur-impregnated ACF clothes by a 0.5-nm -thick layer of Al_2O_3 (Figure 9c).^[181] Such an ALD coating provided sufficient physical and chemical constraints and reactivation for dissolved polysulfides. As a result, capacities were increased by 25% and 114% at the 1^{st} and 40^{th} cycles, respectively, compared to those with unmodified ACF. Maximum capacity of ALD- Al_2O_3 ACF-sulfur electrodes with 12 mg cm^{-2} sulfur reached $13.6 \text{ mA h cm}^{-2}$ (1136 mA h g^{-1}) at a low current density of 40 mA g^{-1} . Other

inorganic/CNF-based 3D assembled electrodes include TiO₂-grafted carbon paper/Li₂S (2.0 mA h cm⁻² at 1.0 C, 2.0 mg cm⁻² sulfur),^[182] TiO₂-wrapped activated CNF/sulfur (2.9 mA h cm⁻² at C/5, 3.2 mg cm⁻² sulfur),^[183] and hollow Co₃S₄ polyhedra/activated CNF/pure sulfur (13 mA h cm⁻² at C/3, 13.5 mg cm⁻² sulfur).^[184]

Compared to CFs, ACFs, or CNFs, CNTs usually have smaller diameters, larger surface area, and better electrical conductivities, serving as superior building blocks to form 3D assembled electrodes. Generally CNTs for 3D assembled electrodes can be classified into three categories: 1) randomly organized small-diameter CNTs with interior incapable of being utilized, 2) vertically grown/aligned CNT forests, and 3) large-diameter CNTs or hollow carbon fibers (HCFs) with internal void accessible to sulfur and ions. CNTs in the first category can be easily processed in solution to form flexible membranes or papers after appropriate surface functionalization. For instance, Jin et al. firstly produced flexible CNT films by filtrating oxidized CNTs and then loaded sulfur by immersing CNT films in sulfur melt (Figure 9d).^[165] After thermal treatment under vacuum to remove excessive sulfur, sulfur–CNT films with a sulfur loading of 3 mg cm⁻² were obtained, delivering a capacity of 1097 mA h g⁻¹ at C/10, higher than that of sulfur–CNT powder electrodes. For the second category, vertically aligned CNTs (VACNTs) have a more ordered structure than CNT membranes, which allows more facile electrolyte penetration. In addition, VACNT forests are normally grown on metal foils, which enable the welding of current collectors to external circuits. Hagen et al. explored various VACNTs grown on different substrates as current collectors for sulfur cathode and investigated different methods to impregnate sulfur in/on the current collectors (Figure 9e).^[171,185] Their systematical studies revealed that VACNTs were ideal substrates for high-sulfur-loading cathode with sulfur loadings up to 15.8 mg cm⁻². As-obtained Li–S cells provided standard platforms to soundly evaluate effects of sulfur contents, areal loadings, current densities, and electrolyte compositions, as well as costs.^[186] Similarly, Xi et al. also fabricated VACNT forests to accommodate sulfur and adsorb polysulfides, gaining enhanced cycling stability.^[187] The last category, large-diameter CNTs or HCFs, offers better encapsulation of sulfur in the hollow void and minimize the exposure to electrolyte.^[48,188] Zhou et al. employed in situ carbothermal method to fabricate sulfur–CNT composites, during which sulfate resided in anodic aluminum oxide (AAO) templates was reduced into sulfur while these sulfur clusters were in situ confined in the microstructure of CNTs grown within AAO templates (Figure 9f).^[189] As-obtained sulfur–CNT composites can be assembled into highly flexible membranes as binder-free sulfur cathodes.

More sophisticated micro-/nanostructures can be obtained by engineering the compositions and structures of CNTs/HCFs, rendering synergistic effects of both physically confining and chemically adsorbing. Li et al. synthesized hollow carbon fibers filled with MnO₂ nanosheets (MnO₂@HCFs) through a multistep template method (Figure 9g).^[190] The resultant MnO₂@HCFs were organized into free-standing electrodes after loading 3.5 mg cm⁻² sulfur in the hollow structure, delivering a high capacity of 1147 mA h g⁻¹ at C/5 and longevity of 300 cycles at C/2 with capacity stabilized at 662 mA h g⁻¹. Such

a remarkable electrochemical performance compared to bare HCF/sulfur composites was attributed to the good integration of electrically conducting nanocarbon, chemisorptive MnO₂ nanosheets, and desirable hollow structure to accommodate sulfur and polysulfides.

Except for tuning the structures and physicochemical properties of 1D nanomaterials towards high-performance 3D assembled electrodes, simply laminating multilayered composite sheets into thicker electrodes effectively multiplies areal loading amounts. Our group proposed a lasagna-like architecture for fabricating free-standing CNT–sulfur paper electrodes with exceptionally high sulfur loadings through a bottom-up approach (Figure 9h).^[168] Routine micrometer-long CNT/sulfur composites based on the melting-diffusion method were firstly prepared and rigorously dispersed in sulfur-saturated ethanol solutions to prevent the loss of active materials. Millimeter-long CNTs were subsequently co-dispersed with short CNT/sulfur to serve as the rigid and long-range conducting backbones. Compared to pre-formed CNT papers with sulfur incorporated afterwards, these in situ assembled CNT–sulfur paper electrodes exhibited enhanced sulfur utilization and cycling stability. By simply stacking one to three CNT–sulfur papers with each containing 5.5–6.3 mg cm⁻² sulfur, high areal capacities of 6.3, 9.4, and 15.1 mA h cm⁻² were attained. Analogously, Qie and Manthiram reported a facile layer-by-layer approach to fabricate high-areal-capacity sulfur cathodes based on CO₂-activated CNF sheets (Figure 9i).^[191] By alternately laminating CNF sheets and commercial sulfur powders, they obtained layered sulfur cathodes with the sulfur loading increased through simply adding extra layers. Highest sulfur loading of 11.4 mg cm⁻² was obtained on six-layer CNF/sulfur electrodes, exhibiting an initial areal capacity of 11.3 mA h cm⁻² and maintaining 7.4 mA h cm⁻² after 100 cycles at 3.84 mA cm⁻².

2D nanomaterials with atomic thickness, such as graphene, are gaining exceptional attention for energy storage due to their unique characteristics compared to their bulk analogues, particularly including extraordinary mobilities (e.g., electrons, ions, and phonons), tunable electronic structures, and hugely exposed surface.^[55,192] Take graphene as an example, it can be easily processed into macroscopic forms so as to fully exert their merits at atomic or nanoscale level. To build 3D assembled electrodes from 2D building blocks, different macroscopic graphene forms such as sponges,^[193,194] aerogels,^[195] and porous foams^[196] have been engineered. For example, Zhou et al. synthesized a fibrous graphene, on which sulfur nanocrystals were anchored through one-pot hydrothermal reduction/co-assembly of graphene oxide (GO)/sulfur in CS₂/alcohol solution, obtaining a binder-free cathode with a sulfur content of up to 71 wt% (in the whole cathode) and a sulfur loading of ≈2 mg cm⁻² (Figure 10a).^[197] Similar hydrothermal approach was employed by Lu et al. to prepare graphene sponge, where sulfur was uniformly distributed after thermal impregnation (Figure 10b). Much higher sulfur loading of 12 mg cm⁻² was achieved, improving the areal capacity to ≈6 mA h cm⁻² and remaining 75.5% after 300 cycles.^[193]

Though 1D CNTs/CNFs and 2D graphene have been regarded as primary building blocks of 3D assembled electrodes owing to good electrical conductivity, high chemical/thermal stability, and ease to form macroscopic monoliths,

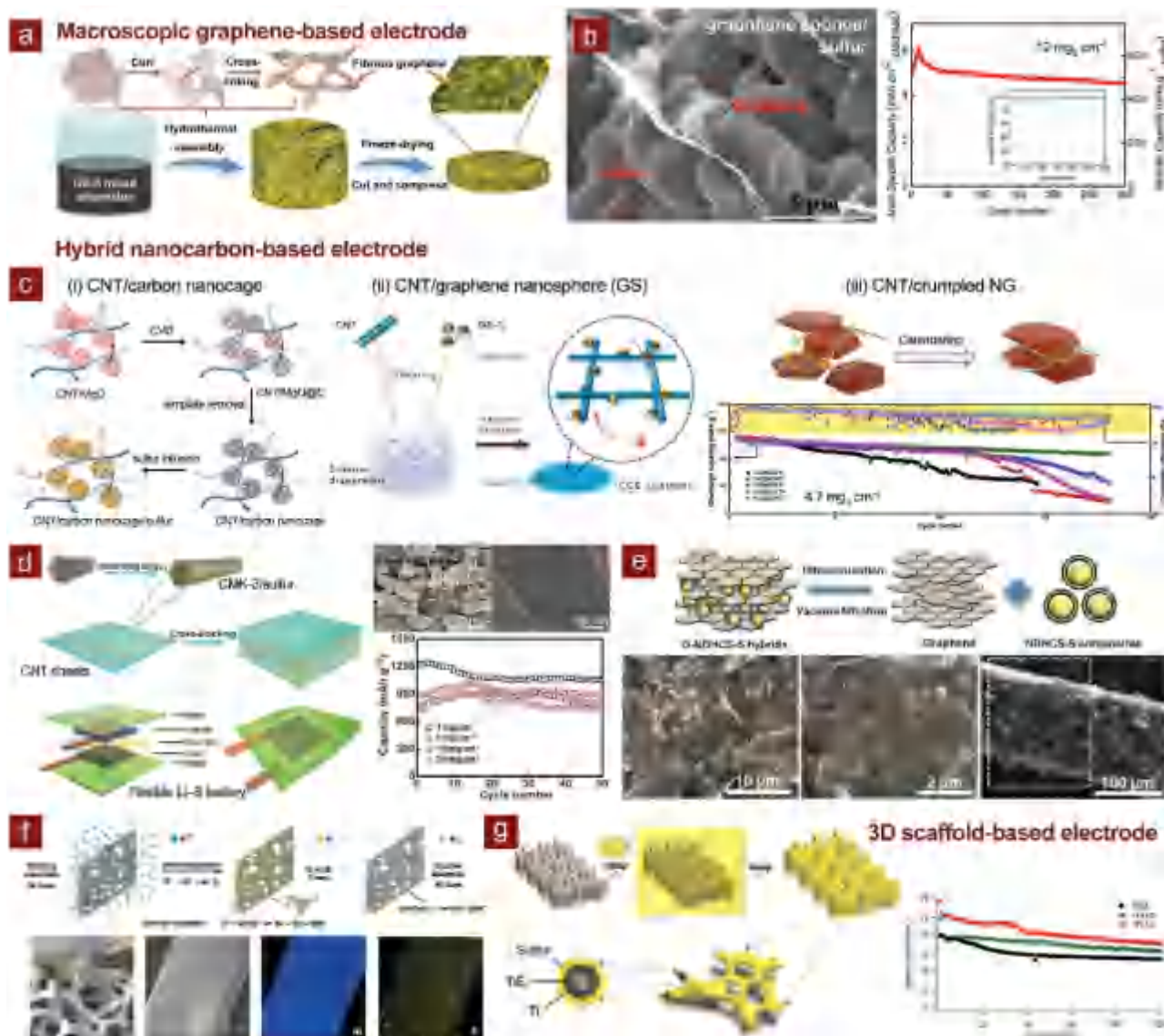


Figure 10. 3D assembled electrodes based on 2D/3D substrates. a) Illustration of the formation process of the fibrous G–S hybrid and schematic of the fabrication of a self-supporting electrode. Reproduced with permission.^[197] Copyright 2013, American Chemical Society. b) SEM image of graphene-sponge/sulfur and cycling performance at C/10. Reproduced with permission.^[193] Copyright 2014, Nature Publishing Group. c) Schematic of i) CNT/graphitic carbon nanocage,^[166] ii) CNT/GS,^[198] and iii) CNT/crumpled NG,^[199] as well as cycling performance of CNT/crumpled-NG/sulfur electrodes after being calendered with different compaction ratios. i) Reproduced with permission.^[166] Copyright 2017, Royal Society of Chemistry. ii) Reproduced with permission.^[198] Copyright 2015, Elsevier. iii) Reproduced with permission.^[199] Copyright 2017, Elsevier. d) Left: schematic of the fabrication process of the laminated CNT/CMK-3@sulfur cathode and for exploded and general views of the flexible Li–S battery; Right: SEM and TEM images of CNT/CMK-3@sulfur, and cycling performance with different sulfur loadings. Reproduced with permission.^[200] Copyright 2015, Wiley-VCH. e) Schematic of the fabrication of graphene–NDHCS–sulfur hybrid paper and its SEM images. Reproduced with permission.^[201] Copyright 2015, Wiley-VCH. f) Schematic of electrodeposition method for preparing sulfur nanodots on Ni foam, SEM image, and corresponding elemental mapping of sulfur nanodot/Ni foam. Reproduced with permission.^[173] Copyright 2015, American Chemical Society. g) Left: schematic of one-step method to prepare Ti/TiS₂/sulfur coaxial foam; Right: cycling performance of Ti/TiS₂/sulfur coaxial foams with different mass ratios of TiS₂ and sulfur. Reproduced with permission.^[172] Copyright 2015, Royal Society of Chemistry.

they are normally lack in extra functionalities, such as internal nanopores for close electrical contact and strong physical confinement, as well as polar interactions with polysulfides, to benefit high-sulfur-loading Li–S batteries. Therefore, more efficient way to utilize them is to assemble other functional building blocks within the mechanically stable and electrical conducting networks composed of 1D CNTs/CNFs

and 2D graphene. For example, our group prepared various flexible sulfur electrodes by co-assembling MgO-templated mesoporous graphitic carbon nanocages,^[166] hollow graphene nanospheres (GS),^[198] or N-doped crumpled graphene^[199] with millimeter-long CNT scaffolds (Figure 10c). These extra graphitic materials possessed better encapsulation and higher contacting surface area between sulfur and carbon than CNTs;

while millimeter-long CNTs were interlinked into robust and conductive skeletons, providing synergistic enhancements in electrochemical performance. Specifically, GS-sulfur/CNT flexible electrodes exhibited the most remarkable cycling stability of 89.0% capacity retention after 500 cycles at C/2.^[198] These flexible electrodes also served as prototypes to evaluate the influence of internal porosity on electrochemical performance by calendaring.^[199] Sun et al. developed an aligned and laminated cathode by alternately cross-stacking aligned CNT sheets and ordered mesoporous carbon/sulfur (CMK-3@S) particles (Figure 10d).^[200] At an extremely high sulfur loading of 20 mg cm⁻², a capacity of nearly 900 mA h g⁻¹ can be achieved. Moreover, such a flexible cathode can be operated under arbitrary bending angles between 0–180° with little performance degradation. Peng and co-workers indicated that such superior electrochemical and mechanical properties were attributed to the unique alignment of CNTs. Apart from CNTs, graphene was also employed as mechanical supports for 3D assembled electrodes. For instance, Zhou et al. employed N-doped double-shelled hollow carbon spheres (NDHCSs) as sulfur hosts and then assembled NDHCS-sulfur composites with graphene to obtain hybrid paper electrodes with a sulfur loading of 3.9 mg cm⁻² (Figure 10e).^[201] The encapsulation of NDHCS and graphene wrapping provided dual-confinements to sulfur and polysulfides, significantly promoting the electrochemical performance compared to bare graphene/sulfur papers. High capacity of 1360 mA h g⁻¹ and nearly 60% lower cyclic decay rate at C/5 were attained.

Hybridizing sulfur and other functional materials on existing 3D scaffolds has also been explored to fabricate high-sulfur-loading electrodes. For example, Zhao et al. reported an electrodeposition method to prepared sulfur nanodots with an average diameter of 2 nm on nickel (Ni) foams in a large area of over 100 cm² (Figure 10f).^[173] By simply controlling the deposition time, sulfur loadings from 0.21 to 4.79 mg cm⁻² can be adjusted. Under a harsher reaction condition at 780 °C, 3D Ti/TiS₂/sulfur coaxial foam was prepared by Ma et al. through the reaction between sulfur powder and commercial Ti foam (Figure 10g).^[172] The resultant TiS₂ not only served as conductive polysulfide absorbers but also provided extra capacity within the working voltage window of 1.6–2.6 V. At an exceptionally high sulfur loading of 40 mg cm⁻², capacities of ≈30 and ≈9 mA h cm⁻² were achieved at 2 and 10 mA cm⁻², respectively. Such unprecedented areal capacities were benefited from high gravimetric densities of metal (e.g., Ni foam and Ti foam with areal densities of ≈28 and ≈38 mg cm⁻²), which, however, inevitably lowered the gravimetric specific energy of the whole electrode. Therefore, 3D porous substrates composed of light weight, high-surface-area materials will probably be the future trend for this approach.

In the aforementioned studies, most 3D assembled electrodes are in the form of films/papers or sponges/aerogels. In recent years, energy storage devices with unconventional configurations, such as fiber- or cable-type rechargeable batteries, are emerging as a novel class of power accessories for wearable devices owing to their spinnability and knitability.^[202] Cable-shaped Li–S batteries are thereby attracting growing attention as they provide much more promising specific energies and linear capacities than cable-type LIBs. For cable-shaped Li–S

batteries, materials utilized to build the composite fiber are similar to their film or aerogel-like counterparts; whereas difficulties mainly lie on the integrating and packaging techniques. Peng's group pioneered the research on cable-shaped Li–S batteries by constructing aligned CNT fibers on which GO-encapsulated CMK-3/sulfur particles were dispersed.^[203] A linear capacity of 0.14 mA h cm⁻¹ was estimated. Niu and colleagues prepared a flexible nanostructured reduced GO (rGO)–sulfur paper via solution assembly, which delivered capacities of 1234, 1042, and 897 mA h g⁻¹ at C/10 at sulfur loadings of 2.2, 3.3, and 5.5 mg cm⁻².^[169] When further wrapped on a separator-protected lithium wire to form a cable-type Li–S battery, the paper cathode provided a comparable capacity of 1360 mA h g⁻¹. Very recently, Chong et al. reported more complicated rGO/CNT/sulfur composite fiber for Li–S battery cables with an initial capacity of 1255 mA h g⁻¹ (2.49 mA h cm⁻²).^[204] Fiber- or cable-like Li–S batteries in an unconventional configuration, with high areal/linear capacities and for unique applications, will be enlightened in the near future under the huge progresses in materials chemistry and engineering.

2.3.3. 3D Infiltrated Electrodes

Unlike 3D assembled electrodes, during the fabrication of which sulfur is incorporated via various complicated approaches such as in situ reactions, co-assembly, melting diffusion, or vapor infusion, 3D infiltrated electrodes are defined as those possessing 3D architectures but employing conventional blade-coating techniques or polysulfides-containing catholytes to infiltrate active slurries or materials into the 3D porous substrates. The basic concept is similar to that of 3D assembled electrodes, rendering enhanced transporting kinetics across the thick electrodes and other desirable attributes. Yet the conventional blade-coating technique or the use of catholyte is more compatible to industrial processes, not necessitating additional steps for sulfur impregnation that should be sophisticatedly engineered for mass production. Some 3D porous substrates, such as metal foams, will be more practically viable than being solely adopted since other functional additives (e.g., nanoscale conductive agents) in the cathode slurry help to compensate the disadvantages of metal foams in heavy weight and low surface area. Generally, the concept of 3D porous electrodes is simplified as building efficient, robust, and multifunctional 3D current collectors.

To replace 2D metal foils, the most primary and straightforward way is to engineer extra porosity into the metal substrates. Since being conventionally utilized in Ni–Cd or Ni–metal hydride batteries,^[205] Ni foams emerge as the most widely employed porous metal current collectors for high-sulfur-loading Li–S batteries. For instance, Chung and Manthiram prepared routine carbon black/sulfur slurries, which were subsequently pasted on and adsorbed in porous Ni foams with a moderate sulfur loading of 2 mg cm⁻².^[206] An average capacity of 810 mA h g⁻¹ was achieved during 50 cycles at C/5; while, in contrast, conventional cathodes applying 2D Al foils exhibited more than 50% capacity fading to only 420 mA h g⁻¹. The enhanced capacity retention was ascribed to the decreased transport impedance in the porous current collector. Ni foams

also enabled good electrochemical performance of high-sulfur-loading electrodes based on various composite materials such as PPy/sulfur (4 mg cm⁻²),^[207] pyrolyzed or dehydrogenated PAN/sulfur or sulfurized PAN (4–15 mg cm⁻²),^[208] Li₂S/ various nanocarbon (5 mg cm⁻²),^[209] N, S-codoped graphene/sulfur (6.3 mg cm⁻²),^[210] and so on. Ni foams were also modified by coating SiO₂ layers to enhance the adsorptivity to polysulfides.^[211] To overcome the drawback of Ni in the heavy density (8.91 g cm⁻³), our group adopted 3D Al foams, engineered with through holes (size of ≈100 μm and distributive density of ≈1000 cm⁻²), as current collectors to provide enlarged contact surface to CNT/sulfur composites (Figure 11a).^[212] At a sulfur loading of 7.0 mg cm⁻², a high initial capacity of 860 mA h g⁻¹ (6.02 mA h cm⁻²) was achieved; whereas the weight of 3D Al foam was ≈4 mg cm⁻², significantly lower than that of Ni foams (20–30 mg cm⁻²). Nara et al. also reported a commercial 3D Al foam with even larger pores of 550 μm and lighter weight as the current collector for Li–S batteries with sulfur loadings of up to 17.7 mg cm⁻² (Figure 11b).^[213] An exceptional areal capacity of 21.9 mA h cm⁻² can be thereby achieved. Therefore, the employment of light-weight raw materials for fabricating 3D porous current collectors unambiguously benefits the specific energy of the packaged cell.

Analogous to 3D assembled electrodes, carbon is one of the most popular and elementary materials for 3D porous current collectors to support blade-coated electrode particles or layers because of its light weight, high chemical stability, and high conductivity. Commercially available 3D carbonaceous substrates such as carbon/CNF papers,^[214,215] ACF clothes,^[216,217] and nonwoven CF clothes^[218,219] have been demonstrated for high-sulfur-loading electrodes. Zhang et al. prepared a sulfur cathode with an extremely high sulfur loading of 13 mg cm⁻² by placing a binder-glued porous sulfur layer on ACF clothes, demonstrating high initial capacities of ≈800 mA h g⁻¹ at 0.5 mA cm⁻².^[216] Chung and Manthiram employed a hybridized nanocellular carbon current collector, in which carbon nanofoams were firmly attached on interwoven CF backbones, possessing a unique micro-/meso-/macroporous architecture and endowing sulfur cathodes (2.2 mg cm⁻² sulfur) with a high initial capacity of 1314 mA h g⁻¹ and enhanced cycling stability at C/10 (Figure 11c).^[215] Nazar's group employed commercial carbon papers as current collectors to test advanced sulfur host materials such as N, S-codoped porous carbon, graphitic C₃N₄, and interwoven MXene/CNT hybrid with sulfur loadings of up to 5 mg cm⁻².^[220]

Despite the low cost and large-scale availability, commercial 3D carbonaceous substrates normally have lower surface area and less possibilities for further architecturing and chemical functionalizing, limiting the further improvement of electrochemical performance. Tremendous efforts have thus been devoted to design nanocarbon-based 3D current collectors. Free-standing, large-scale CNT membranes have already been successfully commercialized, possessing ultralow areal density and extraordinary electrical conductivity.^[221] Therefore, Li et al. invented a foldable Li–S battery by coating cathode slurry on superelastic CNT thin films with chessboard-like patterns (Figure 11d).^[222] At sulfur loadings of 1.8, 3.4, and 6.8 mg cm⁻², capacities of 700–800 mA h g⁻¹ at C/2 and of >400 mA h g⁻¹ at 3.0 C were obtained. More interestingly, more than 87% of

initial capacity can be maintained after folding the patterned electrodes for 100 times. More cost-effective 1D carbonaceous materials were also exploited. Li and Liu's groups synthesized large-area hollow carbon fiber foam (HCFF) through a simple, low-cost, and scalable approach by carbonizing natural cotton textiles (Figure 11e).^[223] The HCFF current collector was infiltrated by CNT/sulfur slurry and as-obtained 3D infiltrated electrodes enabled an ultrahigh sulfur loading of 21.2 mg cm⁻², at which the electrode delivered high initial capacity of 23.3 mA h cm⁻² and 14.8 mA h cm⁻² was maintained after 150 cycles at 3.55 mA cm⁻². Such an extraordinary advancement in battery performance was ascribed to the substantial adsorption of cathode slurry and electrolyte by the macroporous HCFF scaffolds. Wu et al. explored similar concept to prepare high-loading Li₂S cathodes by infiltrating Li₂S solution in porous cellulose sheets and subsequently carbonizing composite sheets into conductive and flexible electrodes (Figure 11f), rendering exceptionally stable 3D Li₂S/carbon electrodes even with an active material loading of 3.2 mg cm⁻².^[224]

Macroscopic graphene has also been developed as 3D current collectors for Li–S batteries since the 2D graphene unit is more advantageous than the 1D CNT/CNF to support and retain sulfur-containing slurry. In 2011, Cheng and Ren's group pioneered the conformal synthesis of 3D graphene foams (GFs) on 3D metal foams through CVD.^[225] Such 3D GFs have interconnected graphene skeletons, thereby possessing much more superb electrical conductivity and structural integrity than other solution-assembled graphene macroscopics to serve as ideal 3D current collectors for high-sulfur-loading Li–S batteries. They firstly reinforced the fragile pristine GF with elastic poly(dimethyl siloxane) (PDMS) to obtain PDMS/GF current collectors and then filtered the sulfur slurry (70 wt% sulfur) into PDMS/GF, which held excellent flexibility and high sulfur loadings of up to 10.1 mg cm⁻² (Figure 11g).^[167] During 1000 cycles at 1.5 A g⁻¹, such an electrode exhibited an initial capacity of ≈1000 mA h g⁻¹ and remained 448 mA h g⁻¹ at the 1000th cycle. This was also the first report that sulfur electrodes with a sulfur loading of >10 mg cm⁻² can survive for at least 1000 cycles. To fully utilize the inner space of several-hundred micrometer pores within GF, GO suspension was casted into pristine GF and then reduced, rendering a nested hierarchical GF-rGO network (Figure 11h).^[226] The sulfur loading and content were therefore increased to 14.4 mg cm⁻² and ≈90 wt% (in the whole cathode). At C/20, a reversible capacity of 846 mA h g⁻¹ was still attained after 90 cycles. Enlightened by these pioneering works, other groups also employed GFs as advanced platforms to test nanostructured sulfur composites (e.g., soybean-derived carbon/sulfur with 5.5 mg cm⁻² sulfur^[227]).

After long-term studies on 3D current collectors, key parameters for designing 3D current collectors are gradually identified by several investigations. Barchasz et al. proposed novel cathode architectures by employing 3D porous current collectors in their pioneering work and systematically compared Ni foams, carbon foams, VACNTs, and nonwoven CF clothes.^[219] They found that high surface area of current collectors (e.g., Ni or carbon foams and VACNTs) rendered higher sulfur utilization, while stable morphologies of current collectors (e.g., nonwoven CF clothes) dominated the cycling performance. They

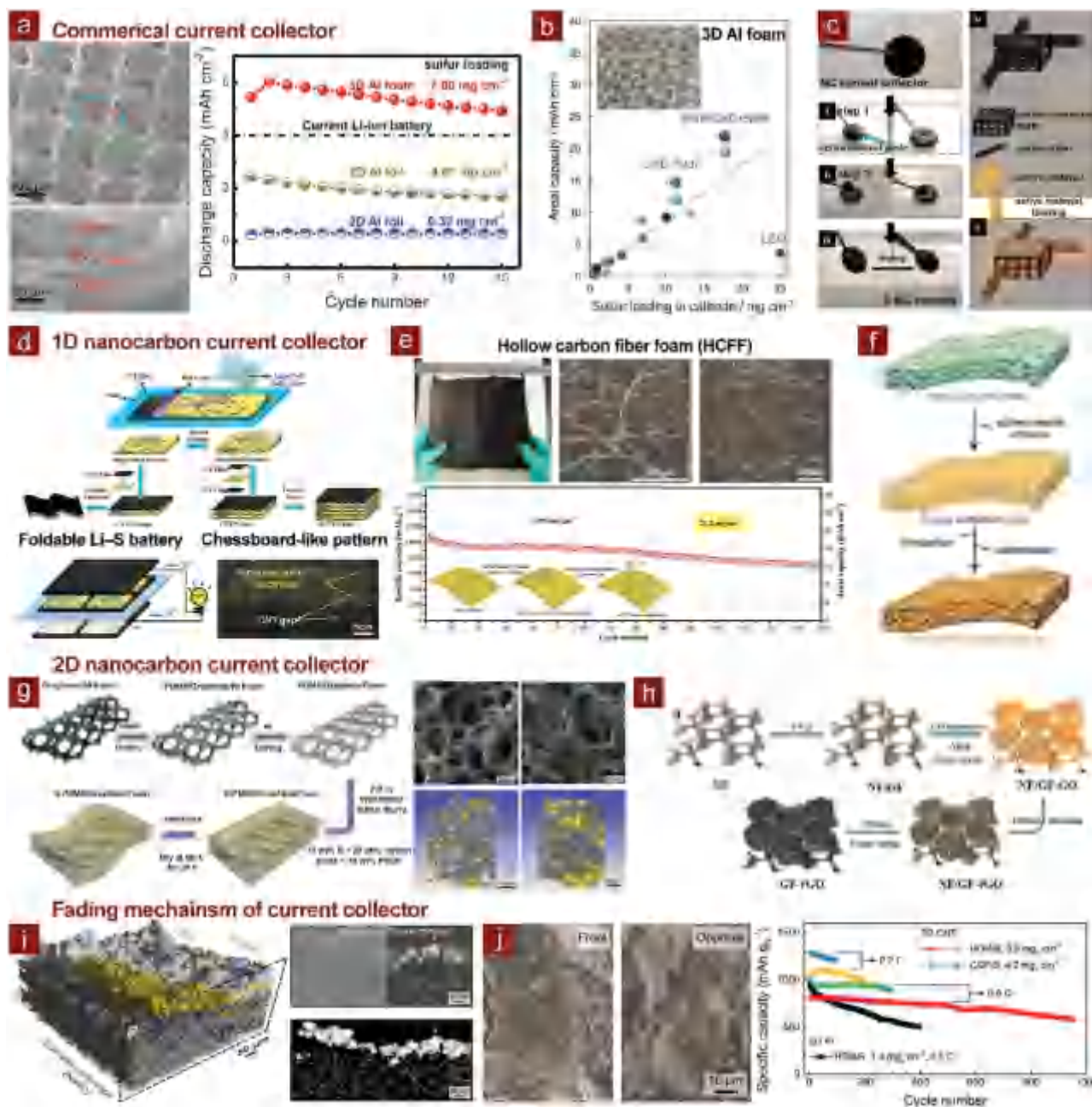


Figure 11. 3D slurry-infiltrated electrodes. a) Left: SEM images of 3D Al foam and CNT/sulfur cathode coated on 3D Al foam; Right: cycling performance of CNT/sulfur cathodes with different sulfur loadings and current collectors. Reproduced with permission.^[212] Copyright 2014, Elsevier. b) The sulfur loading and the areal capacity of the cathodes using commercial 3D Al foams (inset). Reproduced with permission.^[213] Copyright 2017, Electrochemical Society. c) Flowcharts and images showing the nanocellular carbon (NC) current collector, (i–iii) porous cathode preparation process, and (iv, v) schematic models of NC and sulfur-NC. Reproduced with permission.^[215] Copyright 2013, Royal Society of Chemistry. d) Schematics of the electrode preparation process and the designed configurations for foldable Li–S batteries with chessboard-like pattern. Reproduced with permission.^[222] Copyright 2015, American Chemical Society. e) Photograph of a large-area HCFF, SEM image of HCFF, partial 2D projected X-ray microtomography (XRM) of HCFF/sulfur, and cycling performance at 3.55 mA cm⁻². reproduced with permission.^[223] Copyright 2016, Wiley-VCH. f) Schematic of the fabrication of free-standing flexible electrodes from infiltrated porous polymer sheets. Reproduced with permission.^[224] Copyright 2016, Wiley-VCH. g) Schematic of the procedure for fabricating PDMS/GF and sulfur–PDMS/GF electrodes, SEM images and 3D XRM images of reconstructed sulfur–PDMS/GF electrodes with 3.3 (left) and 10.1 (right) mg cm⁻² sulfur loadings. Reproduced with permission.^[167] Copyright 2015, Elsevier. h) Schematic of the fabrication procedure of 3D GF–rGO hybrid nested macrostructure. Reproduced with permission.^[226] Copyright 2016, Wiley-VCH. i) XRM characterization of spatial sulfur distribution within electrode coated on NWC. Reproduced with permission.^[228] Copyright 2015, Nature Publishing Group. j) SEM images of electrochemically-corroded Al current collectors and significant enhancement in cycling performance by replacing 2D Al foils into 3D macroporous CNT membranes. Reproduced with permission.^[148] Copyright 2016, Wiley-VCH.

further employed X-ray phase contrast tomography to probe the degradation mechanism of high-loading sulfur cathodes on 3D current collectors and suggested that active materials migrated and accumulated during cycling, exaggerating the inner resistance and thus lowering the capacity (Figure 11i).^[228] To gain comprehensive insights into the origin of stability enhancement with the presence of 3D current collectors, our group deconvoluted the stability issue into two aspects.^[148] The corrosion and pulverization of Al current collectors in the electrolyte containing bis(trifluoromethanesulfonyl)imide (TFSI) anions led to cathode delamination and drastic increase in cell resistances, accounting for one aspect of the capacity degradation (Figure 11j). The second aspect was in good accordance with Zielke et al. that the migration of active phase passivated the cathode/separator interface and block the ion channels.^[228] Therefore, 3D carbonaceous current collectors, which exhibited superior chemical/electrochemical stability to withstand corrosion and desirable macroporosity at the side close to the separator, as our group demonstrated as self-woven membranes of millimeter-long CNTs, were proved to improve the cycling stability of various high-loading sulfur cathodes universally.^[148] On a hollow graphene nanoshell/sulfur cathode with 3.9 mg cm^{-2} sulfur, the best performance was demonstrated as 71.8% capacity retention after 950 cycles at C/2, which even outperformed the control cathode coated on the Al foil with a much lower sulfur loading of 1.4 mg cm^{-2} .

In 1979, Rauh et al. reported a Li/dissolved polysulfide electrochemical cell for the first time, which unfortunately exhibited rapid capacity decay.^[229] Recently, such a configuration was revisited under tremendous progress in controlling polysulfide shuttle and protecting lithium anodes. For instance, Zhang firstly introduced LiNO_3 as an antishuttle agent in a Li_2S_9 catholyte to promote the reversible conversion between S_8 and Li_2S_8 (Figure 12a).^[230] Since it is easy to scale up the sulfur loading by simply varying the amount of polysulfide catholyte, building Li/dissolved polysulfide cell configuration is another proof-of-concept to evaluate the performance of 3D porous current collectors in a facile and effective way. Different from blade coating or drop casting sulfur slurries on the current collector, directly utilizing polysulfide catholyte demands for 3D porous current collector with higher electrical conductivity and surface area owing to the lack in additional nanoscale conductive agents. Hence, candidates for being current collectors are more strictly screened, mainly focusing on nanocarbon materials.

Manthiram's group have explored a broad range of 3D porous current collectors for Li/dissolved polysulfide batteries based on various nanocarbon materials and their composites. Fu et al. firstly demonstrated this concept by utilizing a self-weaving, free-standing CNT paper as the current collector and Li_2S_6 catholyte as the starting active phase (Figure 12b).^[231] By varying the concentration of sulfur [S] from 1.0 to 3.0 mol L^{-1} (M), they obtained $\text{Li}_2\text{S}_6/\text{CNT}$ paper cathodes with sulfur loadings ranging from 1.2 to 3.4 mg cm^{-2} , all of which were indicated to exhibit high utilization of sulfur at various current rates. However, they also found the corrosion of lithium anodes under the attack of high-concentration polysulfide solutions (Figure 12c). To enhance the adsorption to polysulfides, there are two main approaches. One is to introduce substantial micropores within the current collector to provide exceptional physical adsorption.

For example, Chung et al. fabricated a carbon-cotton current collector by carbonizing commercial cotton fabrics, which intrinsically possessed stereoscopic macroporous structure to stabilize a high amount of active materials and abundant micropores to facilitate the redox reaction of polysulfides (Figure 12d).^[232] Unprecedented sulfur loading of 61.4 mg cm^{-2} was attained, under which the $\text{Li}_2\text{S}_6/\text{carbon-cotton}$ cathodes displayed a peak discharge capacity of 912 mA h g^{-1} ($56.0 \text{ mA h cm}^{-2}$) and a high capacity retention of 77% at C/10 after 50 cycles. More popular one is to introduce chemical anchoring sites with stronger chemisorption to polysulfides. Such an approach can be realized by either chemical doping/functionalizing carbon or compositing it with foreign chemisorptive phase. Zhou et al. synthesized a lightweight 3D N,S-codoped graphene sponge as the current collector for Li/polysulfide batteries (Figure 12e).^[170] Compared to undoped rGO and monodoped (S-doped and N-doped) graphene, N,S-codoped graphene sponges exhibited highest sulfur utilization and rendered smallest impedance and polarization owing to the synergistic binding effects of N,S-dual sites. At a sulfur loading of 8.5 mg cm^{-2} , 1.0 M [S] $\text{Li}_2\text{S}_6/\text{N,S-codoped}$ graphene sponge cathode exhibited capacities of 925 and 670 mA h g^{-1} (7.86 and $5.70 \text{ mA h cm}^{-2}$) at the 1st and 200th cycle at C/2 (7.12 mA cm^{-2}). Yao and Zheng et al. designed a hybrid tin-doped indium oxide (ITO)-decorated CNF scaffold for controlling spatial deposition of sulfur species based on their finding that polysulfides/ Li_2S selectively deposited on polar region (ITO) of patterned ITO/C panels (Figure 12f).^[233] By using 5.0 M [S] Li_2S_8 solution as the catholyte, they achieved stable cycling of Li/polysulfides cells at capacities of $\approx 1000 \text{ mA h g}^{-1}$ and with sulfur loadings of 4.0 mg cm^{-2} . Other doped or hybridized systems as current collectors for Li/dissolved polysulfide batteries include N,O-codoped porous carbon gel (3 mg cm^{-2} sulfur)^[234] or TiO_2 nanowires (3.2 mg cm^{-2} sulfur)^[235] on graphene papers/films, N,S-codoped commercial carbon paper (9 mg cm^{-2} sulfur),^[236] bacterial cellulose-derived N,O-codoped carbon nanoribbon (6.4 mg cm^{-2} sulfur),^[237] and N,O-doped CNT forests (1.7 mg cm^{-2} sulfur),^[238] MnO_2 (2, 4, and 6 mg cm^{-2} sulfur),^[239] Co_3O_4 (4 mg cm^{-2} sulfur),^[240] InCl_3 (2 and 4 mg cm^{-2} sulfur),^[241] or phosphorene (3.3 mg cm^{-2} sulfur)^[242] on CNFs.

Section Summary (2.3.): Despite that tremendous progress made in the past few years have propelled the areal capacities of high-sulfur-loading Li-S batteries to the level above 10 mA h cm^{-2} , there are still many critical issues impeding the practicability of 3D assembled/infiltrated electrodes:

- (1) Large-scale production of 3D porous current collectors. Currently, commercial 3D current collectors such as carbon papers or CF/ACF textiles/cloths are restrained by their relatively low electrical conductivity and surface area; while high-performance CNT films or macroscopic graphene usually necessitate processes in solution, such as dispersion and filtration, which are difficult to be scaled up. Several examples have indicated the bulk production of CNT membranes; however, the high cost is still an issue.
- (2) Compatibility with conventional battery technology. The flexibility and processibility of 3D porous current collectors must be suitable for continuous coating or roll-to-roll procedures, which is quite challenging.

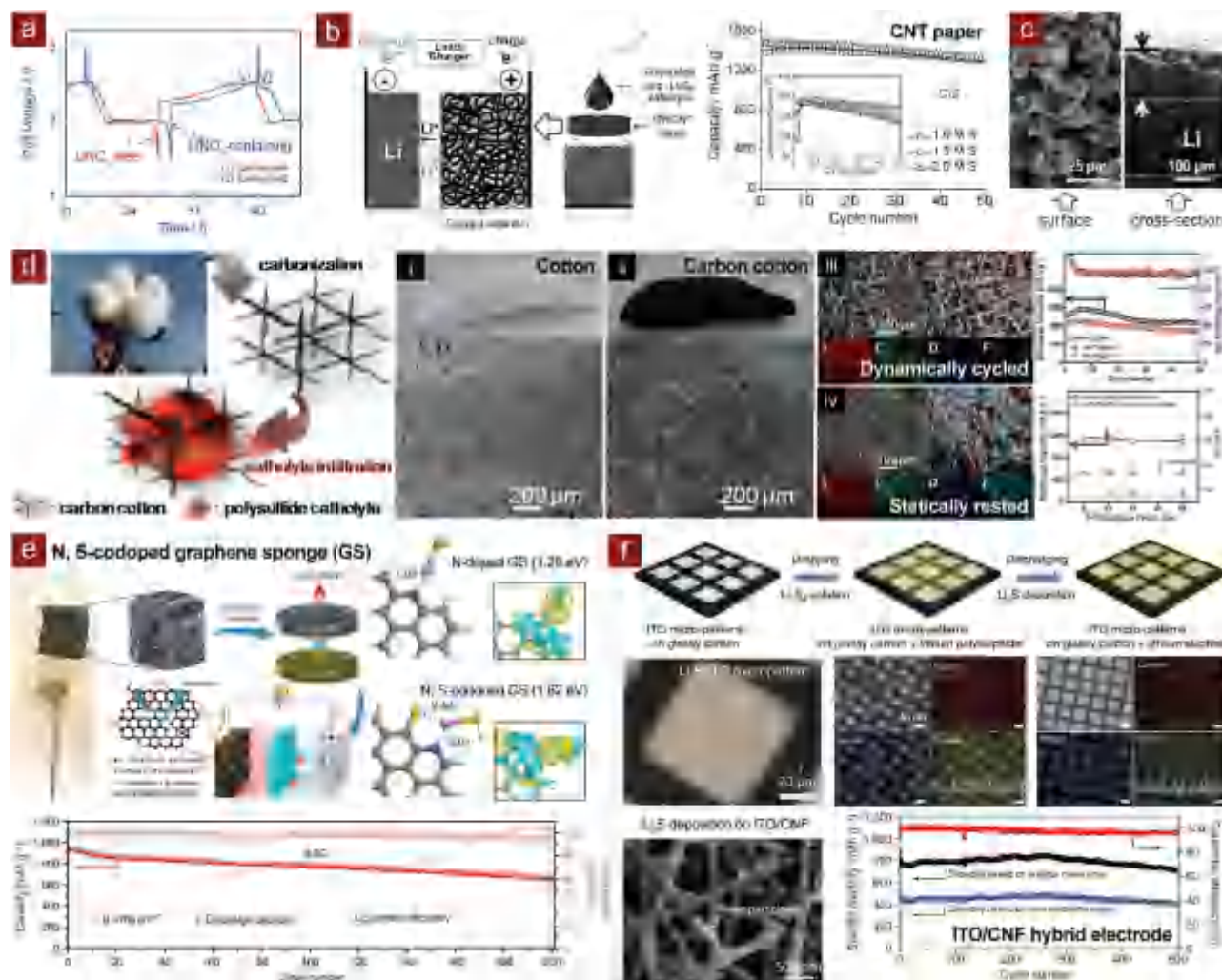


Figure 12. 3D catholyte-infiltrated electrodes. a) Voltage profiles of Li/Li₂S₉ liquid cells with (Catholyte A) or without (Catholyte B) LiNO₃. Reproduced with permission.^[230] Copyright 2012, Elsevier. b) Schematic of the structure of a Li/dissolved polysulfide cell and the addition of polysulfide catholyte into a CNT paper electrode, and cycling performance with different polysulfide concentrations, reproduced with permission.^[231] Copyright 2013, Wiley-VCH. c) SEM images of the surface (left) and cross-section (right) of a cycled lithium metal anode with polysulfide catholytes. Reproduced with permission.^[231] Copyright 2013, Wiley-VCH. d) Schematic of the fabrication process of the carbon-cotton cathode, digital and SEM images of i) cotton and ii) carbon cotton, SEM images, elemental mapping, and stability of iii) dynamically cycled electrodes (after 100 cycles at C/10) and iv) statically rested electrodes (for 60 days). Reproduced with permission.^[232] Copyright 2016, American Chemical Society. e) Left: photograph of a lightweight N,S-codoped GS standing on a dandelion; Middle: schematic of the formation process of the N,S-codoped GS and the fabrication of a Li/dissolved polysulfide cell with N,S-codoped GS after adding polysulfide catholyte; Right: theoretical calculations showing the optimized configuration, charge density difference isosurface, and binding of Li-SH clusters to N-doped GS and N,S-codoped GS; Below: cycling performance of N,S-codoped GS at C/2. Reproduced with permission.^[170] Copyright 2015, Nature Publishing Group. f) Upper: schematic of the fabrication of polysulfide-ITO micropattern glassy carbon cathode to show the nature of polysulfide deposition; Middle: SEM image of Li_xS-ITO micropattern, elemental mapping of ITO glassy carbon electrode after discharging to 1.7 V and charging to 2.6 V; Below: SEM image of ITO/CNF electrode after discharge showing the deposition of Li_xS nanoparticles, and cycling performance of ITO/CNF electrode loaded with solid sulfur (2.0 mg cm⁻²) and polysulfides (2.0 mg cm⁻² sulfur) at C/5. Reproduced with permission.^[233] Copyright 2014, Nature Publishing Group.

- (3) Design of the electrode lug. For the conventional electrode coated on metal foils, the electrode lug is welded to both the metal current collector and external circuits to connect. However, for most of the proof-of-concept 3D nanocarbon electrode, it is almost impossible to weld metal electrode lugs firmly to carbon. Therefore, exploiting alternative strategies for electrode lug design becomes crucial and urgent.
- (4) Huge electrolyte uptake by the 3D porous architecture. It is unambiguous that the sulfur utilization and cycling

stability of high-loading Li-S batteries are in favor of 3D macroporous structures. However, aiming at lowering the E/S ratio, the inner porosity and wetting properties must be deliberately tailored.

In summary, 2D coated electrodes are still the most reliable architectures for practical applications. Yet some conceptually novel and important designs and insights, derived from 3D assembled/infiltrated electrodes, are highly referential for

advanced 2D coated electrodes. Related progress will be discussed in later sections. Alternatively, 3D assembled/infiltrated electrodes can still serve as rational platforms for testing unexplored cathode materials at coin-cell level, thus successively promoting the whole area of energy storage. Whereas at pouch-cell level, none of the mostly studied 3D assembled/infiltrated electrodes based on nanocarbon is readily suitable, unless there is disruptive technical innovation in the structure of practical large cells. Unlike nanocarbon-based, lightweight, high-surface-area 3D electrodes, 3D porous metal current collectors are capable of being continuously produced. Few examples have been commercialized. Therefore, they could be more viable substituents to 2D metal foils. Nonetheless, parameters such as resistance, internal porosity, and areal density must be optimized at an affordable expense. We look forward to numerous related progress.

2.4. Other Sulfur Allotropes

Other sulfur allotropes, serving as the cathode materials, are specifically defined as those capable of being operated in conventional LIB electrolytes using carbonate solvents, including physically confined short sulfur chains (S_2 – S_4)^[37,38] and chemically covalent-bonded organosulfides (e.g., pPAN@S^[39,40] and carbyne polysulfides^[42]). During the electrochemical reactions between these sulfur allotropes and Li^+ ions, no polysulfide formation is expected. Therefore, polysulfide-incompatible carbonate-based electrolyte (e.g., propylene carbonate, ethylene carbonate, dimethyl carbonate) can be utilized.^[243] Generally, unique electrochemistry can be realized with a single-plateau galvanostatic discharge/charge profiles, which is substantially distinguished from that of elemental cyclo- S_8 .

Short sulfur chains or small sulfur molecules (S_2 – S_4) were firstly realized in 2010 by Gao and co-workers.^[244] Typically, sulfur was confined in the micropores^[37,244] or atomic carbon interlayers,^[38] exhibiting a single-plateau electrochemical behavior and normally possessing exceptional cycling stability. However, the mechanisms accounting for such a unique behavior are still in tremendous contradictory. One is the small-sulfur mechanism that within ultramicropores (with pore size <0.5 nm), metastable S_2 – S_4 can be effectively stabilized under very strong geometrical confinement.^[37] Guo's group even extended this mechanism to explain the electrochemistry of single-walled CNT-confined long S chains.^[245] In this case, single plateaus were generally observed either in carbonate-based electrolyte or ether-based electrolyte.^[246] In contrast, other groups found that microporous carbon with pore size >0.5 nm can still allow single-plateau electrochemistry of sulfur even though the pore size was larger than small sulfur allotropes of S_2 – S_4 . A quasi-solid-state mechanism was therefore proposed that a cathodic electrolyte interphase was formed around the aperture of the pore to seal the sulfur and protect it from the electrolyte, suggesting that small sulfur molecules might not be necessary.^[247] pPAN@S can be regarded as one of the earliest cathode materials for rechargeable Li–S batteries based on Wang and co-worker's pioneering works.^[39] In the composite with sulfur content lower than 42 wt%, monodispersed sulfur atoms are covalently bonded to the polymer backbone, preventing

the formation of polysulfides.^[41] Therefore, pPAN@S also exhibit extraordinary cycling stability. Strategies for enhancing the sulfur loading of these cathode materials based on unique sulfur allotropes are similar to those for elemental cyclo- S_8 , mainly focusing on the 3D current collectors.^[208]

Besides much better cycling stability than that of S_8 -based cathode, sulfur allotropes possessing single-plateau electrochemistry have a predominant advantage in specific energies due to the intrinsically low E/S ratio. Since there is no demand for dissolving polysulfides, the amount of the electrolyte, in principle, can be as low as in LIBs. Therefore, the device specific energy can be roughly deduced from the specific energy of the cathode materials using the same empirical standard as for LIBs. Given that one of the highest capacity of pPAN@S ($\approx 600 \text{ mA h g}_{\text{cathode}}^{-1}$) and an average discharge voltage of $\approx 1.8 \text{ V}$, the specific energy of the cathode is calculated to be 1080 W h kg^{-1} , which is higher than those of state-of-art LIB cathode materials (≈ 700 – 900 W h kg^{-1}). Such an advantage will be more predominant if the sulfur content can be further improved while the electrochemical mechanism is maintained. However, for this type of sulfur cathode materials, there is also concern about the relatively low Coulombic efficiency of the first cycle (<80%). The reason for the loss in the initial Coulombic efficiency still remains exclusive. Additional active materials, lithium, or electrolyte might be needed to compensate such loss, which will increase the weight of the whole device and thereby lower its specific energy.

Section Summary (2.4.): Physically confined or chemically bonded sulfur allotropes possesses very promising and distinctive chemistry. The formation of polysulfides is inherently prohibited. That allows efficient stabilization of both the cathode and the lithium anode. Cell operation at electrolyte-starve conditions is also conceptually viable. Nevertheless, many technical obstacles should be overcome before cathode materials based on unique sulfur allotropes can be successfully deployed.

3. Anodes

As coupled with elemental cyclo- S_8 , metallic lithium is the most common anode materials for Li–S batteries. Lithium metal has been regarded as the “Holy Grail” of rechargeable batteries since forty years ago, owing to its extremely high theoretical specific capacity of 3860 mA h g^{-1} and the lowest negative electrochemical potential of -3.040 V vs the standard hydrogen electrode.^[248] These two merits lay a foundation of extraordinary specific energy of Li–S batteries. However, some formidable problems have been hindering the mature of rechargeable lithium metal batteries (LMBs) including Li–S batteries:

- (1) Unlike Li-intercalated graphite or Li-alloyed silicon/tin, lithium metal is, in reality, “hostless” during electrochemical plating/stripping, leading to virtually infinite volume change. Therefore, the composition and morphologies of cycled lithium metal vary significantly from those at the pristine state.
- (2) Solid electrolyte interphase (SEI), the electrically insulating but ionically conducting layer that is naturally formed at

the lithium/electrolyte and solid/liquid boundary, is not chemically, electrochemically, and mechanically stable or spatially and temporally uniform, rendering continuous damage/regeneration of SEI and thus electrochemical inefficiency.^[249]

- (3) Uncontrolled deposition/dissolution of lithium metal makes the interface constantly and dynamically change, resulting in the increase in contact surface area or even rampant growth of large lithium dendrites that pierce the separator and cause short circuit.
- (4) Reactions between metallic lithium and flammable electrolyte solvents are exothermic, probably raising the risk of catastrophic overheating (or thermal runaway), especially when contact surface has been increased.

The above four issues are scientifically strongly coupled, easily triggering undesirable and uncontrolled domino effects once one of the issues is initiated. Such a strongly-coupled feature further increases the global complexity of lithium metal anodes.

To circumvent the formidable challenges of lithium metal anodes, nonmetallic anode materials, such as intercalation-type graphite or other carbon,^[250–253] and alloy-type silicon,^[254,255] tin,^[256,257] or germanium,^[258] have also been demonstrated in Li–S batteries. Inevitably, owing to their relatively low capacities to lithium metal, the specific energies have to be compromised. Such a sacrifice must be offset in other performance such as cycling stability and safety; otherwise, nonmetallic anodes will hold little competitiveness with respect to lithium metal anode.

Compared to the cathode, the research on anode for high-loading Li–S batteries are very little. However, the anode, especially the lithium metal, is gradually becoming the bottleneck for developing practical Li–S batteries, which ought to attract more tremendous attention to impulse the whole devices. In this section, analogous to that of the cathode, we also present an overview in hierarchy of design principles and approaches toward high-loading and high-current-density anodes. Two basic hierarchies are briefly established according to the materials: 1) lithium metal anode and 2) nonmetallic anode.

3.1. Lithium Metal Anode

In a high-loading Li–S batteries, the increase in areal sulfur loading synchronously raises the actual areal current density that pass through the planar lithium metal foils or disks. This is the main confliction between the cathode and the lithium anode. For instance, at a moderate rate of $C/2$ based on the weight of sulfur, the areal current density will be increased from 0.84 to 8.4 mA cm⁻² if the sulfur loading is multiplied from 1.0 to 10 mg cm⁻². Adversely, if the areal current density has to be lower than 1 mA cm⁻², at which it is much easier to stabilize the lithium metal anode, the discharging/charging time for the whole device will be raised to as long as tens of hours, which is unacceptable for practical applications such as electric vehicles.

Some initiative works have revealed the exceptional role of lithium metal anode in stabilizing high-loading Li–S batteries, extending their service life, and determining the cell

failure. Xiao's group indicated that bulk lithium became porous and SEI grew inward the fresh lithium, resulting in sharply increased cell resistances due to the accumulation of insulating SEI (Figure 13a),^[135] which was in accordance with the failure mechanism of fast-charged LMBs (Figure 13b).^[259] In high-loading Li–S batteries, corrosive polysulfides and high areal current density inevitably exaggerated the formation of thick, mossy, and insulating interphase. Qie et al. suggested that even though a Li₂S₆/CNF cathode with an ultrahigh sulfur loading of 18.1 mg cm⁻² can stably cycled at 6.0 mA cm⁻² for more than 75 cycles, the cell suffered from sudden death subsequently.^[260] The cycled cathode and separator became dry while about a half of the pristine lithium anode was etched away concomitantly (Figure 13c). They believed that the serious lithium metal corrosion and electrolyte decomposition and depletion were likely responsible for the failure of the cell with an ultrahigh sulfur loading. And our group also observed the early failure of Li–S batteries at a pouch-cell level, which was attributed to the pulverization and deactivation of anode by forming “dead” lithium (Figure 13d).^[261] We also validated that injecting fresh electrolyte in the failed cell can recover the capacity and lengthen the cycling life to some extent.

These issues correlated to lithium metal anode and exaggerated by the high loading of active materials can broadly classified into two categories: 1) intrinsic kinetics issues of lithium plating/stripping and 2) exotic issues brought by the unique Li–S redox chemistry, specifically the migration of polysulfides to lithium metal anodes and their rampant reactions. Therefore, strategies that potentially improve the lithium metal anodes for high-loading Li–S batteries can be divided into 1) 3D lithium hosts and 2) SEI stabilization. Since anode studies for high-loading Li–S batteries are still at the innocent stage, some concepts for general lithium metal anodes are referenced and discussed with a criterion that areal current density of at least 2 mA cm⁻² has been demonstrated.

3.1.1. 3D Lithium Hosts

One of the fundamental understanding related to the kinetics of anode interfaces can be explained by a widely accepted empirical diffusion model to correlate the “Sand's time τ ” with the transport nature of Li⁺ ions and electrons:^[262]

$$\text{Sand's time } \tau = \pi D \left(\frac{eC_0(\mu_a + \mu_{Li^+})}{2J\mu_a} \right)^2$$

where τ is the time when the growth of lithium dendrites is initiated, D is the diffusion coefficient, e is the elementary charge, C_0 is the initial concentration of Li⁺, μ_a and μ_{Li^+} are the anionic and Li⁺ mobilities, respectively, J is the absolute current density. It can be therefore easily deduced that Sand's time τ is inversely proportional to the absolute current density J , which is further reciprocally correlated to the specific surface area (SSA) of the electrode. Bieker's group has developed several approaches to increase the SSA of lithium metal anodes by adopting either organic-coated lithium powders^[263] or microneedle patterned lithium foils.^[264] Yet the current densities were mainly limited

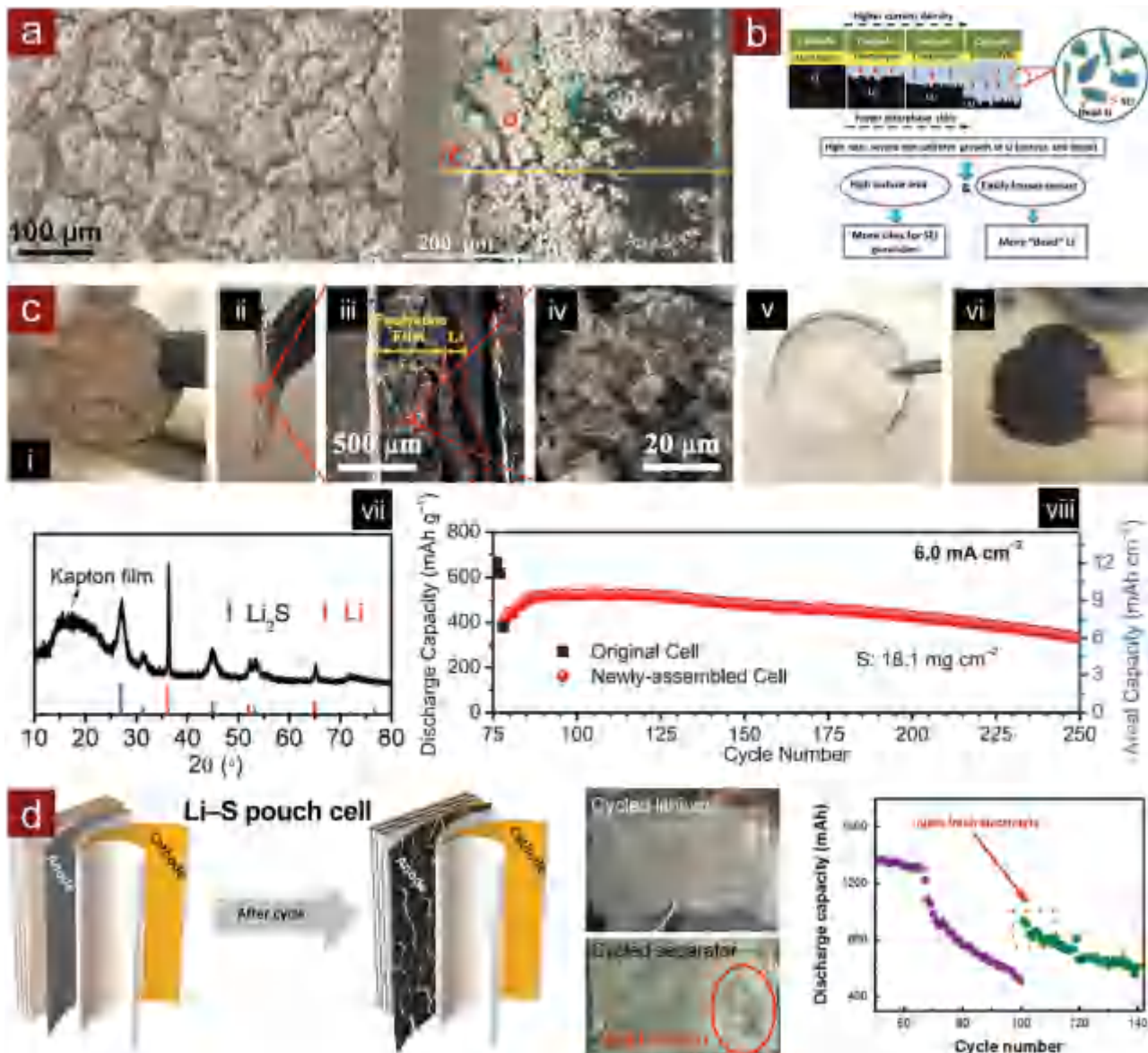


Figure 13. Failure of lithium anode in high-loading Li-S batteries. a) SEM images of lithium anode after 100 cycles combining with thick sulfur cathode. Reproduced with permission.^[135] Copyright 2015, Wiley-VCH. b) Schematic of the failure mechanism of fast-charged LMBs through inward growth of insulating interphases. Reproduced with permission.^[259] Copyright 2015, Wiley-VCH. c) Analysis of the dead ultrahigh-sulfur-loading cells: cycled i–iv) lithium metal anode, v) separator and vi) cathode; vii) X-ray diffraction pattern of cycled lithium metal anode; viii) cycling performances of newly assembled cell using the cycled cathode coupled with fresh lithium metal anode. Reproduced with permission.^[260] Copyright 2016, Wiley-VCH. d) Schematic of evolution of lithium metal anode during cycling, photographs of cycled lithium metal anode and separator, cycling performance after re-injecting electrolyte into a Li-S pouch cell. Reproduced with permission.^[261] Copyright 2017, Elsevier.

lower than 1 mA cm^{-2} . More importantly, owing to the “host-less” feature of lithium metal during plating/stripping, a specifically designed and mechanically robust host is still preferable to reduce the absolute current density and guide the deposition of lithium.

Since copper (Cu) foils are widely employed current collectors for anodes of LIBs and LMBs, nano-/microstructured Cu-based current collector emerges as one of the most studied 3D lithium hosts. Yang et al. synthesized a submicron Cu skeleton through in situ dehydration and reduction of $\text{Cu}(\text{OH})_2$ fibers grown on a Cu foil, allowing lithium metal to be

deposited and accommodated within the 3D skeleton without dendrite formation even at a current density of 5 mA cm^{-2} (Figure 14a).^[265] They also determined an indicator, lithium accommodation (that only deposited inside the 3D structure) percentage, and correlated it to the electroactive area (that contacted with the electrolyte) ratio with respect to the geometrical area of the electrode, highlighting the role of SSA of 3D lithium hosts. Other 3D porous Cu-based current collectors can be obtained by chemically leaching Zn out of commercial Cu–Zn alloy^[266] or assembling Cu nanowires into free-standing networks.^[267]

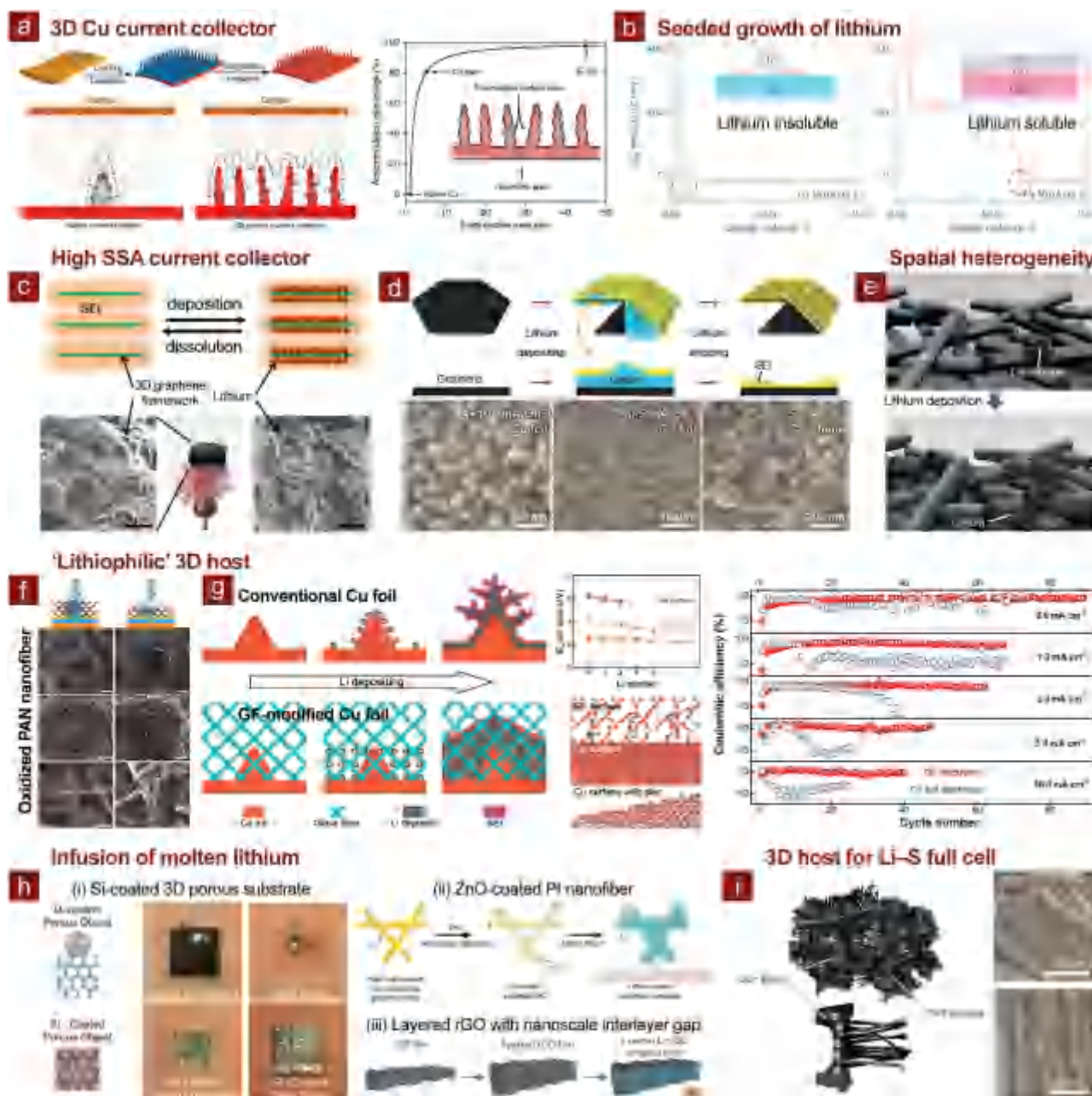


Figure 14. 3D hosts for high-current-density lithium metal anodes. a) Schematic presentation of the procedures to prepare a 3D porous Cu foil from a planar Cu foil, illustration of the electrochemical deposition processes of lithium metal on (left) planar current collector and (right) 3D current collector, and lithium accommodation percentage as a function of electroactive area ratio. Reproduced with permission.^[265] Copyright 2015, Nature Publishing Group. b) Voltage profiles of galvanostatic Li deposition on (left) lithium-insoluble (e.g., Cu) and (right) lithium-soluble (e.g., Au) substrate at $10 \mu\text{A cm}^{-2}$, as well as corresponding schematics for nucleation of lithium on different substrates. Reproduced with permission.^[268] Copyright 2016, Nature Publishing Group. c) Schematics of lithium deposition/dissolution within a SEI-protected 3D porous graphene framework, SEM images of pristine graphene and lithium-coated graphene, and photograph of free-standing graphene framework. Reproduced with permission.^[269] Copyright 2015, American Chemical Society. d) Schematics of Li depositing/stripping process on unstacked graphene, and SEM images of lithium deposits on Cu foils and graphene at different current densities. Reproduced with permission.^[270] Copyright 2016, Wiley-VCH. e) Schematic illustrating the structures of spatially heterogeneous SiO_2/SiC -decorated 3D CF current collector, and the lithium deposition processes on it. Reproduced with permission.^[271] Copyright 2012, Elsevier. f) Top-view SEM images (left) of lithium deposition on Cu-oxidized PAN electrode and (right) of the internal structure of lithium deposition. Reproduced with permission.^[272] Copyright 2015, American Chemical Society. g) Left: schematics of conventional Cu foil and glassy fiber (GF)-modified Cu foil; Middle: theoretical calculation results showing binding energies of lithium atoms to different surfaces and corresponding configurations; Right: comparison of the Coulombic efficiency of lithium plating/stripping on pristine Cu foil and GF-modified Cu foil at different current densities with a lithiation capacity of 0.5 mA h cm^{-2} . Reproduced with permission.^[273] Copyright 2016, Wiley-VCH. h) Infusing molten lithium into 3D “lithiophilic” scaffolds including i) Si-coated 3D porous scaffolds, reproduced with permission.^[274] Copyright 2016, National Academy of Sciences, ii) ZnO-coated PI nanofiber, reproduced with permission.^[275] Copyright 2016, Nature Publishing Group, and iii) layered rGO

Though Cu-based current collectors have been intensively investigated, Yan et al. indicated that metals with the negligible solubility of lithium (e.g., Cu) were incapable of reducing the grain size of lithium nuclei and improving their densities due to high nucleation barriers, inevitably leading to the growth of large lithium dendrites (Figure 14b).^[268] Exploiting alternative current collector materials beyond 3D porous Cu is thereby very promising for dendrite-free deposition of lithium metal, which kinetically addresses the issue of unstable and constantly changed interphases induced by uncontrolled growth of lithium dendrites. There are two main approaches. One is to employ a 3D porous scaffolds with exceptionally higher SSA than that of 3D porous Cu (normally $<1 \text{ m}^2 \text{ g}^{-1}$), resulting in drastically decreased absolute current densities. For example, our group designed a 3D porous graphene scaffold (with SSA of $\approx 500 \text{ m}^2 \text{ g}^{-1}$) protected by a robust SEI layer derived from the reaction between lithium metal and polysulfide-containing electrolyte (Figure 14c).^[269] Such an SEI-coated graphene framework rendered high Coulombic efficiencies of 97 and 93% at 0.5 and 2.0 mA cm^{-2} with no dendrite formation, exhibiting remarkable enhancement compared to planar Cu current collectors. We further adopted a unique unstacked graphene framework with much higher SSA of $1666 \text{ m}^2 \text{ g}^{-1}$ as 3D lithium hosts to realize ultralow absolute current densities, which were drastically decreased from 0.5 mA cm^{-2} on planar current collectors to $\approx 4 \times 10^{-5} \text{ mA cm}^{-2}$ on the graphene (Figure 14d).^[270] Even at a high current density of 2.0 mA cm^{-2} , the Coulombic efficiency remained above 90% with dendrite-free lithium deposition; while that on a Cu foil was basically below 50%, which was attributed to the rampant dendritic growth of lithium under the high absolute current density.

The other one is to engineer a functionalized surface of 3D lithium hosts with desirable capabilities to spatially control the distribution of Li^+ ions and lithium deposition. Ji et al. firstly demonstrated such a fundamentally novel approach by synthesizing spatially heterogeneous SiO_2/SiC -decorated 3D CF current collectors with dendrite-free lithium deposition at high current density of 4.0 mA cm^{-2} (Figure 14e).^[271] Liang et al. designed a 3D oxidized PAN nanofiber network, with polar surface functional groups to guide Li^+ ions, as lithium hosts, demonstrating stable cycling of lithium metal anodes with a dendrite-free morphology and an average Coulombic efficiency of 97.4% over 120 cycles at 3.0 mA cm^{-2} (Figure 14f).^[272] With the insights from theoretical calculations and numerical modeling, our group indicated the enhanced adsorption of Li^+ and electrolyte wetting on SiO_2 (110) surface (to model the majority of glass) compared to on Cu (111)/(221) surfaces, as well as uniform distribution of Li^+ within 3D polar scaffolds.^[273] Based on the understanding, we employed 3D glass fiber cloths with abundant polar functional groups (e.g., Si–O, O–H, O–B, etc.) and an ordered macroscopic textile as insulating lithium hosts, within which the bottom-up growth of lithium was confined without observable formation of dendrites (Figure 14g). Under the current densities of 0.5, 1.0, 2.0, 5.0, and 10.0 mA cm^{-2} , high Coulombic efficiencies of 98, 97, 96, 93, and 91% were

attained, respectively. The stable cycling of modified cells, especially at extremely high current densities of 5.0 and 10.0 mA cm^{-2} , was attributed to the homogenous plating/stripping of lithium, kinetically driven by uniform distribution of Li^+ ions and local currents.

In the works discussed above, lithium was mainly electrochemically deposited within the 3D porous current collectors, demanding for extrinsic lithium sources that cannot be provided by the most conventional Li–S cell configuration with an elemental sulfur cathode. Therefore, effective strategies must be developed to initially accommodate lithium in the 3D hosts. Cu's groups pioneered the method by infusing molten lithium into 3D "lithiophilic" scaffolds (Figure 14h). They firstly demonstrated a "lithiophilic" coating of CVD silicon on various 3D porous substrates, such as carbon frameworks and metal foams, to enable uniform lithium melt-infusion under capillary forces.^[274] As-obtained lithium/silicon-coated CF anodes demonstrated a small lithium plating/stripping overpotential ($<90 \text{ mV}$) at 3.0 mA cm^{-2} over 80 cycles. Such a strategy was further rationalized and extended to a thermostable polyimide (PI)/ALD-coated "lithiophilic" ZnO core/shell nanofiber matrix for accommodating lithium with exceptional cycling stability (plating/stripping overpotential of ≈ 70 and 110 mV at 3.0 and 5.0 mA cm^{-2} over 100 cycles).^[275] Lin and Liu et al. explored the "lithiophilic" capillary effect at the nanoscale by engineering a layered rGO host with nanosized interlayer gaps to soak and confine molten lithium.^[276] The flexible lithium/rGO anodes sustained low plating/stripping overpotential of ≈ 80 at 3.0 mA cm^{-2} over 100 cycles and were paired with LiCoO_2 or $\text{Li}_4\text{Ti}_5\text{O}_{12}$ electrodes as full cell demonstrations with remarkable electrochemical performance.

Most of conceptual advancements were mainly accomplished on lithium metal anode half cells or full cells with LIB counter electrodes. Li–S batteries with lithium anodes applying 3D hosts have still been rarely demonstrated. Our group demonstrated a 3D fibrous boron matrix as an inert host for lithium metal anodes, which was derived from irreversible electrochemical dealloying of Li–B alloy.^[277] Even at 10.0 mA cm^{-2} , no lithium dendrite formation was observed, enabling 2000-cycle long lifespan of Li–S batteries adopting Li–B anodes with Coulombic efficiency higher than 90%. Zhang et al. also revealed the enhancement of Li–S batteries with a sulfur loading of 4.25 mg cm^{-2} by replacing lithium metal with Li–B alloy.^[278] Very recently, Jin and Xin et al. fabricated a covalently connected carbon nanostructure of CNTs grown on ultrathin graphite foam (CNT-UGF), which served as current collectors for both sulfur cathodes and lithium anodes (Figure 14i).^[279] The Li–S full cell, employing sulfur/CNT-UGF cathode (47 wt% sulfur content in the whole cathode and 2.6 mg cm^{-2} sulfur loading) and lithium/CNT-UGF cathode (20 wt% lithium content in the whole anode), delivered high capacity of 860 mAh g^{-1} at 12 C (52 mA cm^{-2}) and were cycled at 2.0 C (8.7 mA cm^{-2}) for 400 cycles with cyclic capacity decay rate of 0.057%.

Subsection Summary (3.1.1.): Though the application of 3D lithium hosts in Li–S batteries is still at an early stage, the

with nanoscale interlayer gap. Reproduced with permission.^[276] Copyright 2016, Nature Publishing Group. i) Schematic of the 3D interconnected network of the CNT-UGF hybrid and SEM images of a lithium/CNT-UGF anode after 800-h plating/stripping. Reproduced with permission.^[279] Copyright 2016, Wiley-VCH.

progress on nanostructured lithium metal anodes with desirable capabilities of being stably cycled at current densities of up to 10 mA cm^{-2} , as well as few very initial proof-of-concepts of Li-S batteries utilizing 3D lithium hosts, undoubtedly encourage the research into the lithium anode and will facilitate the addressment of its issues.

3.1.2. SEI Stabilization

Since 1979 when Peled first named the electrically insulating and ionically conducting surface film, which is naturally formed between lithium metal and electrolytes during the initial electrochemical process, as the SEI,^[280] the significant role of SEI in lithium plating/stripping and the formation of lithium dendrites has been revealed in tremendous studies. Though the formation mechanism of SEI still remains exclusive, several desirable attributes for an ideal SEI have been summarized, including 1) high Li^+ ionic conductivity, 2) proper thickness, 3) compact structure, 4) high mechanical strength, and 5) good chemical stability. Since there are already many high-quality review papers on the SEI for lithium metal anodes,^[249,281] this section will focus on strategies developed specifically to stabilize SEI for Li-S batteries for conciseness. As necessary complements, some predominant efforts on universal lithium metal anodes will also be introduced.

In Li-S batteries, one of the biggest differences in the formation, composition, and structure of SEI on lithium anodes from those in general LMBs is the presence of mobile polysulfides. According to conventional understanding, polysulfides are regarded basically detrimental to the anode as they shuttle to the lithium anode and are reduced by lithium metal, forming an insulating $\text{Li}_2\text{S}/\text{Li}_2\text{S}_2$ film on lithium and passivating the anode interphases. In 2009, Aurbach et al. first introduced lithium nitrate (LiNO_3) as the co-salt in ether-based electrolyte, which can be reduced or oxidize polysulfides to form protective $\text{Li}_x\text{SO}_y/\text{Li}_x\text{NO}_y$ species and remit shuttle effect (Figure 15a).^[282] Zhang indicated that cutoff voltage of discharge must be higher than 1.6 V to prevent the irreversible consumption of LiNO_3 at the cathode side.^[283] Xiong et al. further disclosed the positive role of polysulfides in forming insulating $\text{Li}_2\text{S}/\text{Li}_2\text{S}_2$ layer beneath the $\text{Li}_x\text{SO}_y/\text{Li}_x\text{NO}_y$ surface film to prevent the successive decomposition of electrolyte (Figure 15b).^[284,285] On lithium dendrite formation Li et al. demonstrated that polysulfides and LiNO_3 synergistically provided efficient suppression (Figure 15c).^[286] Through the competition between etching by polysulfides and passivating by LiNO_3 , the growth of lithium dendrites was smoothed and a stable and uniform SEI was formed, leading to a Coulombic efficiency of $>99.0\%$ at 2 mA cm^{-2} for over 300 cycles (demonstrated in Li | stainless steel cells). Our group also systematically investigated the effects of species (from Li_2S to Li_2S_8 with concentration fixed as 0.1 M [S])^[287] and concentration (from 0.005 to 0.2 M [S] in the form of Li_2S_3)^[288] of polysulfides on the lithium metal anode cycled in polysulfide/LiTFSI/ LiNO_3 ternary-salt ether-based electrolyte. We found that both species and concentration impacted significantly on the composition and structure of SEI, thereby rendering drastically different cyclabilities of lithium metal anodes (Figure 15d). One of the optimal formula

was screened as 0.1 M [S] in Li_2S_5 - 1.0 M LiTFSI - 5 wt\% LiNO_3 dissolved in DOL/DME (v/v = 1:1), resulting in LiF-rich SEI layer and a Coulombic efficiency higher than 95% for over 200 cycles.^[288] The SEI induced in this electrolyte rendered dendrite-free Li metal deposits in a working cell. More interestingly, such a robust SEI can be electroplated on lithium anode firstly and then served as an electrochemically derived, 'implantable' SEI for being applied in either Li | $\text{LiNi}_{0.5}\text{Co}_{0.2}\text{Mn}_{0.3}\text{O}_2$ with an ester electrolyte or Li | S full cells with a LiNO_3 -free ether electrolyte, both of which exhibited significantly promoted cycling stability and shelf life (Figure 15e).^[289] Though new insights into the role of LiNO_3 , not strictly in the anode interphase, have emerged very recently,^[290] the synergistic effect of polysulfides and LiNO_3 on stabilizing SEI and inhibiting lithium dendrites existed, at least within a narrow range of polysulfide concentration and equilibrium. Such a narrow range is ascribed to not only the competitive reactions between lithium metal and LiNO_3 /polysulfides, but also the gassing reactions. Jozwiuk and co-workers developed two operando techniques to monitor the gas evolution in Li-S batteries due to the reactions between lithium metal and ether solvents.^[291] They confirmed that LiNO_3 effectively suppressed these undesirable side reactions, while, unfortunately, the gassing was not completely eliminated (Figure 15f). Their results possibly explain why the electrolyte depletion is so easily occurred and suggest that additives beyond LiNO_3 are in urgent demand. Actually, tuning the solvent species could be an alternative approach to suppress the undesirable gas evolution. According to combinatorial experiments and computational simulations, our group suggested that DOL was more likely to be the main origin accounting for gas evolution than DME. Reducing the volume percentage of DOL in the electrolyte thus benefited the cycling stability of Li-S pouch cells.^[292]

Because the synergistic stabilization of SEI by polysulfides/ LiNO_3 strongly depends on the conditions of depletive reactions between them and lithium metal, it is very challenging to control the stabilizing effect, and the depletion of electrolyte components (e.g., LiNO_3) will therefore inevitably lead to the failure of Li-S batteries, especially when they are operated at high current densities and with contact interfaces between lithium and electrolyte increased synchronously. Alternative strategies for SEI stabilization are consequently in urgent demands. Enlightened by recent progress in general lithium metal anodes, such as inorganic additives (e.g., Cs^+ ,^[293] LiF ,^[294] etc.), anion modulation (e.g., bis(fluorosulfonyl)imide (FSI),^[295] trifluoromethyl-4,5-dicyanoimidazole (TDI),^[296] (trifluorosulfonyl)(n-nonafluorobutanesulfonyl)imide,^[297] oxalyldifluoroborate (ODFB),^[298] etc.), solvent engineering (e.g., fluoroethylene carbonate (FEC),^[299] etc.), high-concentrated electrolytes,^[300] and room-temperature ionic liquids (RTILs),^[301] rationally tuning the electrolyte formula became one of the most popular strategies. For example, Zhang and Xu's group proposed a self-healing electrostatic shield mechanism, which can fundamentally alter dendrite formation and thus stabilize SEI, through the addition of non-lithium cations, such as Cs^+ , that have a reduction potential lower than Li^+ (Figure 16a).^[293] Lu and Tu et al. demonstrated stable lithium electrodeposition in both liquid and nanoporous solid electrolytes, which were reinforced by halogenated salts (Figure 16b).^[294] Few attempts have realized superior durability to high current

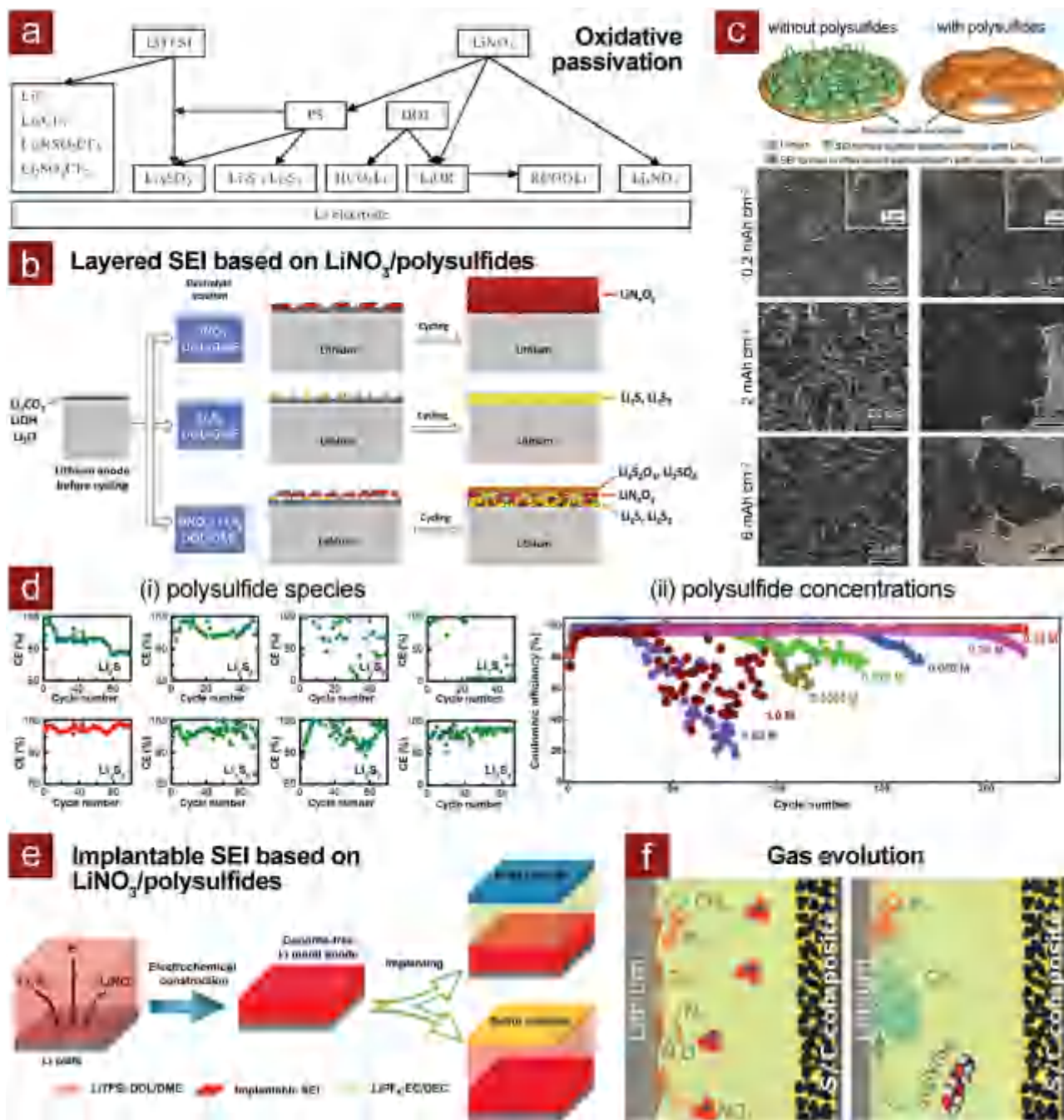


Figure 15. Role of LiNO_3 and its synergy with polysulfides. a) Schematic presentation of an early model that describes the surface chemistry of lithium electrodes with the presence of LiNO_3 in the electrolyte. Reproduced with permission.^[282] Copyright 2009, Electrochemical Society. b) Illustration of the surface film on lithium anode cycling in different electrolyte solutions. Reproduced with permission.^[285] Copyright 2014, Elsevier. c) Schematic and SEM images showing the morphology difference of lithium deposition in the two electrolytes (both contain LiNO_3), but either (left) without polysulfide, or (right) containing lithium polysulfide. Reproduced with permission.^[286] Copyright 2015, Nature Publishing Group. d) The Coulombic efficiency of lithium anodes cycled in polysulfide/ $\text{LiTFSI}/\text{LiNO}_3$ ternary-salt ether-based electrolyte, in terms of polysulfide (i) species^[287] and (ii) concentrations.^[288] Reproduced with permission.^[287,288] Copyright 2016, Elsevier. e) Schematic of the implantable SEI based on the synergy between LiNO_3 and polysulfides. Reproduced with permission.^[289] Copyright 2017, Cell Press. f) Schematic overview of the reactions producing gases in Li-S batteries with the diglyme-based electrolyte with (left) and without LiNO_3 (right). Reproduced with permission.^[291] Copyright 2016, Royal Society of Chemistry.

density of up to 10 mA cm^{-2} . Qian et al. reported highly-concentrated electrolyte composed of 4.0 M LiFSI-DME , enabling high-rate and stable lithium deposition.^[302] For Li | Li symmetric cell, a 6000-cycle shelf life at 10 mA cm^{-2} was achieved. For Li | Cu

asymmetric cell, remarkable Coulombic efficiencies of 99.1 and 98.4% were attained at 1.0 and 4.0 mA cm^{-2} , respectively.

Some specific electrolyte recipes were directly implemented in Li-S batteries. For example, Suo et al. proposed a new class

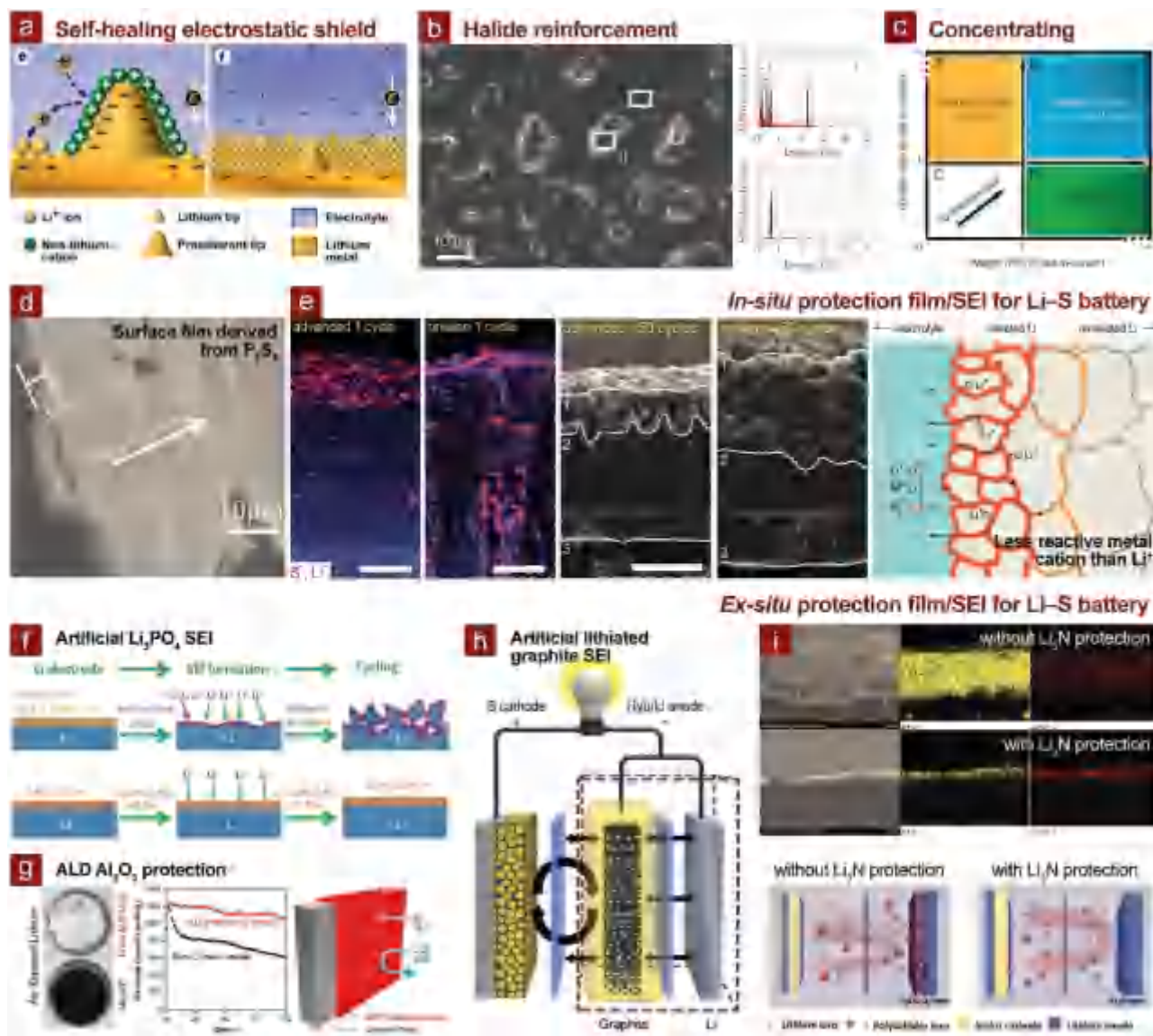


Figure 16. SEI stabilization apart from LiNO_3 /polysulfides synergy. a) Cs^+ additive based on the self-healing electrostatic shield mechanism. Reproduced with permission.^[293] Copyright 2013, American Chemical Society. b) SEM images of halide salt (LiF) clusters on lithium foil and energy dispersive X-ray spectrum of region I and II, respectively. Reproduced with permission.^[294] Copyright 2014, Nature Publishing Group. c) The distribution map of non-aqueous liquid electrolytes with the weight and volume ratios of salt-to-solvent to identify the highly concentrated “Solvent-in-Salt” electrolyte. Reproduced with permission.^[303] Copyright 2013, Nature Publishing Group. d) Cross-sectional SEM image of the passivation layer peeled off from the lithium anode cycled with P_2S_5 in the electrolyte. Reproduced with permission.^[314] Copyright 2013, Wiley-VCH. e) TOF-SIMS cross-sectional chemical mapping (after the 1st cycle) and cross-sectional SEM images (after 150 cycles) of the lithium anodes with (advanced) or without (pristine) the $\text{Cu}(\text{Ac})_2$ additive, and schematic of Li^+ extraction and redeposition pathways during cycling. Reproduced with permission.^[317] Copyright 2016, Wiley-VCH. f) Schematics for general lithium metal and Li_3PO_4 -modified lithium metal anodes. Reproduced with permission.^[319] Copyright 2016, Wiley-VCH. g) Photograph of bare (black) and 14 nm ALD Al_2O_3 -protected lithium metal foils (white) after 20 h exposure to atmosphere, cycling performance of Li-S batteries employing the two lithium anodes, and schematic of ALD Al_2O_3 -protected lithium metal anodes. Reproduced with permission.^[321] Copyright 2015, American Chemical Society. h) Schematic of the hybrid anode design adopting lithiated graphite as an artificial SEI layer. Reproduced with permission.^[322] Copyright 2014, Nature Publishing Group. i) The cross-sectional morphologies and elemental mapping of a lithium metal electrode with or without a Li_3N layer after 100 cycles, and schematic of the design of Li-S batteries with or without anode protection. Reproduced with permission.^[323] Copyright 2014, Royal Society of Chemistry.

of “Solvent-in-Salt” electrolyte, exemplified as LiTFSI –DOL/DME ($v/v = 1:1$) systems with the concentration of LiTFSI varying from 1.0 to 7.0 M, exhibiting exceptional capability of suppressing lithium dendrite growth, which was ascribed to the nature of SEI with reduced thickness (Figure 16c).^[303] Zheng

et al. employed a common RTIL of *N*-methyl-*N*-butylpyrrolidinium (Py_{14}) TFSI as a co-solvent to build more stable SEI on lithium anode, presumably through the pinning effect of stable Py_{14}^+ cations in the mixed reduction products of TFSI⁻ anion and solvents.^[304] Wu et al. studied mixed ether/RTIL

electrolyte^[305] and explored binary salts of LiTFSI and LiODFB for this RTIL-based electrolyte to form inorganic-rich SEI through the reduction of $F_2B[ox]^-$ anions.^[306] Fluorinated ethers, such as 1,1,2,2-tetrafluoro-3-(1,1,2,2-tetrafluoroethoxy)propane (D2),^[307] bis(2,2,2-trifluoroethyl) ether (BTFE)^[308] and 1,1,2,2-tetrafluoroethyl-2,2,3,3-tetrafluoropropyl ether (TTE),^[309,310] have been employed to either completely replace DME solvents or serve as co-solvents. Typically, fluorinated ether possessed lower polysulfide dissolubility, remitting the shuttle effect and self-discharge consequently. More importantly, in two separate studies conducted by Azimi et al.^[309] and Zu et al.,^[310] TTE was found to strengthen the SEI on lithium anode through decomposition into LiF-rich self-limiting layers to suppress the parasitic reactions between lithium metal and polysulfides.

Note that the complexity in the formation and evolution of SEI, as well as in the compositional and structural varieties of as-obtained SEI, may lead to contradictory for a certain electrolyte formula. Take LiFSI salt as a representative example. Gao's group employed a LiFSI–LiTFSI binary-salt electrolyte for Li–S batteries with optimized Li^+ ionic conductivity, viscosity, and lithium protection gained from 1.0 M LiFSI/0.5 M LiTFSI–DOL/DME (v/v = 1: 1) electrolyte.^[311] Kim et al. suggested that at elevated temperature of 60 °C and high concentration of 5.0 M LiFSI dissolved in DME, DME reacted with the oxidized FSI(–F) radical, favoring the formation of Li^+ -permeable protective layers on both cathode and anode.^[312] However, in a study where 3.0 M LiFSI or LiTFSI monosalt was employed in DOL/DME (v/v = 1: 1) solvents, Cao et al. indicated that the anion activity played a key role in tuning the composition and stability of SEI on lithium anode and LiTFSI was more stable than LiFSI.^[313] Therefore, in future studies the discussion on the effects of a certain electrolyte formula or an additive should be cautious with other parameters, such as the concentration, solvents, co-salts, temperature, and conditional process for SEI formation, being deliberately considered.

Owing to the compatibility issue, not all the developed electrolyte systems, which have been proved to be effective for general lithium metal anodes, are able to work well in Li–S batteries. Some unique agents have been explored specifically for Li–S batteries. For instance, Liang's group pioneered the implementation of phosphorous pentasulfide (P_2S_5) in Li–S batteries (Figure 16d).^[314] P_2S_5 not only solubilized insoluble Li_2S into highly soluble complexes to recover capacity loss, but also facilitated the formation of a dense protecting film on lithium anode in a polysulfide-rich environment, which was mainly composed of lithium superionic Li_3PS_4 .^[315] Zu and Manthiram first exploited the role of copper acetate ($Cu(Ac)_2$) additives in stabilizing electrolyte/lithium interfaces through forming a surface passivation layer consisting of a sulfide matrix and decomposition products of the electrolyte.^[316] Subsequently, with the assistance of theoretical calculations and combinatorial characterization tools, Manthiram and co-workers further proposed a more universal mechanism that electrolyte additives containing metal ions having lower reactivity with sulfur than lithium (e.g., Cu, Ag, Au) were capable of inhibiting the long-range crystallinity of the redeposited impurity phases, increasing the grain boundaries, generating amorphous sulfur-rich Li_xS ($x < 2$) structures with higher Li^+ conductivity, and

preventing the lithium from being continuously reacted with the electrolyte (Figure 16e).^[317] As a result, Li–S batteries with a sulfur loading of 5 mg cm^{-2} possessed substantially enhanced capacity and stability.

Beyond in situ stabilization of SEI through electrolyte engineering, coating an exotic protecting layer or an “artificial” SEI on the lithium metal anode emerges as another effective approach. For example, Zheng et al. coated a monolayer of interconnected amorphous hollow carbon nanospheres on the lithium metal anode to isolate the lithium deposition from SEI formation so that the repeated plating/stripping of lithium metal hardly impacted on the SEI morphologies.^[318] Li et al. designed an artificial Li_3PO_4 SEI through the in situ reaction between polyphosphoric acid (PPA) with lithium metal and its native film (mainly Li_2CO_3 , LiOH, and Li_2O) (Figure 16f).^[319] The PPA-derived Li_3PO_4 SEI was more smooth and uniform than the H_3PO_4 -derived counterpart and the native film. Owing to the superior Young's modulus (≈ 10 –11 GPa) and chemical resistance of Li_3PO_4 , such an artificial SEI restrained the unfavorable interfacial side reactions and the dendritic growth of lithium. These works, demonstrated on general lithium metal anodes, indicated the significance of both the selection of suitable materials and fabrication methods for constructing robust SEI layers on lithium anodes.

The concept of artificial SEI has been successfully implemented in high-loading Li–S batteries, typically gaining much enhanced cyclability and Coulombic efficiency. Inert materials such as Al_2O_3 , which are much less reactive with polysulfides than the lithium, have firstly appeared in the scope of screening. Jing et al. fabricated a porous Al_2O_3 layer to protect the lithium anode by spin-coating the mixed Al_2O_3 nanoparticles/binder slurry on lithium foils.^[320] The porous Al_2O_3 layer helped to maintain the smooth surface of lithium metal, but the sulfur loading was relatively low (≈ 1.1 –1.6 mg cm^{-2}). Kozen and co-workers employed ALD to attach a 14-nm-thick Al_2O_3 layer on the lithium metal anode (Figure 16g).^[321] The ALD Al_2O_3 layer was highly efficient in suppressing lithium corrosion due to atmosphere, sulfur, and electrolyte exposure. With an optimized 14-nm-thick Al_2O_3 layer on the anode, high-loading Li–S batteries (5 mg cm^{-2} sulfur) maintained a capacity of >1000 mA h g^{-1} for 100 cycles at 0.31 mA cm^{-2} , which was $\approx 80\%$ higher than those employing bare lithium metal anodes. Li^+ ionic conducting materials are another class of coating materials for lithium metal anodes as they facilitate the ion transportation across the SEI and lower the inner impedance. For instance, Liu and co-workers designed a novel hybrid anode architecture, in which lithiated graphite was placed on metallic lithium, acting as an artificial, self-regulated SEI to manipulate the surface reactions (Figure 16h).^[322] With the protection of such a lithiated graphite layer, the side reactions between lithium metal and polysulfides were considerably suppressed. Wen's group fabricated several protected lithium anodes for highly stable Li–S batteries.^[323,324] Polycrystalline lithium nitrides (Li_3N), with exceptionally high Li^+ conductivity of $\approx 10^{-3}$ S cm^{-1} , were selected to construct a protective layer on lithium anode through the facile reaction between lithium and N_2 gas at room temperature (Figure 16i).^[323] The thickness of resistive Li_2S/Li_2S_2 layer on the lithium anode was substantially reduced from ≈ 100 to ≈ 10 μm by coating a Li_3N layer

on the anode and preventing the corrosive reactions between polysulfides and lithium metal. As a result, at sulfur loadings of 2.5–3 mg cm⁻², Li–S batteries with Li₃N-protected lithium anodes exhibited >100% promotion on the capacity retention at C/5. A Li⁺-conducting PEDOT-co-PEG polymer layer was found to hold analogous function of protecting lithium anode from polysulfide corrosion.^[324]

Subsection Summary (3.1.2.): The nature of SEI is very complicated, while its complexity is further increased due to the spontaneous reactions between polysulfides and lithium metal. Therefore, directly implementing strategies that have been proved from existing studies in general lithium metal anodes might encounter the compatibility issue. Advanced characterization and simulation methods must be adopted to prompt the understanding toward the composition and structure of SEI, as well as its formation and evolution, especially at high current densities and with the presence of corrosive polysulfides. In addition, advanced fabrication methods such as ALD will undoubtedly play a vital role in controlling the morphology, thickness, and adhesion of SEI on lithium anodes, because all these physicochemical properties impact dominantly on the performance.

Section Summary (3.1.): The 3D lithium host and the SEI stabilization are complementary counterparts for enhancing the efficiency and lifespan of the lithium metal anodes. Several efforts have demonstrated high Coulombic efficiency of >90% at an exceptionally high current density of 10 mA cm⁻². However, such a remarkable performance is still insufficient to touch a roughly estimated target, namely an average Coulombic efficiency of >99.93% for more than 1000 cycles, which allows the use of less than 100% excessive lithium. There are still formidable challenges to propel the development of practical LMBs. When focusing on Li–S batteries, things are getting more complicated. But it is hard to say whether it is worse or better because of the duality polysulfides embody on lithium metal anodes. It has to also be pointed out that most of the existing strategies developed for high-efficiency lithium metal anodes are mainly demonstrated on Li | Li symmetrical cells or Li | Cu half cells rather than a Li–S reference cell. When simply implementing them in Li–S systems, as we indicated in (3.1.2), these strategies might not be as applicable as in general LMBs. The effect of polysulfides must be weighed. Li | Li symmetrical cells or Li | Cu asymmetric half cells can serve as primary prototypes to screen out effective strategies, which then deserve further demonstration in Li–S batteries. Since the lithium metal anode is gradually becoming the bottleneck, it appeals for more attention and efforts.

3.2. Nonmetallic Anode

One of the primary purposes of replacing lithium metal anodes by nonmetallic anode materials is to enhance the safety of Li–S batteries. In 2010, Hassoun and Scrosati first reported a polymer Li₂S/tin battery,^[256] and almost at the same time, Yang and McDowell et al. demonstrated a nanostructured Li₂S/silicon battery.^[254] Since then, various nonmetallic anode materials, which are common LIB anodes and broadly classified into the intercalation type (e.g., graphite, hard carbon,^[251] etc.)

and the alloying type (e.g., silicon,^[325] tin,^[257] germanium, etc.), have been explored for Li–S batteries. Nonmetallic anode materials were found to hold some obvious advantages beyond the lithium metal, including high intrinsic safety, lower reactivity with polysulfides, and less probability to grow lithium dendrites. In addition to these merits, nonmetallic anode materials are much more capable of being operated under high current densities than lithium metal as they have been successfully adopted in high-loading LIBs. Therefore, it is particularly interesting and straightforward to adopt nonmetallic anode materials in high-loading Li–S batteries.

On the basis of high-loading anode materials for LIBs, a few kinds of nonmetallic anode materials have been developed for high-loading Li–S batteries. For example, Hagen et al. employed electrochemically prelithiated silicon microwire arrays as the anode, which allowed the operation of full cells (sulfur loadings of 3.0–4.4 mg cm⁻²) in various electrolytes.^[255] Fu and co-workers reported a polysulfide/mesocarbon microbeads (MCMB) battery with a sulfur loading of 4.3 mg cm⁻² and employed a unique electrolyte of 3.0 M LiFSI/1.0 M LiTFSI dissolved in DME.^[253] Zhu and Qian's group reported an alloy-type anode composed of germanium nanoparticles with superior cycling stability for over 1000 cycles in the half cell and paired it with a B,N-codoped graphene supported sulfur cathode.^[258] With a sulfur loading of 4.7 mg cm⁻², the as-obtained sulfur/lithiated germanium full cell exhibited an initial capacity of 1043 mA h g_S⁻¹ at C/5 and extended the longevity to 500 cycles at 1.0 C. Similar to the cases in sulfur cathodes and lithium metal anodes, 3D porous current collectors also benefited the nonmetallic anode. 3D graphene networks were firstly synthesized by Yang and colleagues via a template (commercial sponge)-assisted approach and then served as supports for both the sulfur copolymer cathode (3D cpS-G) and the lithiated silicon anode (3D lithiated Si-G).^[326] The 3D cpS-G | 3D lithiated Si-G full cell, with a sulfur loading of ≈5 mg cm⁻² and a silicon loading of ≈3.9 mg cm⁻², delivered a stable capacity of 620 mA h g⁻¹ (based on the total weight of both the cathode and anode) for over 500 cycles.

Although nonmetallic anode materials are very promising for high-loading Li–S batteries, some fatal problems limited their electrochemical performance and practical reliability. Firstly, prelithiation of the anode or employment of Li₂S-based cathodes is required. Both of them will encounter some practical issues since there are merely effective nor industrial viable prelithiation methods at a large scale, and the use of moisture-sensitive Li₂S is quite challenging. Secondly, commonly employed ether-based electrolytes are incompatible with many existed nonmetallic anode materials. For instance, Lv et al. validated that commercial graphite anodes failed to be operated in 1.0 M LiTFSI–DOL/DME (v/v = 1: 1) electrolyte, the most common electrolyte for Li–S batteries, with comparable capacities to that in carbonate-based LIB electrolytes.^[252] Therefore, alternative electrolyte systems^[250] or ether-compatible nonmetallic anode materials will be very crucial. Thirdly, none of nonmetallic anode materials (at full lithiated state) hold a specific capacity as high as that of lithium metal and in addition, their lithiated potentials are normally higher. Therefore, these two factors inevitably result in the compromise in specific energies.

Section Summary (3.2.): The use of nonmetallic anodes to replace low-efficiency and low-security lithium anodes is a straightforward way to enhance the cycling stability and safety of Li–S batteries and other LMBs. There is always an inevitable balance between the specific energy and shelf life. The major flaw of nonmetallic anodes is their lower specific energy than that of lithium metal. However, considering the formidable challenges in dealing with the lithium metal, as well as the probably interminable research cycle, the alliance of sulfur-based cathodes (either sulfur or Li₂S) and high-capacity non-metallic anodes (e.g., silicon that is either lithiated or pristine) could be a compromised technical scheme that bridges the state-of-art LIBs and the “actual” Li–S batteries using lithium metal anodes. Yet such a compromised route still appeals for substantial efforts.

4. Separator

Separator is a key component in electrochemical energy storage devices and its unique functionalities are indispensable.^[327] For example, the primary function of separators in rechargeable batteries and supercapacitors is to separate the counter electrodes and prevent their short circuit; while in flow batteries and fuel cells, separator should selectively control the mass transportation (e.g., protons or OH[−] anions) as well. Conventional polyolefin separators, such as porous polyethylene (PE) and polypropylene (PP) membranes with micron-sized pores, are commonly employed in rechargeable LIBs owing to their mature fabrication, low resistance, and excellent chemical stability. In Li–S batteries, however, more functionalities are preferably introduced to meet the demand of the unique multi-electron electrochemistry.^[30]

Since a separator is a complete screen between the sulfur cathode and the lithium anode, its contact and interaction with both the cathode and anode will undoubtedly impact on the interfacial properties and the electrochemical performance. In fact, the sulfur cathode and the lithium anode have entirely distinct physicochemical characteristics, and as a result their demands for the separator are also different or even conflicting. As we discussed in the Section 2 and 3, the interfacial stabilities of both the cathode/separator and anode/separator interfaces are extremely important to control the interfacial reactions such as sulfur/polysulfide conversion and lithium deposition/dissolution. Therefore, rationally engineering both sides of the separator will be an effective and efficient way to regulate the Li–S batteries. By fully utilizing commercially viable PE or PP separators as the substrates, it will be much easier to fabricate and modify the functional separators via facile processes.

There have been many insightful review articles on the separators for Li–S batteries.^[30,31] Our group has summarized various multifunctional separator/interlayer systems for Li–S batteries, which were classified in terms of materials.^[30] In this section, however, we focus on the asymmetric sides of the separator with particular concerns in dealing with the issues at the two interfaces: the cathode/separator and anode/separator interfaces. Both of them affect the utilization, efficiency and stability of Li–S batteries dominantly, especially when the areal loading is very high. Besides, to prevent the overlap with

our previous review and to make this section concise, only progress specifically made for high-loading Li–S batteries are highlighted herein. Accordingly, this section is briefly divided into two hierarchies to echo the kernel concepts and understanding discussed in the Section 2 and 3: 1) cathode/separator modulation and 2) anode/separator modulation.

4.1. Cathode/Separator Modulation

Inserting a conductive porous interlayer or coating a functional layer on the routine polymer separator has been proved to be a facile and effective way to enhance Li–S batteries. Basically, both two paths go into equifinality: the modulation of cathode/separator interfaces. Several functions are provided by such an engineered layer, including: 1) controlling the crossover of polysulfides through either rejection or interception, 2) enhancing the sulfur utilization through polysulfide reactivation, and 3) accommodating a migrated active phase to prevent the passivation of the cathode/separator interface. With a high loading of active materials, these functions are in ever-urgent demand. On one hand, the flux of polysulfides diffusing through the separator is enlarged concurrently with the increase in sulfur loading, inducing larger shuttle currents. The parasitic reactions between lithium metal and polysulfides therefore become much severer. On the other hand, high sulfur loading results in more dissolved polysulfides, which are easily intercepted by the porous polymer separator. The intercepted polysulfides can be degraded into immobile solid deposits within the insulating polymeric frameworks, losing the electrical contact and electrochemical activity. Therefore, the component, structure, chemistry, and properties of the engineered functional layer must be deliberately tailored to facilitate the transport and reaction behaviors at the cathode/separator interface when the loading active material is considerable.

According to the specific function of the cathode-side engineering, we generally classified this hierarchy into: 1) polysulfide-rejection layer and 2) polysulfide-reativation layer.

4.1.1. Polysulfide-Rejection Layer

Considering the negatively charged nature of polysulfides and their typical hydraulic radius (>1 nm), either the electrostatic repulsion (e.g., anionic polymer such as Nafion^[328,329] and PP grafted with styrenesulfonate^[330]), size sieve (e.g., ultramicroporous carbon^[331] and ultramicroporous polymer^[332]), steric retardment (e.g., ceramic films^[333]), or their combination (e.g., GO^[334] and MOF^[335]) can be utilized for constructing efficient polysulfide-rejection layers. Our group first fabricated Nafion-coated PP separators to realize highly stable cycling of Li–S batteries.^[328] Negatively charged sulfonate (SO₃[−]) groups on Nafion enabled ion hopping of Li⁺ but rejected polysulfide anions electrostatically, resulting in significantly suppressed shuttle effect. To introduce additional steric retardment, our group further employed 2D GO films as cation permselective membranes to control the shuttle.^[334] On one hand, GO contained rich oxygenated functional groups to afford electrostatic repulsion to polysulfide anions. On the other hand, the laminated pores of

GO membranes also sterically inhibit the rapid diffusion of polysulfides. Very recently, Zhou's group fabricated a MOF/GO hybrid membrane via in situ reactions to offer an ionic sieve for Li-S batteries.^[335] The MOF/GO separator exhibited substantial suppression of polysulfide shuttle. Nevertheless, relatively low sulfur loadings of $<1.5 \text{ mg cm}^{-2}$ were reported in the aforementioned works. The effectiveness of these polysulfide-rejection layer should be further verified in high-loading Li-S batteries.

The major challenge for the application of polysulfide-rejection layers in high-loading Li-S batteries is the Li^+ ion transportation. It will be easily deduced that the areal current density will be proportional to the areal loading if the C-rate remains the same. Correspondingly, the Li^+ -ion flux will also be proportional to the loading. The polysulfide-rejection layer, however, inevitably retards the diffusion of Li^+ ions. For example, Jin et al. synthesized a perfluorinated ionomer film with lithium sulfonyl dicyanomethide functional groups (Li-PFSD), which possessed similar chemical structure to Nafion but higher Li^+ ionic conductivity.^[336] Li-S batteries employing Li-PFSD ($\approx 3 \text{ mg cm}^{-2}$ sulfur) exhibited high capacity of $\approx 1260 \text{ mA h g}^{-1}$ at 0.2 mA cm^{-2} ($\approx C/25$); while the capacity dropped to 550 mA h g^{-1} at 1.2 mA cm^{-2} ($\approx C/4$). Wang and co-workers separated the Li_2S cathode and the anode by a lithium superionic conductor (LISICON)-type $\text{Li}_{1+x}\text{Al}_x\text{Ti}_{2-x}\text{Si}_y\text{P}_{3-y}\text{O}_{12}$ (LATP) glass film, enabling very stable cycling of the Li-S cells with a Li_2S loading of 7 mg cm^{-2} (Figure 17a).^[337] Nevertheless, the current densities were restrained lower than $C/10$ ($\approx 0.8 \text{ mA cm}^{-2}$) to obtain a capacity higher than 800 mA h g^{-1} at room temperature. Yu et al. also explored the use of ceramic electrolyte films, including LATP^[338] and a more chemically stable $\text{Li}_{1+x}\text{Y}_x\text{Zr}_{2-x}(\text{PO}_4)_3$ (LYZP) alternative,^[339] as the interlayers for Li/CNF-polysulfide cells with a sulfur loading of 4 mg cm^{-2} . The rate capabilities were facilitated by the 3D CNF current collectors, but capacities higher than 800 mA h g^{-1} can only be attained at current densities lower than $C/2$ ($\approx 3.35 \text{ mA cm}^{-2}$). Although these rejection layers completely blocked the crossover of polysulfides and held certain Li^+ permeabilities, their Li^+ ionic conductivities ($\approx 10^{-7}$ – $10^{-4} \text{ S cm}^{-1}$) are still much lower than that of the liquid electrolyte ($\approx 10^{-2} \text{ S cm}^{-1}$).

One approach to reduce the ion-diffusion resistance is to adopt a porous polysulfide-rejection layer. For example, Zeng et al. grafted SO_3^- groups onto acetylene blacks and coated these sulfonated acetylene blacks (AB-SO_3^-) on the polymer separator.^[340] The AB-SO_3^- -coated separator exhibited similar permselective sieving effect to Nafion-coated separator while the porous structure allow more facile Li^+ transportation. At $3C/2$ (7.5 mA cm^{-2}), the Li-S batteries with a sulfur loading of 3 mg cm^{-2} still exhibited a capacity of 751 mA h g^{-1} after 100 cycles. Yim et al. coated barium titanium oxide (BaTiO_3 , BTO) particles on the separator to form a porous polysulfide-rejection layer (Figure 17b).^[341] By applying an electric field, aligned permanent dipoles were induced in the ferroelectric BTO, affording sufficient electrostatic repulsion to polysulfides. The Li-S batteries applying a poled BTO-coated separator ($\approx 3 \text{ mg cm}^{-2}$ sulfur) exhibited stable cycling with capacities over 900 mA h g^{-1} at $C/2$ (2.5 mA cm^{-2}). Another approach is to reduce the thickness of the polysulfide-rejection layer. Our group fabricated a rationally integrated PP/GO/Nafion

ternary-layered separator (Figure 17c).^[342] Ultrathin layer of GO ($3.2 \times 10^{-3} \text{ mg cm}^{-2}$; $\approx 30 \text{ nm}$) was firstly filtrated onto the PP substrate to completely conceal the underneath pores and subsequently, a dense Nafion ($5 \times 10^{-2} \text{ mg cm}^{-2}$; $\approx 100 \text{ nm}$) layer was coated on the GO layer without penetration and loss in the porous PP matrix. Such a rational integration allowed an extremely low loading of the rejection layer ($5.32 \times 10^{-2} \text{ mg cm}^{-2}$) with an ultrathin thickness ($\approx 130 \text{ nm}$), simultaneously maintaining efficient polysulfide blockage and Li^+ channels. As a result, not only the cycling stability but also the rate performance was improved. Even at a high sulfur loading of 4 mg cm^{-2} , the Li-S cell utilizing a PP/GO/Nafion separator delivered a high capacity of 1225 mA h g^{-1} at $C/5$ and attained a Coulombic efficiency of 92% without the aid of LiNO_3 additives in the electrolyte.

Subsection Summary (4.1.1.): The concept of a polysulfide-rejection layer has a fundamentally preferable attribute, namely the suppression of shuttle effect. Such an attribute raises several technical advantages, including 1) enhanced Coulombic efficiency, 2) mitigated capacity loss, 3) self-discharge inhibition, and 4) anode stabilization. However, in practical use, the ion-diffusion resistance brought by the additional rejection layer should be primarily addressed, otherwise the operation of high-loading Li-S batteries will be unsatisfactorily time-consuming.

4.1.2. Polysulfide-Reactivation Layer

Since 2012, when Manthiram's group first inserted a multi-walled CNT interlayer between the separator and the sulfur cathode,^[343] introducing a conductive porous layer to the cathode/separator interface has attracted fantastic popularity for Li-S battery research. Such a strategy can be achieved through either coating various conductive agents on the separator or placing a free-standing interlayer in between the separator and the sulfur cathode. Except for the fabrication procedures, their functions are essentially analogous. By varying the architecturing materials, ranging from carbon blacks,^[344,345] CNFs/CNTs,^[346] graphene,^[347] porous carbon^[348] and their composites,^[349] for this layer and tuning its properties such as electrical conductivity, porosity, and polysulfide binding affinities, at least one of the following functions can be realized: 1) intercepting the shuttling polysulfides through either physical, chemical, or synergistic adsorption; 2) reactivating polysulfides that are intercepted by the layer or diffuse back from the anode side; 3) accommodating the migrated active phase from the cathode; 4) minimizing the volume fluctuation induced by polysulfide dissolution and phase migration.

Such a layer is termed as the "polysulfide-reactivation layer" based on its mechanism. Chung and Manthiram adopted a hierarchical carbonized paper with controllable thickness as a modularized platform to enclose the polysulfide interception mechanism.^[350] They placed six layers of identical carbonized paper between the separator and the sulfur cathode, and analyzed the elemental distribution in the cycled interlayer modules. It was found that the sulfur content decreased from the innermost layer to the outermost layer, fitting the concentration gradient of polysulfides. The polysulfides were gradually intercepted and continuously reutilized, affording high and stable capacity. In

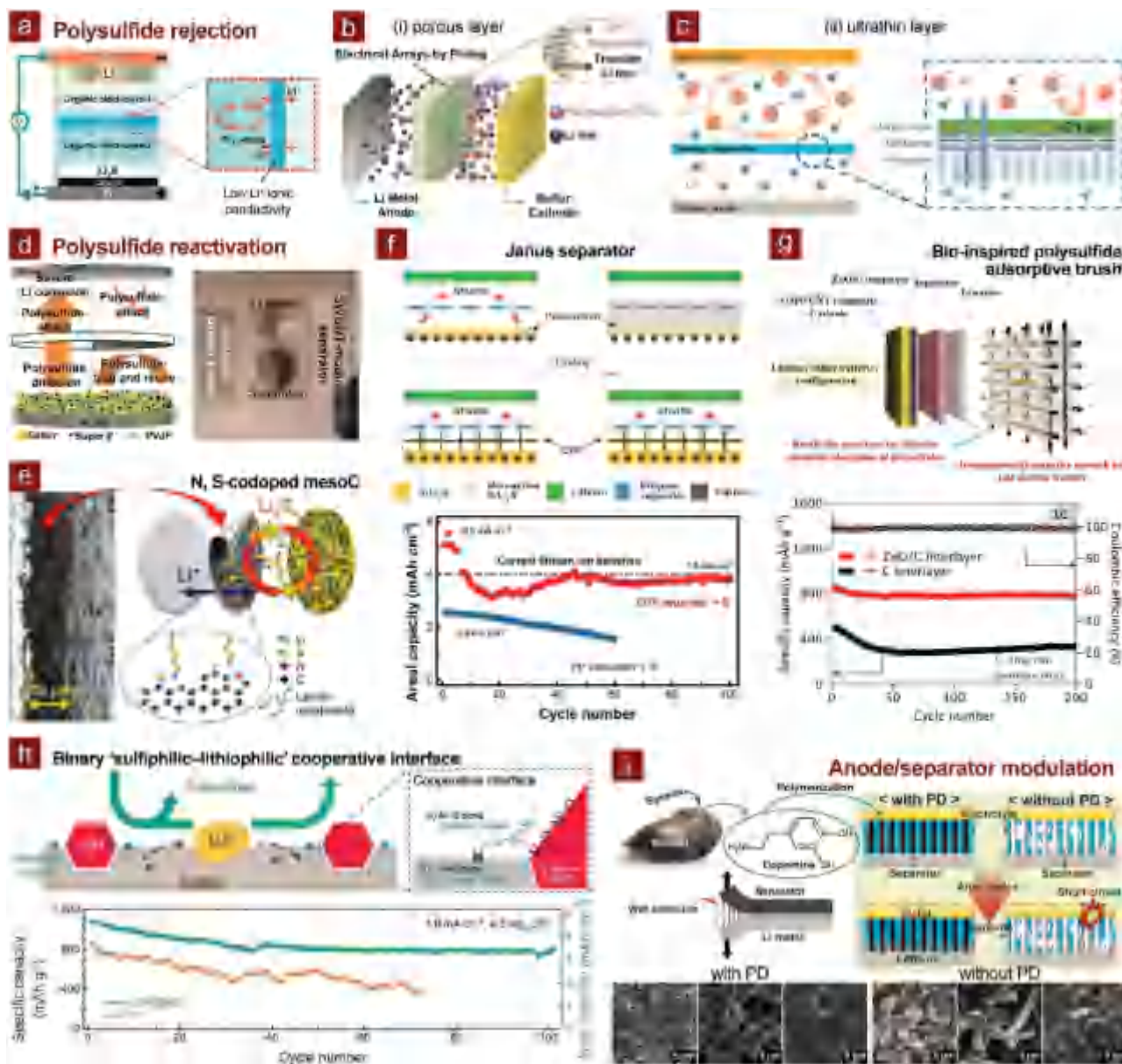


Figure 17. Separator engineering. a) Schematic of the architecture for the Li-S battery employing a ceramic separator. Reproduced with permission.^[337] Copyright 2015, Royal Society of Chemistry. b) Schematic of the effect of the poled BTO particles toward polysulfide rejection. Reproduced with permission.^[341] Copyright 2016, Wiley-VCH. c) Schematic of a ternary PP/GO/Nafion separator with ultrathin and ultralight coating layer. Reproduced with permission.^[342] Copyright 2016, Wiley-VCH. d) The improvement mechanism of the single-walled CNT-modulated separator and the demonstration with a half-side modulated separator. Reproduced with permission.^[351] Copyright 2016, Wiley-VCH. e) Cross-sectional SEM image and schematic configuration of the N,S-codoped mesoporous carbon (mesoC) separator. Reproduced with permission.^[355] Copyright 2016, American Chemical Society. f) Schematic of a routine PP separator and a Janus separator with a CGF layer, and cycling performance of Li-S batteries with the two separators. Reproduced with permission.^[356] Copyright 2016, Wiley-VCH. g) Schematic of illustrating the structural and chemical function of the hybrid ZnO nanowire/CNF interlayer, and cycling performance of Li-S batteries with the two interlayers. Reproduced with permission.^[365] Copyright 2016, Wiley-VCH. h) Schematic of the binary 'sulfiphilic-lithiophilic' cooperative interface of LDH@NG and cycling performance Li-S batteries with a LDH@NG separator. Reproduced with permission.^[369] Copyright 2016, Wiley-VCH. i) Mussel-inspired PD coating onto the separator to mitigate lithium dendrite growth via uniform Li⁺-ionic flux and wet-adhesion, and SEM images of lithium deposition with or without PD. Reproduced with permission.^[374] Copyright 2014, Wiley-VCH.

Yao et al.'s work, operando Raman spectroscopy was employed to reveal that polysulfides can also be intercepted by the routine porous polymer separators, and precipitate as deactivated phase, blocking the ion channels and passivating the cathode/separator interface.^[344] They also suggested that a conductive

coating can effectively eliminate the passivation and reactivate the inactive sediment. Surface area and electrical conductivity were regarded as the key parameter of such a reactivation layer. Chang et al. further indicated that enhancing the reutilization ratio of shuttling polysulfides also simultaneously stabilized the

lithium metal anode through the suppression of side reactions between lithium metal and polysulfides (Figure 17d).^[351] These works provided mechanistic insights into the working mechanism of the polysulfide-reactivation layer, shedding fresh light on the design of novel functional separators/interlayers.

For high-loading Li–S batteries, the trapping capability of the reactivation layer will become more important than in case of the low loading if the areal loading of the reactivation layer remains the same (normally less than 0.5 mg cm^{-2}). As the loading increases, the amount of polysulfides that the layer ought to deal with rises simultaneously. Therefore, two new parameters of the layer emerge as the key. One is the pore volume, which is used to accommodate a substantial amount of polysulfides and allow their precipitation without blocking electrolyte channels and destructing the overall porous structure. The other one is the binding affinity to polysulfides. The amount of polysulfides that can be adsorbed by the reactivation layer must be further increased to meet the greatly promoted shuttle phenomenon.

Unlike microporous carbon or routine carbon blacks, carbon materials with mesopores or macropores normally have more interior pore volume to store trapped polysulfides and solid precipitates, which is highly beneficial for building the reactivation layer for high-loading Li–S batteries. For instance, Balach et al. explored a variety of mesoporous carbon (mesoC) derived from phenolic resin using silica hard templates and fabricated mesoC-coated separators for Li–S batteries with sulfur loadings of at least 3 mg cm^{-2} .^[352–355] All the cathodes were made of simple and scalable carbon black/sulfur composites. The mesoC possessed tunable pore volume^[353] and can be modified with N-dopants^[354] or N,S-dual-dopants.^[355] They found that undoped mesoC with the highest pore volume of $3.23 \text{ cm}^3 \text{ g}^{-1}$ provided the most remarkable enhancement in the electrochemical performance, highlighting the role of the pore volume.^[353] While for the heteroatom-doped mesoC with a comparable pore volume, N,S-codoped mesoC-coated separators enabled the best battery performance even when the sulfur loading was as high as 5.4 mg cm^{-2} (Figure 17e).^[355] At C/10 and C/2 (0.9 and 4.5 mA cm^{-2}), high areal capacities of 5.9 and 2.9 mA h cm^{-2} were achieved, respectively. Our group proposed a Janus separator by attaching a conductive layer of cellular graphene frameworks (CGFs), which were derived from CVD growth on a unique MgO templates, on the commercial PP membrane (Figure 17f).^[356] The PP substrate was flexible and insulating; while CGFs had extraordinary electrical conductivity (100 S cm^{-1}), high surface area ($2120 \text{ m}^2 \text{ g}^{-1}$), and exceptional mesopore volume ($3.1 \text{ cm}^3 \text{ g}^{-1}$), serving as an ideal building block for constructing reactivation layer. We found that coating the same amount of CGFs on the separator was much more efficient than mixing them in the cathode, which Liu et al. also experimentally verified.^[357] Only 0.3 mg cm^{-2} coating of CGF on the separator significantly boosted the capacity and cycling stability of a double-high sulfur cathode with sulfur content of 80 wt% in the slurry (68 wt% in the whole cathode with a CNT current collector) and an areal sulfur loading of 5.3 mg cm^{-2} . A high areal capacity of 5.5 mA h cm^{-2} was obtained at 0.9 mA cm^{-2} and $\approx 4.0 \text{ mA h cm}^{-2}$ was retained after 100 cycles at 1.8 mA cm^{-2} . To further reduce the cost of such Janus-type separators and enable their continuous production,

our group developed a facile, scalable, and green process to fabricate porous graphene (PG)/PVP-coated separators via continuous aqueous coating.^[358] Amphiphilic PVP was employed as a bifunctional binder to simultaneously enable the aqueous processability and provide sufficient binding to polysulfides. Such a scaled-up fabrication of PG/PVP-coated separators allowed the electrochemical evaluation at a pouch-cell level. With a sulfur loading of 7.8 mg cm^{-2} , the Li–S pouch cell delivered a high initial capacity of 1135 mA h g^{-1} (8.9 mA h cm^{-2}) at 1.3 mA cm^{-2} .

Although heteroatom doping significantly promotes the chemisorptivity of carbon materials, polymer and inorganics are believed to possess more abundant binding sites and stronger adsorption to polysulfides. Therefore, a wide range of polymer, inorganics, or their hybrids with carbon have been explored as interlayers or coating layers of the separator for high-loading Li–S batteries, including PAA,^[359] PEDOT:PSS,^[360] PEG/PEO,^[361] PPY,^[362] C_3N_4 ,^[363] $\text{Fe}_3\text{C/C}$,^[364] ZnO ,^[365] SnO_2 ,^[366] RuO_2 ,^[367] hydroxyapatite,^[368] etc. Among them, the combination of conductive carbon and chemisorptive polymer/inorganics is a holistic way to realize both high trapping efficiency and high conversion rate of polysulfides. For example, Chen and Kumar's group designed a bio-inspired, brush-like interlayer consisting of ZnO nanowires grown on interconnected conductive frameworks such as Ni foams and porous CNFs (Figure 17g).^[365] When ZnO nanowires were grown on a free-standing, lightweight CNF mat, they formed a “brush border” to increase the contact area with the electrolyte, and an individual nanowire acted “microvilli” to chemically adsorb the dissolved polysulfides in electrolytes. As a result, the ZnO/CNF interlayer (1.3 mg cm^{-2}) rendered very stable cycling performance of high-loading Li–S cells (3.0 mg cm^{-2} sulfur). At C/5 and 1.0 C (1.0 and 5.0 mA cm^{-2}), capacities of 1031 and 776 mA h g^{-1} were retained after 50 and 200 cycles, respectively. Our group synthesized a nanosized NiFe layered double hydroxide (LDH)/nitrogen-doped graphene (NG) hybrid (termed as LDH@NG) to form a cooperative interface, at which NG was “lithiophilic” to favor the binding to terminal Li^+ in polysulfides and serve as immobilized Li^+ -transfer media; while NiFe LDH was “sulfiphilic” with the capability of directly forming metal–S bond and catalyzing the conversion of polysulfides (Figure 17h).^[369] By integrating the high conductivity, large pore volume, and optimal binding to polysulfides/ Li_2S , LDH@NG-modified separators facilitated the nucleation/growth of $\text{Li}_2\text{S}/\text{Li}_2\text{S}_2$, mitigated shuttle effect, and promoted electrochemical kinetics. The Li–S cell applying a LDH@NG (0.3 mg cm^{-2})-modified separator and a routine carbon/sulfur cathode (4.3 mg cm^{-2} sulfur) coated on the Al foil exhibited an initial capacity of 1043 mA h g^{-1} and retained $\approx 800 \text{ mA h g}^{-1}$ after 100 cycles at 1.0 mA cm^{-2} . Even lower loading of the reactivation layer (0.12 mg cm^{-2}) can be achieved on layer-by-layer multi-walled CNT/PEG-coated separators, which facilitate the Li–S batteries with a sulfur loading of up to 6.5 mg cm^{-2} .^[361] The weight ratio of sulfur and reactivation layer will be a more important parameter for fair comparison in the future.

The large-scale deployment of these functional separators demands for advanced fabrication techniques. Similar to 3D porous current collectors, it is also quite challenging to continuously produce large-area free-standing conductive films or other macroscopic forms as interlayers. The coated separators

might be more practically reliable if filtration, which is difficult to be scaled up, can be replaced by industrially oriented blade coating. As discussed above, our group demonstrated that continuous aqueous coating could be very facile to fabricate large-area functional separators for pouch-cell evaluation.^[358] But even so, it is still valuable to explore alternative coating methods to push forward both technologies and understanding. For example, Niu and Lv et al. developed a simple, one-step electrostatic spray deposition technique to compactly coat ultrathin PEDOT:PSS layer as polysulfide-blocking layer with a thickness of only ≈ 100 nm and a loading of ≈ 0.09 mg cm⁻².^[370] Archer's group reported Langmuir–Blodgett technique for efficiently preparing multifunctional and multicomponent nanoparticle membranes to fully utilize each building blocks.^[371,372] Separators coated with CNT/SiO₂/CNT (0.13 mg cm⁻²)^[372] or CNT/PANI/TiO₂ (0.43 mg cm⁻²)^[371] laminates were adopted for Li–S batteries with a sulfur loading of 3.5 mg cm⁻², which exhibited outstanding electrochemical performance. The advancement in membrane manufacture will undoubtedly promote the development of functional separators with ultrathin but effective polysulfide-rejection/reactivation layers.

Section Summary (4.1.): Placing a multifunctional layer between the routine polymer separator and sulfur cathode has been proved to be an effective and efficient way to trap polysulfides and reactivate them. Such an approach judiciously adapt the natural gradient distribution of polysulfides within a working Li–S cell. However, a major technical concern about the interlayer is the additional weight and thickness that it brings in. Would the enhancement just be the result of adding more carbon (or other beneficial components)? The concept of cathode/separator modulation must be challenged at a relevant condition (e.g., with a comparable fraction of sulfur in the whole cathode/separator integration). Moreover, advanced fabrication technologies are always the bottleneck for bulk applications.

4.2. Anode/Separator Modulation

Unlike the cathode/separator modulation, engineering the anode side of the separator to modulate the interfacial properties is still at an illuminative stage for the development of Li–S batteries. In this area, Choi's group has carried out several pioneering works by applying “lithiophilic” separators. In their early exploitation, they found that mussel-inspired PD-treated separators exhibited remarkable wetting properties by both the electrolyte and lithium anode, effectively suppressing the dendrite growth and allowing remarkable high-rate capabilities.^[373] Such a separator was further adopted in Li–S batteries and coupled with a carbonized PAN/S composite cathode and CsNO₃-containing electrolyte (Figure 17i).^[374] The PD-treated separator, in combination with Cs⁺ additives, significantly reduced the thickness of resistive mossy lithium and inhibited dendrite growth. Therefore, the Li–S cell with an active material loading of 17 mg cm⁻² (≈ 6.74 mg cm⁻² sulfur) exhibited a high initial capacity of 9 mA h cm⁻² (≈ 1300 mA h g_S⁻¹) and maintained more than 70% after 90 cycles at a discharge rate of 4.2 mA cm⁻². Note that the charge rate was much smaller (0.42 mA cm⁻²), further indicating the significance

of stabilizing lithium metal anodes especially during lithium plating. They also applied a poreless urea-urethane copolymer (spandex) separator to replace the PD-coated separator. Even better cycling stability ($\approx 80\%$ capacity retention of initial capacity of ≈ 4 mA h cm⁻² after 200 cycles) was achieved at a sulfur loading of 3 mg cm⁻² when both charge and discharge rates were 1 mA cm⁻² ($\approx C/4$).^[375] Similar PD-coated separators were also reported for the modification of anode/separator interfaces.^[19,376] Except for the polymer, other materials have also been employed to modulate the anode/separator interface. For example, Li and co-workers proposed a trilayer graphene/PP/Al₂O₃ separator with Al₂O₃ contacting with the lithium to enhance the thermal stability and prevent lithium dendrites.^[377] Goodenough and co-workers replaced the PP separator by a porous cellulose membrane to afford much enhanced interfacial stability of lithium metal, therefore attaining extended longevity to 1000 cycles.^[378]

Section Summary (4.2.): Although the popularity of research into the engineered separators for Li–S battery anodes is not as much as that for the cathode side, the anode/separator modulation will be very interesting and important to control the interfacial behaviors of lithium metal when it contacts with electrolyte-infiltrated separators. If the strength, surface affinities, and spatial distribution of Li⁺ can be rationally regulated by the separator, lithium dendrites might be prohibited, thereby allowing stable operation of lithium metal anodes within long-term duration even under high current densities. Progress in the separators for general lithium metal anodes (e.g., boron nitride-coated separator,^[379] all-integrated PI separator,^[380] etc.) will also shed a light on the anode/separator modulation for Li–S anodes. We believe that this area is burgeoning, and in the near future it will make a huge difference.

4.3. Integrated Electrode/Separator Systems

Roles of individual components such as sulfur cathode, lithium anode, and separator, as well as their strategic optimizations and key concepts, are reviewed in the aforementioned sections. Nevertheless, Li–S batteries, especially with practically desirable high loadings of active materials, suffer from influences of each individual components; whereas these influences, in general, are strongly coupled. Decoupling the contributions of each components from a combinatorial consequence promotes the understanding toward Li–S batteries. In turn, integrative design also gives rise to synergistic enhancement in the battery performance. Therefore, the target of this section is to review several conceptual advancements in integrated electrode/separator systems toward high-loading Li–S batteries.

One example is the integration of a deliberately engineered cathode and a polysulfide-reactivation interlayer. Sun and co-workers demonstrated a series of bilayer integrated cathode/interlayer.^[381–383] Some valuable principles can be extracted, including the addition of polar conductive scaffolds (e.g., hollow mesoporous TiO₂ embedded CNT,^[382] N-doped carbon blacks/CNTs,^[381] and N-doped carbon packed TiO₂^[383]), the use of chitosan binder to adsorb polysulfides, and the insertion of porous conductive interlayers (e.g., CNT or N-doped CNT membranes). Among them, the combination of a sulfur/N-doped carbon

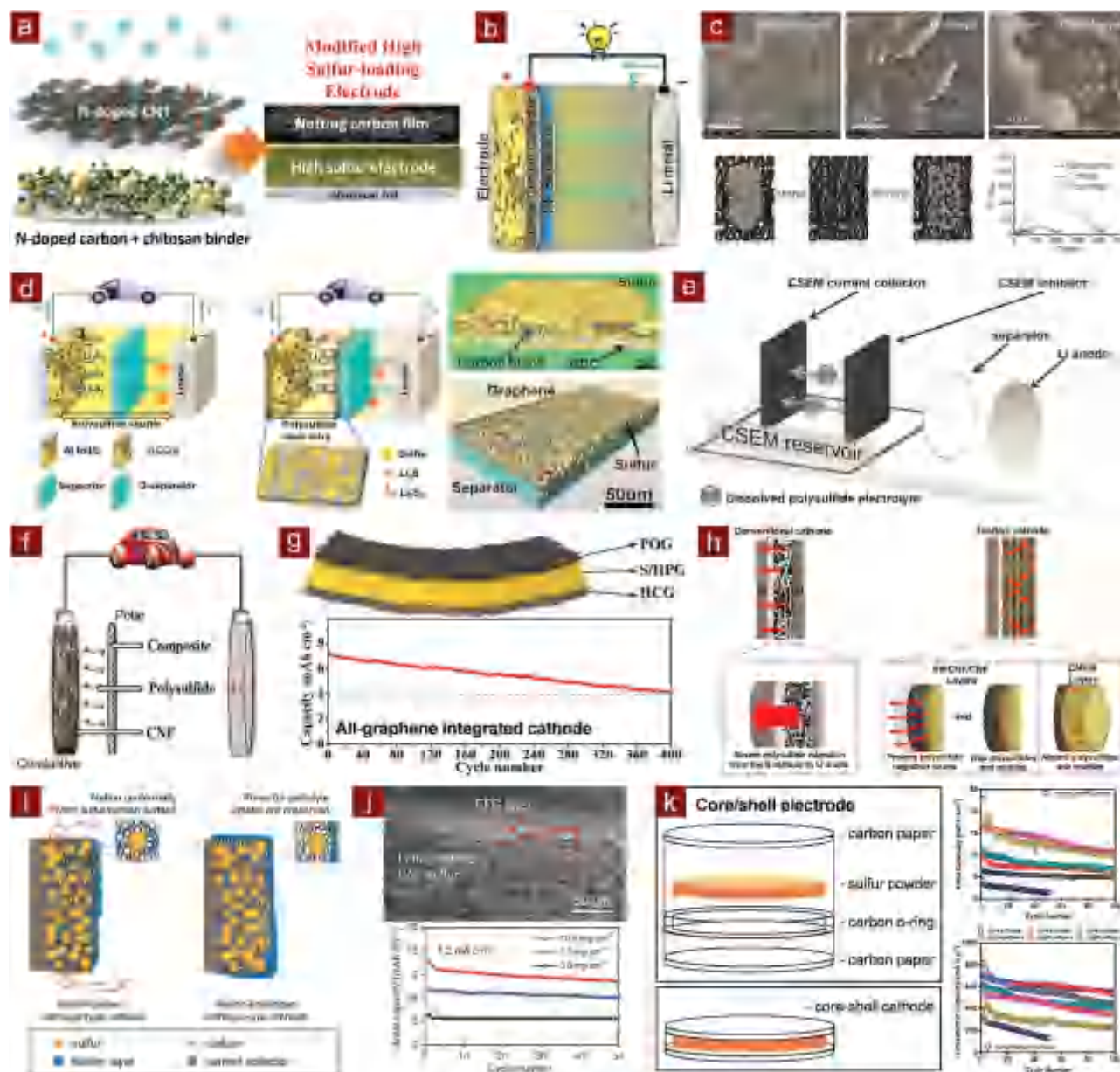


Figure 18. Integrated electrode/separator systems. a) Schematic design of the modified high sulfur-loading electrode with a netting carbon film. Reproduced with permission.^[381] Copyright 2016, American Chemical Society. b) Schematic of the electrode configuration using an integrated structure of sulfur and G-separator. Reproduced with permission.^[389] Copyright 2015, Wiley-VCH. c) The activation of pristine Li_2S particles through CNT sandwich during the 1st cycle. Reproduced with permission.^[391] Copyright 2014, Wiley-VCH. d) Schematic of a Li-S battery with conventional configuration and with GCC/pure-sulfur/G-separator sandwich configuration, and 3D XRM image of the reconstructed sulfur electrode (upper) and G-separator (below). Reproduced with permission.^[392] Copyright 2014, Wiley-VCH. e) Schematic model of the sandwiched CSEM reservoir configuration. Reproduced with permission.^[393] Copyright 2014, Wiley-VCH. f) Schematic showing a lithium/dissolved polysulfide cell with an asymmetric sandwich cathode. Reproduced with permission.^[399] Copyright 2014, Wiley-VCH. g) Schematic of the all-graphene integrated cathode and cycling performance at 0.34 A g^{-1} . Reproduced with permission.^[400] Copyright 2016, American Chemical Society. h) Schematic of the Li-S cells with the conventional sulfur cathode and with the tandem cathode. Reproduced with permission.^[402] Copyright 2017, Royal Society of Chemistry. i) Schematic of (left) Nafion-coated cathode and (right) Nafion-enveloped cathode. Reproduced with permission.^[403] Copyright 2014, Wiley-VCH. j) Cross-sectional SEM image of a dissected lotus root multichannel CNF/S@EFG electrode and cycling performance with different sulfur loadings. Reproduced with permission.^[404] Copyright 2015, Nature Publishing Group. k) Schematic of the (upper) various split parts and (below) core/shell cathode, and cycling performance with different sulfur loadings (marked as the CSX cathode, where X represents the sulfur loading). Reproduced with permission.^[405] Copyright 2016, Royal Society of Chemistry.

black/N-doped CNT/chitosan cathode and a N-doped CNT interlayer enabled the most remarkable performance of Li-S batteries (Figure 18a).^[381] At a high sulfur loading of 10 mg cm^{-2} , an initial capacity of 1332 mA h g^{-1} was attained at C/10 with

91% retention after 50 cycles, and 2.0 C (33.5 mA cm^{-2}) rate capability was also enabled with a capacity of 845 mA h g^{-1} . 3D assembled/infiltrated electrodes are also explored to cooperate with the functional separators/interlayers, including a

CNF/polysulfide (2.4 and 18.1 mg cm⁻² sulfur)–bare CNF dual-layer electrode^[260] and a rGO-coated cellulose fiber current collector-supported sulfur cathode (4 mg cm⁻² sulfur) with a TiO₂ nanocrystal-embedded N-doped porous carbon interlayer.^[384]

The deliberate cathode can even be replaced by pure sulfur powders. For example, Qie and Manthiram reported a blade-coated pure sulfur powder cathode in combination with a CNF interlayer, which also served as an upper current collector.^[385] A wide range of sulfur loadings was achieved from 2.5 to 16.2 mg cm⁻². When the sulfur loading was 13.9 mg cm⁻², a high initial capacity of 1383 mA h g⁻¹ (19.2 mA h cm⁻²) was achieved at C/20 (1.2 mA cm⁻²) and a capacity of 741 mA h g⁻¹ (10.3 mA h cm⁻²) was remained after 100 cycles at C/3 (7.8 mA cm⁻²). The concept of combining pure sulfur powder electrode with an upper current collector was further realized by other groups through either modifying the vapor grown carbon fiber (VGCF) interlayer by polar PEO (9.8 mg cm⁻² sulfur)^[386] or applying alternative Ni foam current collectors (2.3^[387] or 50 mg cm⁻² sulfur^[388]). Directly coating the cathode on the upper current collector could be an alternative route to prevent sophisticated design of the cathode. For example, Cheng and Li's group developed a slot coating method to continuously fabricate large-area graphene-coated separators (G-separators), on which sulfur slurry was coated to form integrated electrode/separator systems (Figure 18b).^[389] The rough surface of G-separators ensured better adhesion of sulfur layer than Al foils, and graphene also served as physical barriers for polysulfide diffusion. To further enhance the adsorption to polysulfides, N-dopants and Ni nanoparticles were introduced to the nanocarbon coating layer as polar sites.^[390] A high sulfur loading of 8.5 mg cm⁻² was realized with high rate capabilities at 2.0 C (≈28 mA cm⁻²) and a capacity of 772 mA h g⁻¹ (6.6 mA h cm⁻²) retained after 200 cycles at C/5.

Another configuration is the sandwich-type integrated cathode/interlayer, which has attracted considerable interests for high-loading Li–S batteries and enabled improved electrochemical performance in comparison with the routine cell configuration. The general sandwiched configuration is realized by placing active materials, in form of either sulfur/Li₂S powders, slurry, or polysulfide catholyte, between two identical conductive porous membranes or papers. Fu et al. first demonstrated this concept by simply placing 1, 2, and 3 mg cm⁻² pristine Li₂S powder between two CNT sheets.^[391] It was found that the pristine Li₂S can be electrochemically activated by CNTs after the 1st cycle, and capacities of 752 and 442 mA h g_{Li₂S}⁻¹ (1081 and 635 mA h g_S⁻¹) were obtained at C/2 when Li₂S loadings were 1 and 3 mg cm⁻², respectively (Figure 18c). Later on, Cheng and Li's group reported a graphene–pure sulfur–graphene sandwich structure for ultrafast, long-life Li–S batteries (Figure 18d).^[392] Large-area graphene current collectors (GCCs) and G-separators were fabricated. The GCC/S/G-separator sandwich efficiently decreased the contact impedance, provided rapid ion/electron-transport paths, accommodated volumetric expansion and reutilized migrating polysulfides. Graphene loading in the GCC and G-separator was only 1.3 mg cm⁻² in contrast to the loading of the cathode was 3–4 mg cm⁻². The sandwich-structured electrodes exhibited good cycling stability and retained a capacity of 680 mA h g⁻¹ after 300 cycles at 1.5 A g⁻¹. Almost at the same time, Chung and Manthiram proposed a

natural polysulfide reservoir composed of two pieces of carbonized eggshell membranes (CSEM) for Li/polysulfide cells (Figure 18e).^[393] The biomass-derived hierarchical micro/macroporous scaffolds localized the dissolved polysulfides and stabilized the electrochemical reaction within the cathode region, offering the Li/polysulfide cells with a high discharge capacity (1327 mA h g⁻¹ at C/10), long-term cycle stability (over 100 cycles), and a high sulfur loading (3.2 mg cm⁻²). Since then, various symmetric sandwiched electrode/interlayer systems have been explored, including binder-glued carbon black matrices (4 mg cm⁻² sulfur),^[394] carbon papers (6.7 mg cm⁻² sulfur),^[395] buckypapers (5.1 mg cm⁻² sulfur),^[396] CF clothes (6.8 mg cm⁻² sulfur),^[397] CNT/hydroxyl functionalized nanofibrillated cellulose (8.1 mg cm⁻² sulfur),^[398] etc.

To meet the different demands for serving as current collectors and interlayers/separators, the symmetric sandwich structure can be further tuned to fabricate the asymmetric structure, which could be probably termed as more sophisticated “burger” structure. Zu and Manthiram employed a hydrophilic polymer (sodium alginate and polyvinyl alcohol)/carbon-black-modified CNF film as the interlayer and coupled it with a pristine CNF film as the current collector to improve Li/polysulfide batteries (Figure 18f).^[399] The polymer/carbon black composite layer reduced the interspace within CNF frameworks and afforded desirable hydrophilic immobilization to enhance the interception/reactivation efficiency of polysulfides. As a result, the capacity was much higher than that of the cell employing only CNF scaffolds with a sulfur loading of 5.4 mg cm⁻². Fang et al. proposed an all-graphene cathode structure based on specifically designed graphene materials, in which the highly conductive graphene (HCG, ≈1 mg cm⁻²) served as a lightweight current collector with a low square resistance, highly porous graphene (HPG) with a pore volume of up to 3.51 cm³ g⁻¹ accommodated at least 80 wt% sulfur, and partially oxygenated graphene (POG, ≈0.2 mg cm⁻²) served as an interlayer to adsorb mobile polysulfides (Figure 18g).^[400] The rational adoption of graphene and integrative design allowed very high utilization of sulfur with a sulfur loading of 5 mg cm⁻². Capacities of 1500 and 841 mA h g⁻¹ (7.5 and 4.2 mA h cm⁻²) were obtained initially and after 400 cycles at C/5. Modification of carbon to tune the surface functionality into hydrophilicity or “sulfiphilicity” normally sacrifices the electrical conductivity. Therefore, Fan and co-workers systematically investigated the effect of replacing pristine CNFs by hydrophilic surfactant-modified CNFs in current collectors or interlayers for the sandwich-type configurations.^[401] They found that a pristine CNF bottom layer and a modified CNF top layer gave rise to the best electrochemical performance, offering an insight into how the intrinsic properties influenced Li–S batteries.

Very recently, Chang et al. proposed a tandem-electrode concept to fully exert the advantages of the sandwich-type configuration.^[402] The tandem cathode was composed of alternately stacked CNF/S active material layer and CNF/single-walled CNT polysulfide-trapping layer. Compared to conventional cathode configuration, such a tandem configuration can be regarded as sequential ‘sulfur cathode–polysulfide-reactivation layer’ series, and therefore the migration of polysulfides outward each CNF cathode layer can be mitigated through each closely attached CNF/single-walled CNT layer (Figure 18h). As

a result, the polysulfide shuttle across a long path can be suppressed by sequential segmented short paths. Even with high loading of 16 mg cm^{-2} , high initial capacity of $12.3 \text{ mA h cm}^{-2}$ was attained at C/10. Moreover, such a tandem electrode was highly foldable, delivering comparable capacity at bended states to that at original state.

Enlightened by the advantageous core/shell particle design, the final configuration could be termed as “core/shell” electrode design. Such a concept can be traced as a Nafion-enveloped cathode proposed by Song et al. (Figure 18i).^[403] The authors suggested that a significant leakage of polysulfides could happen through the edge of the cathode even a conformal protective coating was formed in between the cathode and the separator. Probably owing to the insulating nature of Nafion, Li–S batteries with sulfur loadings higher than 2 mg cm^{-2} were not demonstrated. Lou’s group reported a pie-like electrode to achieve such a concept and remarkable electrochemical performance (Figure 18j).^[404] Lotus-root-like multichannel CNFs served as nanoscale reactors to store active materials and can easily form a 3D assembled electrode, which was regarded as the “filling” or the core; while amino-functionalized graphene (EFG) was coated on the electrode to serve as the “crust” or the shell, which suppressed the leakage of polysulfides. As a result, the EFG-coated electrode exhibited much enhanced cycling stability than uncoated one at an identical sulfur loading of 3.6 mg cm^{-2} . At an even three-folded sulfur loading (10.8 mg cm^{-2}), a high capacity of 993 mA h g^{-1} ($10.7 \text{ mA h cm}^{-2}$) was retained, comparable to that at 3.6 mg cm^{-2} , indicating the great potential of such a pie-like electrode to scale up the areal capacities. Very recently, Chung et al. thoroughly demonstrated the concept of “core/shell” electrode by placing a carbon paper O-ring between two pieces of carbon papers, and pristine sulfur powders were dispersed with the electrolyte in the hollow space of O-ring (Figure 18k).^[405] Such a structure completely retarded the outward diffusion of polysulfides at all the directions and afforded efficient electron transporting networks. Therefore, sulfur loadings ranging from 4 to 30 mg cm^{-2} was realized. Even at extremely high 30 mg cm^{-2} sulfur, dynamically and statically Li–S battery chemistry was exerted with an areal capacity as high as 23 mA h cm^{-2} at C/10 (5 mA cm^{-2}), and at C/2 (25 mA cm^{-2}), the battery can still be stably operated for longer than 100 cycles. They also demonstrated such a concept on sulfur cathodes coated on Al foils by sealing them with carbon film shields. A high sulfur loading of up to 10 mg cm^{-2} was obtained.^[406]

Section Summary (4.3.): In summary, the rational integration of novel electrode architectures and functional separator/inter-layer systems has been demonstrated as very efficient approach to fully exert the advantages of individual components. Synergistic benefits might also be rendered if the electrochemical reactions and polysulfide shuttle are well manipulated within the cathode region. Such a combinatorial strategy will also bring substantial opportunities to optimize the battery performance and deepen the understanding of working Li–S batteries at a practical loading. Nonetheless, several concerns still existed: 1) quantitative description of the essential intrinsic properties should be defined to guide the design of current collectors, electrode scaffolds, and separators; 2) methods that are suitable for large-scale production or continuous processes are

preferred; 3) the enhancement in the electrochemical performance, such as the capacity, rate capability, and cycling stability must take negligible expense of the increase in the additional weight, which appeals for fairer comparison (e.g., capacity based on the total weight of the current collector, electrode, separator, and other introduced additives instead of on merely sulfur).

5. Conclusions and Perspective

As summarized in this review, huge progress has been achieved through multifaceted and multidisciplinary endeavors, including novel host materials, advanced binder, mesoscale engineering of energy particles, rational electrode architectures, high-efficiency and high-current anodes, multifunctional separators and their inspiration for designing unique cell configurations, and holistic integrations of all desirable attributes. In this review, these efforts are rationally organized into several parts. Evaluations of each approach, as well as considerations into its necessity, merits, drawbacks, and potential directions, are summarized in each section. Brief conclusions are listed below (Table 3).

Up to date, most of the efforts have realized superb battery performance at sulfur loadings of $3\text{--}10 \text{ mg cm}^{-2}$. Moreover, battery prototypes with an areal capacity higher than 20 mA h cm^{-2} have also been proposed. Based on these advancements, there are breakthroughs in Li–S pouch cells as well. Most of them maintained a specific energy of 350 W h kg^{-1} for nearly 100 cycles. Further improving the specific energy to 500 W h kg^{-1} is also achievable, but cyclic life is significantly shortened owing to the starvation of electrolyte. Regardless the cyclability, prototype primary Li–S batteries can deliver a specific energy of 900 W h kg^{-1} . According to our experience on Li–S pouch cells, key parameters for achieving a cell specific energy of 350 W h kg^{-1} include 1) a sulfur content of $>75 \text{ wt\%}$ in the cathode, 2) sulfur utilization of $>70\%$ (or a capacity of $>900 \text{ mA h g}^{-1}$ based on the weight of the whole cathode), 3) a single-side areal sulfur loading of $>5 \text{ mg cm}^{-2}$, 4) an E/S ratio of <3 , and 5) excess lithium of $<100\%$. If higher specific energy was targeted, a lower E/S ratio would be the primary prerequisite. These parameters are not the absolutely exact standard but for reference only. In previous analyses,^[20,25,26] other sets of parameters have been proposed in regards to the aforementioned parameters as well.

Compared to Li–S coin cells that demonstrate superior performance in laboratory, the performance of Li–S pouch cells is still below the great expectation from the market. So why is there a huge gap between the state-of-the-art and the expectation? And is there any possible route to fill it in?

One of the main reason lies in the difference in cell configurations, which may lead to completely different understanding towards pouch cells from that of coin cells. The coupling between charge/ion transfer, polysulfide dissolution/precipitation, and reactions in solution/at surface might be remarkably altered, rendering Li–S pouch cells with distinct behaviors. This, however, may subversively change our mind. For example, it has been commonly known that employing a high current rate benefits the cycling stability of a low-sulfur-loading Li–S coin cell through reducing the percentage of shuttle current

Table 3. Brief summary of key considerations and conclusions for high-loading Li–S batteries.

Cathode	<p>a) Surface polarity and electrical conductivity are two key properties of sulfur host materials as they strongly impact on the interfacial reactions kinetics and manipulation of heterogeneous phase transfer.</p> <p>b) Nanomaterials are preferably organized into large, rationally engineered energy particles to enable optimized contact between electrolyte and active phase, high tap density, and macroscopic uniformity.</p> <p>c) 2D coated electrodes are the most reliable architectures for practical applications, whereas it is formidably challenging for 2D coated electrodes to simultaneously satisfy transport phenomena, dispersion/separation of functional building blocks, and structural compactness/mechanical robustness at multiscale.</p> <p>d) 3D assembled/infiltrated electrodes possess an exceptional advantage in enhancing the areal loading/capacity for researches in laboratory, while intrinsic drawbacks need to be overcome for real applications. Some effective concepts of 3D electrode design are highly referential for 2D counterparts.</p> <p>e) Development of advanced binder materials is urgent for stabilizing in-particle/interparticle connections and enhancing 2D coated electrodes.</p>
Anode	<p>a) The lithium metal anode is becoming the bottleneck for developing Li–S batteries and other analogues. It is so pivotal that some proof-of-concepts of high-areal-capacity sulfur cathodes have to be paired with lithium foils with substantially larger area.^[223,226,232]</p> <p>b) Dendrite growth and SEI destabilization are two determinants that are strongly coupled. They accounts for the vast consumption and eventual depletion of both the metallic lithium and electrolyte.</p> <p>c) 3D lithium hosts reduce the absolute current density and the probability of dendritic growth. Nevertheless, further demonstration in full cells is necessitated. Moreover, effective lithium impregnation strategies are highly desirable to allow the use of lithium-free cathodes such as sulfur.</p> <p>d) Approaches for SEI stabilization should be not only applicable at a high current density but also compatible with the polysulfide-existing environment.</p> <p>e) Since 3D lithium hosts with large exposed surface, which increases the consumption of electrolytes for SEI formation, burgeoning tactics (e.g., 3D hosts protected by preformed SEI)^[407] may help with addressing such an issue.</p>
Separator	<p>a) Separator is an indispensable and important cell component to regulate the interfacial properties and transport behaviors at both sides.</p> <p>b) Either polysulfide-rejection or reaction layer is efficient in controlling the shuttle, redox of polysulfides, and lithium corrosion. However, such an extra layer ought not to take expense in sacrificing total specific energy/energy density.</p> <p>c) Researches into the functional separator/interlayer systems should be in regard to both the cathode and anode. Asymmetric or Janus structures might be quite promising to meet the distinct requirements from the two sides.</p> <p>d) Advanced fabrication methods are promising for functional separator/interlayer systems being deployed in large-scale applications.</p>

in the total. However, high rate is conspicuously detrimental to operating a high-sulfur-loading Li–S pouch cell owing to the earlier failure of lithium anode under a higher current density. Meanwhile, it is impossible to exactly evaluate the effect of E/S ratio in a coin cell because extra electrolyte is needed to fill in the ‘dead’ volume. Also the space confinement in a coin cell, a pouch cell, and a winding-type cell is quite different, which play a critical role to tolerate the volume expansion and contraction in a working battery. A reliable binder are strongly considered to build a robust cell with nanostructured electrode materials. Basically, several challenges, from both fundamental, materials and techniques, are interdicting the road towards practically viable Li–S batteries (Table 4). Accordingly, new opportunities may be created upon navigating through these challenges.

Besides, in the battery industry, single-cell uniformity is essential for assembling huge battery packs, demanding for standardization and modularization, as well as systematic management. Moreover, unprecedented enthusiasm about high-energy rechargeable batteries overemphasizes the significance of energy density and aims at developing high-energy but potentially dangerous electrode materials, such as lithium. The safety concern must gain more attention and the enthusiasm must be slightly cooled down. Last but not the least, although Li–S batteries have overwhelming advantages in specific energy and cost, the low tap density of sulfur, as well as the hazard of using lithium, restrains the wide applications of Li–S batteries. Considering the rapidly growing of other energy storage technologies, it is urgent and noteworthy to define unique applications where Li–S batteries are indispensable.

Besides the high loading, it has generally accepted that the E/S ratio for current research into Li–S batteries is far from satisfactory. However, strategies to lower the E/S ratio are still in demand. At the end of this review, we attempt to propose several potential solutions to address the electrolyte-starvation problem:

- (1) Learning from current progress in advanced sulfur hosts, a surface-dominant reaction pathway holds a great promise as the formation of Li_2S is facilitated and strongly bound to the surface.^[17,78,79,409] Accordingly, the full dissolution of polysulfides is not as essential as in the case of non-polar hosts. Polysulfide-non-soluble electrolyte can be a candidate.^[70]
- (2) Since the needed amount of electrolyte for the as-mentioned sulfur allotropes (e.g., pPAN@S) is essentially the same as that for LIB cathodes, it is very interesting and important to exert the chemistry of covalent-bonded sulfur. To overcome the drawback of pPAN@S, which is that the sulfur content is low, polysulfide chains, instead of mono-dispersed sulfur atoms, could be grafted or tethered on either organic crosslinkers,^[410] polymeric matrices,^[411] organosulfur solvents,^[412] or even carbon.^[413] These attempts may find to be more promising as long as low E/S ratio is demonstrated in the future.^[414]
- (3) The depletion of electrolyte due to the reactions with lithium metal also accounts for the relatively high E/S ratios that are currently required. Engineering a polymeric or ceramic solid electrolyte thin film on the lithium anode can greatly reduce the possibility of side reactions. There have also

Table 4. Challenges and opportunities for practically viable Li–S batteries.

Fundamental	<p>a) The multielectron conversion chemistry renders the rearrangement and redistribution of energy-storage molecules. The complexity of multielectron conversion chemistry ought to be unveiled through the combination of ab initio calculation, modelling, and advanced operando characterization.</p> <p>b) It is still controversial about the speciation of intermediates. Are they charged ions, neutral ion pairs, or radicals? The distribution and contribution of these species are still unclear. Precise regulation of their adsorption, diffusion, and conversion is consequently quite difficult.</p> <p>c) It has been found that a high overpotential is required for charging and there is always a voltage hysteresis (though it is much smaller than those of Li–O₂ batteries). Does such an energy penalty exist inherently? Can it be overcome through electrocatalysis? These questions need to be answered.^[82,408]</p>
Materials	<p>a) Emerging polar or even electrocatalytic host materials for sulfur possess remarkable performance superiorities. However, the chemical instability of heteroatom-containing polymer or carbon, and possible incompatibility of inorganic materials may contribute to the degradation of overall cell performance. Electrocatalysts or redox mediators must be carefully investigated to prevent undesirable catalysis of decomposition of other components such as the electrolyte and binder.</p> <p>b) Metallic lithium is intrinsically active and vulnerable. Effective and efficient strategies must be developed to protect lithium metal both statically and dynamically. The amount of excess lithium should also be reduced, demanding for extraordinary cyclic efficiency (e.g., Coulombic efficiency of at least 99.93% for 100% excess of lithium).</p> <p>c) Separator is indispensable. However, its weight, thickness, porosity, selectivity, and stability have to be comprehensively considered.</p>
Techniques	<p>a) Systematic integration has a lot of engineering issues and difficulties.</p> <p>b) Thermal management is still lacking. On the contrary, it is crucial to control the temperature field within the whole cell since temperature strongly affects the reaction/transporting kinetics.</p> <p>c) Electrode lug plays a key role in practical cell. Substantial heat is generated upon large current flowing through it. Besides, widely studied 3D assembled/infiltrated electrodes employ a carbonaceous scaffold, which cannot be weld to a normally metal electrode lug.</p> <p>d) Robust technology featuring continuous production and uniform products is strongly recommended. The standards and related test methods are urgently requested.</p> <p>e) The recipe to consistently exert multi-electron conversion chemistry and regulate SEI in a working cell should be exploited. Reliable stabilization of both the cathode and anode is very critical to obtain qualified Li–S batteries. The uniformity of as-fabricated Li–S cells also benefits the battery operation in a safe state.</p> <p>f) Strategies and recipes of battery managements targeting specific applications should be further rationalized not only for Li–S batteries but also other LMBs. Business models for emerging Li–S battery technology are still immature.</p>

been some prototype all-solid-state Li–S batteries.^[315,415] Nevertheless, low Li⁺ ionic conductivity and high interfacial impedance are the remaining intractable issues.^[416]

In conclusion, the development of Li–S batteries, especially high-loading Li–S batteries, significantly promotes the understanding towards the fundamentals of multielectron conversion chemistry and initiates prototype substitutive rechargeable batteries with higher performance than LIBs. We have to admit that Li–S batteries might be overrated without addressing the aforementioned remaining issues. But note that it took at least twenty years for LIBs to be delivered to markets. We believe that Li–S batteries remain in the early stages of the research cycle, and there are tremendous challenges and opportunities to be explored. There is still a long way to go. In such a golden age for battery development, these challenges and opportunities are appealing to deeper understanding, wiser concepts, and better technologies. Since the Li–S battery is a highly integrative system, it demands multidisciplinary, multiscale, and multidimensional exploration. Where is the Li–S battery going next? Be patient, be inquisitive, be diligent, be collaborative, and we will see.

Acknowledgements

This work was supported by National Key Research and Development Program (Nos. 2016YFA0202500, 2016YFA0200101, and

2015CB932500), National Natural Science Foundation of China (Nos. 21422604 and 21676160), and Tsinghua University Initiative Scientific Research Program.

Keywords

composite cathodes, electrolytes, lithium–sulfur batteries, lithium metal anodes, multifunctional separators, polysulfides

Received: January 26, 2017

Revised: February 10, 2017

Published online:

- [1] a) M. Armand, J. M. Tarascon, *Nature* **2008**, 451, 652; b) B. Dunn, H. Kamath, J.-M. Tarascon, *Science* **2011**, 334, 928.
- [2] J. B. Goodenough, Y. Kim, *Chem. Mater.* **2010**, 22, 587.
- [3] N. Nitta, F. Wu, J. T. Lee, G. Yushin, *Mater. Today* **2015**, 18, 252.
- [4] P. G. Bruce, S. A. Freunberger, L. J. Hardwick, J.-M. Tarascon, *Nat. Mater.* **2012**, 11, 19.
- [5] A. Manthiram, Y. Fu, S.-H. Chung, C. Zu, Y.-S. Su, *Chem. Rev.* **2014**, 114, 11751.
- [6] Z. W. Seh, Y. Sun, Q. Zhang, Y. Cui, *Chem. Soc. Rev.* **2016**, 45, 5605.
- [7] D. Herber, J. Ulam, *US Patent 3043896* **1962**.
- [8] X. Ji, K. T. Lee, L. F. Nazar, *Nat. Mater.* **2009**, 8, 500.
- [9] A. Manthiram, S.-H. Chung, C. Zu, *Adv. Mater.* **2015**, 27, 1980.
- [10] Y. Yang, G. Zheng, Y. Cui, *Chem. Soc. Rev.* **2013**, 42, 3018.
- [11] a) X. Fang, H. Peng, *Small* **2015**, 11, 1488; b) W. Kang, N. Deng, J. Ju, Q. Li, D. Wu, X. Ma, L. Li, M. Naebe, B. Cheng, *Nanoscale*

- 2016, 8, 16541; c) Y.-X. Yin, H.-R. Yao, Y.-G. Guo, *Chinese Phys. B* **2016**, 25, 018801; d) X. Zhang, X. Cheng, Q. Zhang, *J. Energy Chem.* **2016**, 25, 967.
- [12] a) H.-J. Peng, J. Liang, L. Zhu, J.-Q. Huang, X.-B. Cheng, X. Guo, W. Ding, W. Zhu, Q. Zhang, *ACS Nano* **2014**, 8, 11280; b) H. Chen, C. Wang, W. Dong, W. Lu, Z. Du, L. Chen, *Nano Lett.* **2015**, 15, 798; c) K. Cai, M.-K. Song, E. J. Cairns, Y. Zhang, *Nano Lett.* **2012**, 12, 6474.
- [13] a) S. Evers, L. F. Nazar, *Chem. Commun.* **2012**, 48, 1233; b) W.-C. Du, Y.-X. Yin, X.-X. Zeng, J.-L. Shi, S.-F. Zhang, L.-J. Wan, Y.-G. Guo, *ACS Appl. Mater. Interfaces* **2016**, 8, 3584.
- [14] X.-B. Cheng, J.-Q. Huang, Q. Zhang, H.-J. Peng, M.-Q. Zhao, F. Wei, *Nano Energy* **2014**, 4, 65.
- [15] a) H.-J. Peng, J.-Q. Huang, M.-Q. Zhao, Q. Zhang, X.-B. Cheng, X.-Y. Liu, W.-Z. Qian, F. Wei, *Adv. Funct. Mater.* **2014**, 24, 2772; b) M.-Q. Zhao, Q. Zhang, J.-Q. Huang, G.-L. Tian, J.-Q. Nie, H.-J. Peng, F. Wei, *Nat. Commun.* **2014**, 5, 3410; c) S. Moon, Y. H. Jung, W. K. Jung, D. S. Jung, J. W. Choi, D. K. Kim, *Adv. Mater.* **2013**, 25, 6547; d) J.-Q. Huang, X.-F. Liu, Q. Zhang, C.-M. Chen, M.-Q. Zhao, S.-M. Zhang, W. Zhu, W.-Z. Qian, F. Wei, *Nano Energy* **2013**, 2, 314; e) L. Sun, M. Li, Y. Jiang, W. Kong, K. Jiang, J. Wang, S. Fan, *Nano Lett.* **2014**, 14, 4044; f) J.-L. Shi, C. Tang, H.-J. Peng, L. Zhu, X.-B. Cheng, J.-Q. Huang, W. Zhu, Q. Zhang, *Small* **2015**, 11, 5243; g) Y. Pan, Y. Zhou, Q. Zhao, Y. Dou, S. Chou, F. Cheng, J. Chen, H. K. Liu, L. Jiang, S. X. Dou, *Nano Energy* **2017**, 33, 205.
- [16] Y. Qiu, W. Li, W. Zhao, G. Li, Y. Hou, M. Liu, L. Zhou, F. Ye, H. Li, Z. Wei, S. Yang, W. Duan, Y. Ye, J. Guo, Y. Zhang, *Nano Lett.* **2014**, 14, 4821.
- [17] Z. Yuan, H.-J. Peng, T.-Z. Hou, J.-Q. Huang, C.-M. Chen, D.-W. Wang, X.-B. Cheng, F. Wei, Q. Zhang, *Nano Lett.* **2016**, 16, 519.
- [18] Z. W. Seh, W. Li, J. J. Cha, G. Zheng, Y. Yang, M. T. McDowell, P.-C. Hsu, Y. Cui, *Nat. Commun.* **2013**, 4, 1331.
- [19] F. Wu, Y. Ye, R. Chen, J. Qian, T. Zhao, L. Li, W. Li, *Nano Lett.* **2015**, 15, 7431.
- [20] M. Hagen, D. Hanselmann, K. Ahlbrecht, R. Maca, D. Gerber, J. Tuebke, *Adv. Energy Mater.* **2015**, 5, 1401986.
- [21] a) A. Rosenman, E. Markevich, G. Salitra, D. Aurbach, A. Garsuch, F. F. Chesneau, *Adv. Energy Mater.* **2015**, 5, 1500212; b) J. W. Choi, D. Aurbach, *Nat. Rev. Mater.* **2016**, 1, 16013.
- [22] J. Song, T. Xu, M. L. Gordin, P. Zhu, D. Lv, Y.-B. Jiang, Y. Chen, Y. Duan, D. Wang, *Adv. Funct. Mater.* **2014**, 24, 1243.
- [23] L. Zhu, W. Zhu, X.-B. Cheng, J.-Q. Huang, H.-J. Peng, S.-H. Yang, Q. Zhang, *Carbon* **2014**, 75, 161.
- [24] a) N. Ding, S. W. Chien, T. S. A. Hor, Z. Liu, Y. Zong, *J. Power Sources* **2014**, 269, 111; b) M. Hagen, P. Fanz, J. Tuebke, *J. Power Sources* **2014**, 264, 30.
- [25] M. A. Pope, I. A. Aksay, *Adv. Energy Mater.* **2015**, 5, 1500124.
- [26] D. Eroglu, K. R. Zavadil, K. G. Gallagher, *J. Electrochem. Soc.* **2015**, 162, A982.
- [27] a) C. Fu, J. Guo, *Curr. Opin. Chem. Eng.* **2016**, 13, 53; b) S. S. Zhang, *Energies* **2012**, 5, 5190; c) X.-B. Cheng, J.-Q. Huang, H.-J. Peng, J.-Q. Nie, X.-Y. Liu, Q. Zhang, F. Wei, *J. Power Sources* **2014**, 253, 263; d) J. Zheng, D. Lv, M. Gu, C. Wang, J.-G. Zhang, J. Liu, J. Xiao, *J. Electrochem. Soc.* **2013**, 160, A2288.
- [28] a) O. Ogoke, G. Wu, X. Wang, A. Casimir, L. Ma, T. Wu, J. Lu, *J. Mater. Chem. A* **2017**, 5, 448; b) S. Rehman, K. Khan, Y. Zhao, Y. Hou, *J. Mater. Chem. A* **2017**, DOI: 10.1039/C6TA10111A.
- [29] a) R. Cao, W. Xu, D. Lv, J. Xiao, J.-G. Zhang, *Adv. Energy Mater.* **2015**, 5, 1402273; b) K. Zhang, G.-H. Lee, M. Park, W. Li, Y.-M. Kang, *Adv. Energy Mater.* **2016**, 6, 1600811; c) R. Zhang, N.-W. Li, X.-B. Cheng, Y.-X. Yin, Q. Zhang, Y.-G. Guo, *Adv. Sci.* **2017**, 4, 1600445.
- [30] J.-Q. Huang, Q. Zhang, F. Wei, *Energy Storage Mater.* **2015**, 1, 127.
- [31] a) Y. Xiang, J. Li, J. Lei, D. Liu, Z. Xie, D. Qu, K. Li, T. Deng, H. Tang, *ChemSusChem* **2016**, 9, 3023; b) N. Deng, W. Kang, Y. Liu, J. Ju, D. Wu, L. Li, B. S. Hassan, B. Cheng, *J. Power Sources* **2016**, 331, 132.
- [32] J.-Q. Huang, Y.-Z. Sun, Y.-F. Wang, Q. Zhang, *Acta Chim. Sinica.* **2017**, DOI: 10.6023/A16080454.
- [33] a) J. Scheers, S. Fantini, P. Johansson, *J. Power Sources* **2014**, 255, 204; b) Z. Lin, C. Liang, *J. Mater. Chem. A* **2015**, 3, 936; c) S. Zhang, K. Ueno, K. Dokko, M. Watanabe, *Adv. Energy Mater.* **2015**, 5, 1500117.
- [34] Y.-X. Yin, S. Xin, Y.-G. Guo, L.-J. Wan, *Angew. Chem., Int. Ed.* **2013**, 52, 13186.
- [35] a) S. Evers, L. F. Nazar, *Accounts. Chem. Res.* **2013**, 46, 1135; b) A. Manthiram, Y. Fu, Y.-S. Su, *Accounts. Chem. Res.* **2013**, 46, 1125.
- [36] Y. Son, J.-S. Lee, Y. Son, J.-H. Jang, J. Cho, *Adv. Energy Mater.* **2015**, 5, 1500110.
- [37] S. Xin, L. Gu, N.-H. Zhao, Y.-X. Yin, L.-J. Zhou, Y.-G. Guo, L.-J. Wan, *J. Am. Chem. Soc.* **2012**, 134, 18510.
- [38] J. Guo, Y. Xu, C. Wang, *Nano Lett.* **2011**, 11, 4288.
- [39] J. Wang, Y.-S. He, J. Yang, *Adv. Mater.* **2015**, 27, 569.
- [40] J. L. Wang, J. Yang, J. Y. Xie, N. X. Xu, *Adv. Mater.* **2002**, 14, 963.
- [41] L. Wang, X. He, J. Li, M. Chen, J. Gao, C. Jiang, *Electrochim. Acta* **2012**, 72, 114.
- [42] B. Duan, W. Wang, A. Wang, K. Yuan, Z. Yu, H. Zhao, J. Qiu, Y. Yang, *J. Mater. Chem. A* **2013**, 1, 13261.
- [43] a) Y. V. Mikhaylik, J. R. Akridge, *J. Electrochem. Soc.* **2004**, 151, A1969; b) W.-T. Xu, H.-J. Peng, J.-Q. Huang, C.-Z. Zhao, X.-B. Cheng, Q. Zhang, *ChemSusChem* **2015**, 8, 2892.
- [44] X. He, J. Ren, L. Wang, W. Pu, C. Jiang, C. Wan, *J. Power Sources* **2009**, 190, 154.
- [45] Q. Pang, X. Liang, C. Y. Kwok, L. F. Nazar, *Nat. Energy* **2016**, 1, 16132.
- [46] X. Ji, L. F. Nazar, *J. Mater. Chem.* **2010**, 20, 9821.
- [47] a) S. C. Han, M. S. Song, H. Lee, H. S. Kim, H. J. Ahn, J. Y. Lee, *J. Electrochem. Soc.* **2003**, 150, A889; b) L. Yuan, H. Yuan, X. Qiu, L. Chen, W. Zhu, *J. Power Sources* **2009**, 189, 1141; c) L. Ji, M. Rao, S. Aloni, L. Wang, E. J. Cairns, Y. Zhang, *Energy Environ. Sci.* **2011**, 4, 5053; d) X. Liu, Q. Zhang, J. Huang, S. Zhang, H. Peng, F. Wei, *J. Energy Chem.* **2013**, 22, 341; e) L. Zeng, Y. Yao, J. Shi, Y. Jiang, W. Li, L. Gu, Y. Yu, *Energy Storage Mater.* **2016**, 5, 50.
- [48] G. Zheng, Y. Yang, J. J. Cha, S. S. Hong, Y. Cui, *Nano Lett.* **2011**, 11, 4462.
- [49] H. Wang, Y. Yang, Y. Liang, J. T. Robinson, Y. Li, A. Jackson, Y. Cui, H. Dai, *Nano Lett.* **2011**, 11, 2644.
- [50] a) J.-Z. Wang, L. Lu, M. Choucair, J. A. Stride, X. Xu, H.-K. Liu, *J. Power Sources* **2011**, 196, 7030; b) Y. Cao, X. Li, I. A. Aksay, J. Lemmon, Z. Nie, Z. Yang, J. Liu, *Phys. Chem. Chem. Phys.* **2011**, 13, 7660; c) Y.-X. Wang, L. Huang, L.-C. Sun, S.-Y. Xie, G.-L. Xu, S.-R. Chen, Y.-F. Xu, J.-T. Li, S.-L. Chou, S.-X. Dou, S.-G. Sun, *J. Mater. Chem.* **2012**, 22, 4744; d) N. Li, M. Zheng, H. Lu, Z. Hu, C. Shen, X. Chang, G. Ji, J. Cao, Y. Shi, *Chem. Commun.* **2012**, 48, 4106; e) C. Tang, B.-Q. Li, Q. Zhang, L. Zhu, H.-F. Wang, J.-L. Shi, F. Wei, *Adv. Funct. Mater.* **2016**, 26, 577.
- [51] a) J. Schuster, G. He, B. Mandlmeier, T. Yim, K. T. Lee, T. Bein, L. F. Nazar, *Angew. Chem., Int. Ed.* **2012**, 51, 3591; b) C. Liang, N. J. Dudney, J. Y. Howe, *Chem. Mater.* **2009**, 21, 4724; c) B. Ding, C. Yuan, L. Shen, G. Xu, P. Nie, X. Zhang, *Chem. Eur. J.* **2013**, 19, 1013; d) N. Tachikawa, K. Yamauchi, E. Takashima, J.-W. Park, K. Dokko, M. Watanabe, *Chem. Commun.* **2011**, 47, 8157; e) G. He, S. Evers, X. Liang, M. Cuisinier, A. Garsuch, L. F. Nazar, *ACS Nano* **2013**, 7, 10920; f) F. Xu, J. Xu, H. Xu, Y. Lu, H. Yang, Z. Tang, Z. Lu, R. Fu, D. Wu, *Energy Storage Mater.* **2017**, 7, 8; g) Y. Wei, Y. Tao, Z. Kong, L. Liu, J. Wang, W. Qiao, L. Ling, D. Long, *Energy Storage Mater.* **2016**, 5, 171.

- [52] J. T. Lee, Y. Zhao, S. Thieme, H. Kim, M. Oschatz, L. Borchardt, A. Magasinski, W.-I. Cho, S. Kaskel, G. Yushin, *Adv. Mater.* **2013**, *25*, 4573.
- [53] a) X. Yang, L. Zhang, F. Zhang, Y. Huang, Y. Chen, *ACS Nano* **2014**, *8*, 5208; b) M.-Q. Zhao, X.-F. Liu, Q. Zhang, G.-L. Tian, J.-Q. Huang, W. Zhu, F. Wei, *ACS Nano* **2012**, *6*, 10759; c) D. Wang, Y. Yu, W. Zhou, H. Chen, F. J. DiSalvo, D. A. Muller, H. D. Abruna, *Phys. Chem. Chem. Phys.* **2013**, *15*, 9051; d) C. Tang, Q. Zhang, M.-Q. Zhao, J.-Q. Huang, X.-B. Cheng, G.-L. Tian, H.-J. Peng, F. Wei, *Adv. Mater.* **2014**, *26*, 6100; e) M.-Q. Zhao, H.-J. Peng, G.-L. Tian, Q. Zhang, J.-Q. Huang, X.-B. Cheng, C. Tang, F. Wei, *Adv. Mater.* **2014**, *26*, 7051.
- [54] a) L. Borchardt, M. Oschatz, S. Kaskel, *Chem. Eur. J.* **2016**, *22*, 7324; b) J. Liang, Z.-H. Sun, F. Li, H.-M. Cheng, *Energy Storage Mater.* **2016**, *2*, 76; c) J.-G. Wang, K. Xie, B. Wei, *Nano Energy* **2015**, *15*, 413; d) D.-W. Wang, Q. Zeng, G. Zhou, L. Yin, F. Li, H.-M. Cheng, I. R. Gentle, G. Q. M. Lu, *J. Mater. Chem. A* **2013**, *1*, 9382; e) Z. Li, Y. Huang, L. Yuan, Z. Hao, Y. Huang, *Carbon* **2015**, *92*, 41; f) Q. Zhang, X.-b. Cheng, J.-q. Huang, H.-j. Peng, F. Wei, *New Carbon Mater.* **2014**, *29*, 241.
- [55] W. Lv, Z. Li, Y. Deng, Q.-H. Yang, F. Kang, *Energy Storage Mater.* **2016**, *2*, 107.
- [56] R. Xu, J. Lu, K. Amine, *Adv. Energy Mater.* **2015**, *5*, 1500408.
- [57] M. Hagen, P. Schiffels, M. Hammer, S. Doerfler, J. Tuebke, M. J. Hoffmann, H. Althues, S. Kaskel, *J. Electrochem. Soc.* **2013**, *160*, A1205.
- [58] a) S. Walus, C. Barchasz, R. Bouchet, J.-C. Lepretre, J.-F. Colin, J.-F. Martin, E. Elkaim, C. Baetz, F. Alloin, *Adv. Energy Mater.* **2015**, *5*, 1500165; b) S. Walus, C. Barchasz, J.-F. Colin, J.-F. Martin, E. Elkaim, J.-C. Lepretre, F. Alloin, *Chem. Commun.* **2013**, *49*, 7899.
- [59] M. Cuisinier, P.-E. Cabelguen, S. Evers, G. He, M. Kolbeck, A. Garsuch, T. Bolin, M. Balasubramanian, L. F. Nazar, *J. Phys. Chem. Lett.* **2013**, *4*, 3227.
- [60] a) M. U. M. Patel, I. Arcon, G. Aquilanti, L. Stievano, G. Mali, R. Dominko, *ChemPhysChem* **2014**, *15*, 894; b) T. A. Pascal, K. H. Wujcik, J. Velasco-Velez, C. Wu, A. A. Teran, M. Kapilashrami, J. Cabana, J. Guo, M. Salmeron, N. Balsara, D. Prendergast, *J. Phys. Chem. Lett.* **2014**, *5*, 1547.
- [61] X. Yu, H. Pan, Y. Zhou, P. Northrup, J. Xiao, S. Bak, M. Liu, K.-W. Nam, D. Qu, J. Liu, T. Wu, X.-Q. Yang, *Adv. Energy Mater.* **2015**, *5*, 1500072.
- [62] a) Q. Wang, J. Zheng, E. Walter, H. Pan, D. Lv, P. Zuo, H. Chen, Z. D. Deng, B. Y. Liaw, X. Yu, X. Yang, J.-G. Zhang, J. Liu, J. Xiao, *J. Electrochem. Soc.* **2015**, *162*, A474; b) J. Xiao, J. Z. Hu, H. Chen, M. Vijayakumar, J. Zheng, H. Pan, E. D. Walter, M. Hu, X. Deng, J. Feng, B. Y. Liaw, M. Gu, Z. D. Deng, D. Lu, S. Xu, C. Wang, J. Liu, *Nano Lett.* **2015**, *15*, 3309.
- [63] M. U. M. Patel, R. Demir-Cakan, M. Morcrette, J.-M. Tarascon, M. Gaberscek, R. Dominko, *ChemSusChem* **2013**, *6*, 1177.
- [64] Q. Zou, Y.-C. Lu, *J. Phys. Chem. Lett.* **2016**, *7*, 1518.
- [65] a) S. S. Zhang, *J. Power Sources* **2013**, *231*, 153; b) M. Wild, L. O'Neill, T. Zhang, R. Purkayastha, G. Minton, M. Marinescu, G. J. Offer, *Energy Environ. Sci.* **2015**, *8*, 3477.
- [66] a) N. B. Aetukuri, B. D. McCloskey, J. M. Garcia, L. E. Krupp, V. Viswanathan, A. C. Luntz, *Nat. Chem.* **2015**, *7*, 50; b) L. Johnson, C. Li, Z. Liu, Y. Chen, S. A. Freunberger, P. C. Ashok, B. B. Praveen, K. Dholakia, J.-M. Tarascon, P. G. Bruce, *Nat. Chem.* **2014**, *6*, 1091.
- [67] C. M. Burke, V. Pande, A. Khetan, V. Viswanathan, B. D. McCloskey, *Proc. Natl. Acad. Sci. U. S. A.* **2015**, *112*, 9293.
- [68] B. D. Adams, C. Radtke, R. Black, M. L. Trudeau, K. Zaghbi, L. F. Nazar, *Energy Environ. Sci.* **2013**, *6*, 1772.
- [69] a) M. Cuisinier, C. Hart, M. Balasubramanian, A. Garsuch, L. F. Nazar, *Adv. Energy Mater.* **2015**, *5*, 1401801; b) Y.-C. Lu, Q. He, H. A. Gasteiger, *J. Phys. Chem. C* **2014**, *118*, 5733.
- [70] M. Cuisinier, P. E. Cabelguen, B. D. Adams, A. Garsuch, M. Balasubramanian, L. F. Nazar, *Energy Environ. Sci.* **2014**, *7*, 2697.
- [71] H.-J. Peng, G. Zhang, X. Chen, Z.-W. Zhang, W.-T. Xu, J.-Q. Huang, Q. Zhang, *Angew. Chem., Int. Ed.* **2016**, *55*, 12990.
- [72] X. Tao, J. Wang, C. Liu, H. Wang, H. Yao, G. Zheng, Z. W. Seh, Q. Cai, W. Li, G. Zhou, C. Zu, Y. Cui, *Nat. Commun.* **2016**, *7*, 11203.
- [73] a) H.-J. Peng, Q. Zhang, *Angew. Chem., Int. Ed.* **2015**, *54*, 11018; b) Q. Pang, X. Liang, C. Y. Kwok, L. F. Nazar, *J. Electrochem. Soc.* **2015**, *162*, A2567; c) M. Liu, F. Ye, W. Li, H. Li, Y. Zhang, *Nano Res.* **2016**, *9*, 94.
- [74] a) L. Xiao, Y. Cao, J. Xiao, B. Schwenzer, M. H. Engelhard, L. V. Saraf, Z. Nie, G. J. Exarhos, J. Liu, *Adv. Mater.* **2012**, *24*, 1176; b) Y. Yang, G. Yu, J. J. Cha, H. Wu, M. Vosgueritchian, Y. Yao, Z. Bao, Y. Cui, *ACS Nano* **2011**, *5*, 9187; c) J. Wang, J. Chen, K. Konstantinov, L. Zhao, S. H. Ng, G. X. Wang, Z. P. Guo, H. K. Liu, *Electrochim. Acta* **2006**, *51*, 4634; d) X. Liang, Y. Liu, Z. Wen, L. Huang, X. Wang, H. Zhang, *J. Power Sources* **2011**, *196*, 6951; e) W. Li, Q. Zhang, G. Zheng, Z. W. Seh, H. Yao, Y. Cui, *Nano Lett.* **2013**, *13*, 5534.
- [75] H. Chen, W. Dong, J. Ge, C. Wang, X. Wu, W. Lu, L. Chen, *Sci. Rep.* **2013**, *3*, 1910.
- [76] a) F. Sun, J. Wang, H. Chen, W. Li, W. Qiao, D. Long, L. Ling, *ACS Appl. Mater. Interfaces* **2013**, *5*, 5630; b) C.-P. Yang, Y.-X. Yin, H. Ye, K.-C. Jiang, J. Zhang, Y.-G. Guo, *ACS Appl. Mater. Interfaces* **2014**, *6*, 8789; c) H.-J. Peng, T.-Z. Hou, Q. Zhang, J.-Q. Huang, X.-B. Cheng, M.-Q. Guo, Z. Yuan, L.-Y. He, F. Wei, *Adv. Mater. Interfaces* **2014**, *1*, 1400227; d) L. Ji, M. Rao, H. Zheng, L. Zhang, Y. Li, W. Duan, J. Guo, E. J. Cairns, Y. Zhang, *J. Am. Chem. Soc.* **2011**, *133*, 18522; e) T.-Z. Hou, X. Chen, H.-J. Peng, J.-Q. Huang, B.-Q. Li, Q. Zhang, B. Li, *Small* **2016**, *12*, 3283; f) S. Yuan, J. L. Bao, L. Wang, Y. Xia, D. G. Truhlar, Y. Wang, *Adv. Energy Mater.* **2016**, *6*, 1501733; g) K. A. See, Y.-S. Jun, J. A. Gerbec, J. K. Sprafke, F. Wudl, G. D. Stucky, R. Seshadri, *ACS Appl. Mater. Interfaces* **2014**, *6*, 10908; h) X.-G. Sun, X. Wang, R. T. Mayes, S. Dai, *ChemSusChem* **2012**, *5*, 2079; i) T.-Z. Hou, H.-J. Peng, J.-Q. Huang, Q. Zhang, B. Li, *2D Mater.* **2015**, *2*, 014011; j) Z. Cao, J. Zhang, Y. Ding, Y. Li, M. Shi, H. Yue, Y. Qiao, Y. Yin, S. Yang, *J. Mater. Chem. A* **2016**, *4*, 8636; k) L. Li, G. Zhou, L. Yin, N. Koratkar, F. Li, H.-M. Cheng, *Carbon* **2016**, *108*, 120; l) M.-q. Guo, J.-q. Huang, X.-y. Kong, H.-j. Peng, H. Shut, F.-y. Qian, L. Zhu, W.-c. Zhu, Q. Zhang, *New Carbon Mater.* **2016**, *31*, 352.
- [77] a) S. Evers, T. Yim, L. F. Nazar, *J. Phys. Chem. C* **2012**, *116*, 19653; b) X. Tao, J. Wang, Z. Ying, Q. Cai, G. Zheng, Y. Gan, H. Huang, Y. Xia, C. Liang, W. Zhang, Y. Cui, *Nano Lett.* **2014**, *14*, 5288; c) Z. Liang, G. Zheng, W. Li, Z. W. Seh, H. Yao, K. Yan, D. Kong, Y. Cui, *ACS Nano* **2014**, *8*, 5249; d) X. Wang, T. Gao, X. Fan, F. Han, Y. Wu, Z. Zhang, J. Li, C. Wang, *Adv. Funct. Mater.* **2016**, *26*, 7164.
- [78] X. Liang, C. Hart, Q. Pang, A. Garsuch, T. Weiss, L. F. Nazar, *Nat. Commun.* **2015**, *6*, 5682.
- [79] Q. Pang, D. Kundu, M. Cuisinier, L. F. Nazar, *Nat. Commun.* **2014**, *5*, 4759.
- [80] a) S. S. Zhang, D. T. Tran, *J. Mater. Chem. A* **2016**, *4*, 4371; b) H. Wang, Q. Zhang, H. Yao, Z. Liang, H.-W. Lee, P.-C. Hsu, G. Zheng, Y. Cui, *Nano Lett.* **2014**, *14*, 7138; c) Y. Lu, X. Li, J. Liang, L. Hu, Y. Zhu, Y. Qian, *Nanoscale* **2016**, *8*, 17616; d) Z. Ma, Z. Li, K. Hu, D. Liu, J. Huo, S. Wang, *J. Power Sources* **2016**, *325*, 71.
- [81] Q. Pang, D. Kundu, L. F. Nazar, *Mater. Horiz.* **2016**, *3*, 130.
- [82] G. Zhou, H. Tian, Y. Jin, X. Tao, B. Liu, R. Zhang, Z. W. Seh, D. Zhuo, Y. Liu, J. Sun, J. Zhao, C. Zu, D. S. Wu, Q. Zhang, Y. Cui, *Proc. Natl. Acad. Sci. U. S. A.* **2017**, *114*, 840.
- [83] a) X. Liang, A. Garsuch, L. F. Nazar, *Angew. Chem., Int. Ed.* **2015**, *54*, 3907; b) Z. Hao, L. Yuan, C. Chen, J. Xiang, Y. Li, Z. Huang, P. Hu, Y. Huang, *J. Mater. Chem. A* **2016**, *4*, 17711; c) Z. Cui,

- C. Zu, W. Zhou, A. Manthiram, J. B. Goodenough, *Adv. Mater.* **2016**, *28*, 6926.
- [84] a) R. Demir-Cakan, M. Morcrette, F. Nouar, C. Davoisne, T. Devic, D. Gonbeau, R. Dominko, C. Serre, G. Ferey, J.-M. Tarascon, *J. Am. Chem. Soc.* **2011**, *133*, 16154; b) J. Zheng, J. Tian, D. Wu, M. Gu, W. Xu, C. Wang, F. Gao, M. H. Engelhard, J.-G. Zhang, J. Liu, J. Xiao, *Nano Lett.* **2014**, *14*, 2345; c) Y.-J. Li, J.-M. Fan, M.-S. Zheng, Q.-F. Dong, *Energy Environ. Sci.* **2016**, *9*, 1998; d) J. Zhou, R. Li, X. Fan, Y. Chen, R. Han, W. Li, J. Zheng, B. Wang, X. Li, *Energy Environ. Sci.* **2014**, *7*, 2715; e) M. Zhang, C. Yu, C. Zhao, X. Song, X. Han, S. Liu, C. Hao, J. Qiu, *Energy Storage Mater.* **2016**, *5*, 223; f) T. Chen, B. Cheng, G. Zhu, R. Chen, Y. Hu, L. Ma, H. Lv, Y. Wang, J. Liang, Z. Tie, Z. Jin, J. Liu, *Nano Lett.* **2017**, *17*, 437.
- [85] X. Liu, J.-Q. Huang, Q. Zhang, L. Mai, *Adv. Mater.* **2017**, *29*, 1601759.
- [86] a) Y. Sun, N. Liu, Y. Cui, *Nat. Energy* **2016**, *1*, 16071; b) L. Ma, K. E. Hendrickson, S. Wei, L. A. Archer, *Nano Today* **2015**, *10*, 315; c) P. G. Bruce, B. Scrosati, J.-M. Tarascon, *Angew. Chem., Int. Ed.* **2008**, *47*, 2930.
- [87] C. Zhang, W. Lv, Y. Tao, Q.-H. Yang, *Energy Environ. Sci.* **2015**, *8*, 1390.
- [88] A. Magasinski, P. Dixon, B. Hertzberg, A. Kvit, J. Ayala, G. Yushin, *Nat. Mater.* **2010**, *9*, 353.
- [89] a) C. Wang, H. Wu, Z. Chen, M. T. McDowell, Y. Cui, Z. Bao, *Nat. Chem.* **2013**, *5*, 1042; b) Y. Li, K. Yan, H.-W. Lee, Z. Lu, N. Liu, Y. Cui, *Nat. Energy* **2016**, *1*, 15029.
- [90] I. Kovalenko, B. Zdyrko, A. Magasinski, B. Hertzberg, Z. Milicev, R. Burtovyy, I. Luzinov, G. Yushin, *Science* **2011**, *334*, 75.
- [91] S.-L. Chou, Y. Pan, J.-Z. Wang, H.-K. Liu, S.-X. Dou, *Phys. Chem. Chem. Phys.* **2014**, *16*, 20347.
- [92] a) M. J. Lacey, F. Jeschull, K. Edstrom, D. Brandell, *J. Phys. Chem. C* **2014**, *118*, 25890; b) Y.-J. Choi, K.-W. Kim, H.-J. Ahn, J.-H. Ahn, *J. Alloy. Compd.* **2008**, *449*, 313; c) S. E. Cheon, K. S. Ko, J. H. Cho, S. W. Kim, E. Y. Chin, H. T. Kim, *J. Electrochem. Soc.* **2003**, *150*, A796.
- [93] Z. W. Seh, Q. Zhang, W. Li, G. Zheng, H. Yao, Y. Cui, *Chem. Sci.* **2013**, *4*, 3673.
- [94] M. J. Lacey, F. Jeschull, K. Edstrom, D. Brandell, *Chem. Commun.* **2013**, *49*, 8531.
- [95] Y. Jung, S. Kim, *Electrochem. Commun.* **2007**, *9*, 249.
- [96] W. Chen, T. Qian, J. Xiong, N. Xu, X. Liu, J. Liu, J. Zhou, X. Shen, T. Yang, Y. Chen, C. Yan, *Adv. Mater.* **2017**, *29*, 1605160.
- [97] S. S. Zhang, *J. Electrochem. Soc.* **2012**, *159*, A1226.
- [98] a) J. Sun, Y. Huang, W. Wang, Z. Yu, A. Wang, K. Yuan, *Electrochim. Acta* **2008**, *53*, 7084; b) J. Sun, Y. Huang, W. Wang, Z. Yu, A. Wang, K. Yuan, *Electrochem. Commun.* **2008**, *10*, 930.
- [99] J. Wang, Z. Yao, C. W. Monroe, J. Yang, Y. Nuli, *Adv. Funct. Mater.* **2013**, *23*, 1194.
- [100] W. Zhou, H. Chen, Y. Yu, D. Wang, Z. Cui, F. J. DiSalvo, H. D. Abruna, *ACS Nano* **2013**, *7*, 8801.
- [101] F. Zeng, W. Wang, A. Wang, K. Yuan, Z. Jin, Y.-s. Yang, *ACS Appl. Mater. Interfaces* **2015**, *7*, 26257.
- [102] P. Bhattacharya, M. I. Nandasiri, D. Lv, A. M. Schwarz, J. T. Darsell, W. A. Henderson, D. A. Tomalia, J. Liu, J.-G. Zhang, J. Xiao, *Nano Energy* **2016**, *19*, 176.
- [103] Y. Ma, H. Zhang, B. Wu, M. Wang, X. Li, H. Zhang, *Sci. Rep.* **2015**, *5*, 14949.
- [104] Y.-S. Su, A. Manthiram, *Electrochim. Acta* **2012**, *77*, 272.
- [105] L. Wang, Y. Zhao, M. L. Thomas, H. R. Byon, *Adv. Funct. Mater.* **2014**, *24*, 2248.
- [106] Y. Fu, A. Manthiram, *J. Phys. Chem. C* **2012**, *116*, 8910.
- [107] X. Liang, M. R. Kaiser, K. Konstantinov, R. Tandiono, Z. Wang, C. Chen, H.-K. Liu, S.-X. Dou, J. Wang, *ACS Appl. Mater. Interfaces* **2016**, *8*, 25251.
- [108] T. Xu, J. Song, M. L. Gordin, H. Sohn, Z. Yu, S. Chen, D. Wang, *ACS Appl. Mater. Interfaces* **2013**, *5*, 11355.
- [109] J. Song, M. L. Gordin, T. Xu, S. Chen, Z. Yu, H. Sohn, J. Lu, Y. Ren, Y. Duan, D. Wang, *Angew. Chem., Int. Ed.* **2015**, *54*, 4325.
- [110] H. Sohn, M. L. Gordin, M. Regula, D. H. Kim, Y. S. Jung, J. Song, D. Wang, *J. Power Sources* **2016**, *302*, 70.
- [111] M. S. Whittingham, *Chem. Rev.* **2004**, *104*, 4271.
- [112] D. S. Jung, T. H. Hwang, J. H. Lee, H. Y. Koo, R. A. Shakoor, R. Kahraman, Y. N. Jo, M.-S. Park, J. W. Choi, *Nano Lett.* **2014**, *14*, 4418.
- [113] Y. Tao, Y. Wei, Y. Liu, J. Wang, W. Qiao, L. Ling, D. Long, *Energy Environ. Sci.* **2016**, *9*, 3230.
- [114] X. Ye, J. Ma, Y.-S. Hu, H. Wei, F. Ye, *J. Mater. Chem. A* **2016**, *4*, 775.
- [115] a) C. Zhang, D.-H. Liu, W. Lv, D.-W. Wang, W. Wei, G.-M. Zhou, S. Wang, F. Li, B.-H. Li, F. Kang, Q.-H. Yang, *Nanoscale* **2015**, *7*, 5592; b) H. Li, X. Yang, X. Wang, M. Liu, F. Ye, J. Wang, Y. Qiu, W. Li, Y. Zhang, *Nano Energy* **2015**, *12*, 468.
- [116] J.-L. Shi, H.-J. Peng, L. Zhu, W. Zhu, Q. Zhang, *Carbon* **2015**, *92*, 96.
- [117] J. Song, Z. Yu, M. L. Gordin, D. Wang, *Nano Lett.* **2016**, *16*, 864.
- [118] Y.-L. Ding, P. Kopold, K. Hahn, P. A. van Aken, J. Maier, Y. Yu, *Adv. Funct. Mater.* **2016**, *26*, 1112.
- [119] Z. Zhang, L.-L. Kong, S. Liu, G.-R. Li, X.-P. Gao, *Adv. Energy Mater.* **2017**, *7*, 1602543.
- [120] J. W. F. To, Z. Chen, H. Yao, J. He, K. Kim, H.-H. Chou, L. Pan, J. Wilcox, Y. Cui, Z. Bao, *ACS Cent. Sci.* **2015**, *1*, 68.
- [121] K. Zhang, F. Qin, Y. Lai, J. Li, X. Lei, M. Wang, H. Lu, J. Fang, *ACS Appl. Mater. Interfaces* **2016**, *8*, 6072.
- [122] A. Schneider, C. Weidmann, C. Suchomski, H. Sommer, J. Janek, T. Brezesinski, *Chem. Mater.* **2015**, *27*, 1674.
- [123] a) H. Li, H. Zhou, *Chem. Commun.* **2012**, *48*, 1201; b) J. Wang, X. Sun, *Energy Environ. Sci.* **2012**, *5*, 5163.
- [124] N. Liu, H. Wu, M. T. McDowell, Y. Yao, C. Wang, Y. Cui, *Nano Lett.* **2012**, *12*, 3315.
- [125] J. Wang, W. Li, F. Wang, Y. Xia, A. M. Asiri, D. Zhao, *Nanoscale* **2014**, *6*, 3217.
- [126] S. Li, J. Niu, Y. C. Zhao, K. P. So, C. Wang, C. A. Wang, J. Li, *Nat. Commun.* **2015**, *6*, 7872.
- [127] a) C. Nan, Z. Lin, H. Liao, M.-K. Song, Y. Li, E. J. Cairns, *J. Am. Chem. Soc.* **2014**, *136*, 4659; b) C. Wang, J.-j. Chen, Y.-n. Shi, M.-s. Zheng, Q.-f. Dong, *Electrochim. Acta* **2010**, *55*, 7010.
- [128] a) F. Wu, J. Chen, R. Chen, S. Wu, L. Li, S. Chen, T. Zhao, *J. Phys. Chem. C* **2011**, *115*, 6057; b) W. Zhou, X. Xiao, M. Cai, L. Yang, *Nano Lett.* **2014**, *14*, 5250.
- [129] a) N. Ding, Y. Lum, S. Chen, S. W. Chien, T. S. A. Hor, Z. Liu, Y. Zong, *J. Mater. Chem. A* **2015**, *3*, 1853; b) Q. Sun, B. He, X.-Q. Zhang, A.-H. Lu, *ACS Nano* **2015**, *9*, 8504.
- [130] N. Jayaprakash, J. Shen, S. S. Moganty, A. Corona, L. A. Archer, *Angew. Chem., Int. Ed.* **2011**, *50*, 5904.
- [131] a) W. Zhou, Y. Yu, H. Chen, F. J. DiSalvo, H. D. Abruna, *J. Am. Chem. Soc.* **2013**, *135*, 16736; b) X. Zhou, F. Chen, J. Yang, *J. Energy Chem.* **2015**, *24*, 448.
- [132] a) J. Zhang, H. Hu, Z. Li, X. W. Lou, *Angew. Chem., Int. Ed.* **2016**, *55*, 3982; b) X. Wang, G. Li, J. Li, Y. Zhang, A. Wook, A. Yu, Z. Chen, *Energy Environ. Sci.* **2016**, *9*, 2533.
- [133] N. Liu, Z. Lu, J. Zhao, M. T. McDowell, H.-W. Lee, W. Zhao, Y. Cui, *Nat. Nanotechnol.* **2014**, *9*, 187.
- [134] F. Wu, J. T. Lee, F. Fan, N. Nitta, H. Kim, T. Zhu, G. Yushin, *Adv. Mater.* **2015**, *27*, 5579.
- [135] D. Lv, J. Zheng, Q. Li, X. Xie, S. Ferrara, Z. Nie, L. B. Mehdi, N. D. Browning, J.-G. Zhang, G. L. Graff, J. Liu, J. Xiao, *Adv. Energy Mater.* **2015**, *5*, 1402290.
- [136] a) Y. Shi, W. Lv, S. Niu, Y. He, G. Zhou, G. Chen, B. Li, Q.-H. Yang, F. Kang, *Chem. Asian J.* **2016**, *11*, 1343; b) C. Lai, Z. Wu, X. Gu, C. Wang, K. Xi, R. V. Kumar, S. Zhang, *ACS Appl. Mater. Interfaces*

- 2015, 7, 23885; c) S. Liu, K. Xie, Z. Chen, Y. Li, X. Hong, J. Xu, L. Zhou, J. Yuan, C. Zheng, *J. Mater. Chem. A* **2015**, 3, 11395; d) M. Yu, R. Li, Y. Tong, Y. Li, C. Li, J.-D. Hong, G. Shi, *J. Mater. Chem. A* **2015**, 3, 9609; e) L. Suo, Y. Zhu, F. Han, T. Gao, C. Luo, X. Fan, Y.-S. Hu, C. Wang, *Nano Energy* **2015**, 13, 467.
- [137] G.-C. Li, G.-R. Li, S.-H. Ye, X.-P. Gao, *Adv. Energy Mater.* **2012**, 2, 1238.
- [138] W. Li, Z. Liang, Z. Lu, H. Yao, Z. W. Seh, K. Yan, G. Zheng, Y. Cui, *Adv. Energy Mater.* **2015**, 5, 1500211.
- [139] M. Wang, W. Wang, A. Wang, K. Yuan, L. Miao, X. Zhang, Y. Huang, Z. Yu, J. Qiu, *Chem. Commun.* **2013**, 49, 10263.
- [140] L.-X. Miao, W.-K. Wang, A.-B. Wang, K.-G. Yuan, Y.-S. Yang, *J. Mater. Chem. A* **2013**, 1, 11659.
- [141] Z. Sun, M. Xiao, S. Wang, D. Han, S. Song, G. Chen, Y. Meng, *J. Mater. Chem. A* **2014**, 2, 15938.
- [142] Z. Gong, Q. Wu, F. Wang, X. Li, X. Fan, H. Yang, Z. Luo, *RSC Adv.* **2015**, 5, 96862.
- [143] J. Jiang, J. Zhu, W. Ai, X. Wang, Y. Wang, C. Zou, W. Huang, T. Yu, *Nat. Commun.* **2015**, 6, 8622.
- [144] X. Liang, L. F. Nazar, *ACS Nano* **2016**, 10, 4192.
- [145] X. Liang, C. Y. Kwok, F. Lodi-Marzano, Q. Pang, M. Cuisinier, H. Huang, C. J. Hart, D. Houtarde, K. Kaup, H. Sommer, T. Brezesinski, J. Janek, L. F. Nazar, *Adv. Energy Mater.* **2016**, 6, 1501636.
- [146] Z. W. Seh, J. H. Yu, W. Li, P.-C. Hsu, H. Wang, Y. Sun, H. Yao, Q. Zhang, Y. Cui, *Nat. Commun.* **2014**, 5, 5017.
- [147] S.-T. Myung, Y. Hitoshi, Y.-K. Sun, *J. Mater. Chem.* **2011**, 21, 9891.
- [148] H.-J. Peng, W.-T. Xu, L. Zhu, D.-W. Wang, J.-Q. Huang, X.-B. Cheng, Z. Yuan, F. Wei, Q. Zhang, *Adv. Funct. Mater.* **2016**, 26, 6351.
- [149] J. Ma, Z. Fang, Y. Yan, Z. Yang, L. Gu, Y.-S. Hu, H. Li, Z. Wang, X. Huang, *Adv. Energy Mater.* **2015**, 5, 1500046.
- [150] G. Ai, Y. Dai, W. Mao, H. Zhao, Y. Fu, X. Song, Y. En, V. S. Battaglia, V. Srinivasan, G. Liu, *Nano Lett.* **2016**, 16, 5365.
- [151] X. Yang, Y. Chen, M. Wang, H. Zhang, X. Li, H. Zhang, *Adv. Funct. Mater.* **2016**, 26, 8427.
- [152] S. Thieme, J. Brueckner, I. Bauer, M. Oschatz, L. Borchardt, H. Althues, S. Kaskel, *J. Mater. Chem. A* **2013**, 1, 9225.
- [153] C. Hoffmann, S. Thieme, J. Brueckner, M. Oschatz, T. Biemelt, G. Mondin, H. Althues, S. Kaskel, *ACS Nano* **2014**, 8, 12130.
- [154] P. Strubel, S. Thieme, T. Biemelt, A. Helmer, M. Oschatz, J. Brueckner, H. Althues, S. Kaskel, *Adv. Funct. Mater.* **2015**, 25, 287.
- [155] a) M. He, L.-X. Yuan, W.-X. Zhang, X.-L. Hu, Y.-H. Huang, *J. Phys. Chem. C* **2011**, 115, 15703; b) M.-K. Song, Y. Zhang, E. J. Cairns, *Nano Lett.* **2013**, 13, 5891.
- [156] Z. Zhang, W. Bao, H. Lu, M. Jia, K. Xie, Y. Lai, J. Li, *ECS Electrochemistry Letters* **2012**, 1, A34.
- [157] a) Y. Li, D. Ye, W. Liu, B. Shi, R. Guo, H. Zhao, H. Pei, J. Xu, J. Xie, *ACS Appl. Mater. Interfaces* **2016**, 8, 28566; b) J. Pan, G. Xu, B. Ding, J. Han, H. Dou, X. Zhang, *RSC Adv.* **2015**, 5, 13709; c) K. Mi, S. Chen, B. Xi, S. Kai, Y. Jiang, J. Feng, Y. Qian, S. Xiong, *Adv. Funct. Mater.* **2017**, 27, 1604265.
- [158] a) W. Bao, Z. Zhang, Y. Gan, X. Wang, J. Li, *J. Energy Chem.* **2013**, 22, 790; b) A. Ghosh, R. Manjunatha, R. Kumar, S. Mitra, *ACS Appl. Mater. Interfaces* **2016**, 8, 33775.
- [159] L. Wang, Z. Dong, D. Wang, F. Zhang, J. Jin, *Nano Lett.* **2013**, 13, 6244.
- [160] Q. Pang, X. Liang, C. Y. Kwok, J. Kulisch, L. F. Nazar, *Adv. Energy Mater.* **2017**, 7, 1601630.
- [161] G. Li, C. Wang, W. Cai, Z. Lin, Z. Li, S. Zhang, *NPG Asia Mater.* **2016**, 8, e317.
- [162] a) Q. Li, H. Yang, L. Xie, J. Yang, Y. Nuli, J. Wang, *Chem. Commun.* **2016**, 52, 13479; b) T. Qiu, H. Shao, W. Wang, H. Zhang, A. Wang, Z. Feng, Y. Huang, *RSC Adv.* **2016**, 6, 102626; c) Y.-Q. Lu, J.-T. Li, X.-X. Peng, T. Zhang, Y.-P. Deng, Z.-Y. Wu, L. Deng, L. Huang, X.-D. Zhou, S.-G. Sun, *Electrochem. Commun.* **2016**, 72, 79.
- [163] G. Li, M. Ling, Y. Ye, Z. Li, J. Guo, Y. Yao, J. Zhu, Z. Lin, S. Zhang, *Adv. Energy Mater.* **2015**, 5, 1500878.
- [164] J. Liu, D. G. Galpaya, L. Yan, M. Sun, Z. Lin, C. Yan, C. Liang, S. Zhang, *Energy Environ. Sci.* **2017**, DOI: 10.1039/C6EE03033E.
- [165] K. Jin, X. Zhou, L. Zhang, X. Xin, G. Wan, Z. Liu, *J. Phys. Chem. C* **2013**, 117, 21112.
- [166] J.-Q. Huang, H.-J. Peng, X.-Y. Liu, J.-Q. Nie, X.-B. Cheng, Q. Zhang, F. Wei, *J. Mater. Chem. A* **2014**, 2, 10869.
- [167] G. Zhou, L. Li, C. Ma, S. Wang, Y. Shi, N. Koratkar, W. Ren, F. Li, H.-M. Cheng, *Nano Energy* **2015**, 11, 356.
- [168] Z. Yuan, H.-J. Peng, J.-Q. Huang, X.-Y. Liu, D.-W. Wang, X.-B. Cheng, Q. Zhang, *Adv. Funct. Mater.* **2014**, 24, 6105.
- [169] J. Cao, C. Chen, Q. Zhao, N. Zhang, Q. Lu, X. Wang, Z. Niu, J. Chen, *Adv. Mater.* **2016**, 28, 9629.
- [170] G. Zhou, E. Paek, G. S. Hwang, A. Manthiram, *Nat. Commun.* **2015**, 6, 7760.
- [171] M. Hagen, S. Doerfler, H. Althues, J. Tuebke, M. J. Hoffmann, S. Kaskel, K. Pinkwart, *J. Power Sources* **2012**, 213, 239.
- [172] L. Ma, S. Wei, H. L. Zhuang, K. E. Hendrickson, R. G. Hennig, L. A. Archer, *J. Mater. Chem. A* **2015**, 3, 19857.
- [173] Q. Zhao, X. Hu, K. Zhang, N. Zhang, Y. Hu, J. Chen, *Nano Lett.* **2015**, 15, 721.
- [174] G. Zhou, F. Li, H.-M. Cheng, *Energy Environ. Sci.* **2014**, 7, 1307.
- [175] R. Elazari, G. Salitra, A. Garsuch, A. Panchenko, D. Aurbach, *Adv. Mater.* **2011**, 23, 5641.
- [176] S. S. Zhang, *Electrochem. Commun.* **2013**, 31, 10.
- [177] a) L. Miao, W. Wang, K. Yuan, Y. Yang, A. Wang, *Chem. Commun.* **2014**, 50, 13231; b) J. Zhang, J. Xiang, Z. Dong, Y. Liu, Y. Wu, C. Xu, G. Du, *Electrochim. Acta* **2014**, 116, 146; c) S. Lu, Y. Chen, X. Wu, Z. Wang, L. Lv, W. Qin, L. Jiang, *RSC Adv.* **2014**, 4, 18052.
- [178] S. Lu, Y. Cheng, X. Wu, J. Liu, *Nano Lett.* **2013**, 13, 2485.
- [179] A. Schneider, C. Suchomski, H. Sommer, J. Janek, T. Brezesinski, *J. Mater. Chem. A* **2015**, 3, 20482.
- [180] W. Zhou, B. Guo, H. Gao, J. B. Goodenough, *Adv. Energy Mater.* **2016**, 6, 1502059.
- [181] X. Han, Y. Xu, X. Chen, Y.-C. Chen, N. Weadock, J. Wan, H. Zhu, Y. Liu, H. Li, G. Rubloff, C. Wang, L. Hu, *Nano Energy* **2013**, 2, 1197.
- [182] Z. Zhang, Q. Li, K. Zhang, W. Chen, Y. Lai, J. Li, *J. Power Sources* **2015**, 290, 159.
- [183] K. Xie, K. Zhang, Y. Han, K. Yuan, Q. Song, J.-g. Wang, C. Shen, X. Liu, B. Wei, *Electrochim. Acta* **2016**, 210, 415.
- [184] H. Xu, A. Manthiram, *Nano Energy* **2017**, 33, 124.
- [185] M. Hagen, G. Feisthamm, P. Fanz, H. T. Grossmann, S. Doerfler, J. Tuebke, M. J. Hoffmann, D. Boerner, M. Joos, H. Althues, S. Kaskel, *J. Electrochem. Soc.* **2013**, 160, A996.
- [186] a) J. Brueckner, S. Thieme, H. T. Grossmann, S. Doerfler, H. Althues, S. Kaskel, *J. Power Sources* **2014**, 268, 82; b) M. Hagen, S. Doerfler, P. Fanz, T. Berger, R. Speck, J. Tuebke, H. Althues, M. J. Hoffmann, C. Scherr, S. Kaskel, *J. Power Sources* **2013**, 224, 260.
- [187] K. Xi, B. Chen, H. Li, R. Xie, C. Gao, C. Zhang, R. V. Kumar, J. Robertson, *Nano Energy* **2015**, 12, 538.
- [188] a) Y. Zhao, W. Wu, J. Li, Z. Xu, L. Guan, *Adv. Mater.* **2014**, 26, 5113; b) F. Jin, S. Xiao, L. Lu, Y. Wang, *Nano Lett.* **2016**, 16, 440.
- [189] G. Zhou, D.-W. Wang, F. Li, P.-X. Hou, L. Yin, C. Liu, G. Q. Lu, I. R. Gentle, H.-M. Cheng, *Energy Environ. Sci.* **2012**, 5, 8901.
- [190] Z. Li, J. Zhang, X. W. Lou, *Angew. Chem., Int. Ed.* **2015**, 54, 12886.
- [191] L. Qie, A. Manthiram, *Adv. Mater.* **2015**, 27, 1694.
- [192] a) R. Raccichini, A. Varzi, S. Passerini, B. Scrosati, *Nat. Mater.* **2015**, 14, 271; b) L. Ji, P. Meduri, V. Agubra, X. Xiao, M. Alcoutlabi, *Adv. Energy Mater.* **2016**, 6, 1502159; c) M. Yu, R. Li, M. Wu, G. Shi, *Energy Storage Mater.* **2015**, 1, 51.

- [193] S. Lu, Y. Chen, X. Wu, Z. Wang, Y. Li, *Sci. Rep.* **2014**, *4*, 4629.
- [194] B. Papandrea, X. Xu, Y. Xu, C.-Y. Chen, Z. Lin, G. Wang, Y. Luo, M. Liu, Y. Huang, L. Mai, X. Duan, *Nano Res.* **2016**, *9*, 240.
- [195] a) Y. Jiang, M. Lu, X. Ling, Z. Jiao, L. Chen, L. Chen, P. Hu, B. Zhao, *J. Alloy. Compd.* **2015**, *645*, 509; b) J. He, Y. Chen, W. Lv, K. Wen, C. Xu, W. Zhang, W. Qin, W. He, *ACS Energy Lett.* **2016**, *1*, 820.
- [196] D. H. Wang, D. Xie, T. Yang, Y. Zhong, X. L. Wang, X. H. Xia, C. D. Gu, J. P. Tu, *J. Power Sources* **2016**, *313*, 233.
- [197] G. Zhou, L.-C. Yin, D.-W. Wang, L. Li, S. Pei, I. R. Gentle, F. Li, H.-M. Cheng, *ACS Nano* **2013**, *7*, 5367.
- [198] L. Zhu, H.-J. Peng, J. Liang, J.-Q. Huang, C.-M. Chen, X. Guo, W. Zhu, P. Li, Q. Zhang, *Nano Energy* **2015**, *11*, 746.
- [199] P.-Y. Zhai, J.-Q. Huang, L. Zhu, J.-L. Shi, W. Zhu, Q. Zhang, *Carbon* **2017**, *111*, 493.
- [200] Q. Sun, X. Fang, W. Weng, J. Deng, P. Chen, J. Ren, G. Guan, M. Wang, H. Peng, *Angew. Chem., Int. Ed.* **2015**, *54*, 10539.
- [201] G. Zhou, Y. Zhao, A. Manthiram, *Adv. Energy Mater.* **2015**, *5*, 1402263.
- [202] a) S.-Y. Lee, K.-H. Choi, W.-S. Choi, Y. H. Kwon, H.-R. Jung, H.-C. Shin, J. Y. Kim, *Energy Environ. Sci.* **2013**, *6*, 2414; b) D. Yu, K. Goh, H. Wang, L. Wei, W. Jiang, Q. Zhang, L. Dai, Y. Chen, *Nat. Nanotechnol.* **2014**, *9*, 555.
- [203] X. Fang, W. Weng, J. Ren, H. Peng, *Adv. Mater.* **2016**, *28*, 491.
- [204] W. G. Chong, J. Q. Huang, Z. L. Xu, X. Qin, X. Wang, J. K. Kim, *Adv. Funct. Mater.* **2017**, *27*, 1604815.
- [205] M. Yao, K. Okuno, T. Iwaki, S. Tanase, K. Harada, M. Kato, K. Emura, T. Sakai, *J. Power Sources* **2007**, *171*, 1033.
- [206] S.-H. Chung, A. Manthiram, *Electrochim. Acta* **2013**, *107*, 569.
- [207] Y. Zhao, Y. Zhang, Z. Bakkenov, P. Chen, *Solid State Ionics* **2013**, *234*, 40.
- [208] D. The Nam Long, M. Ghaznavi, Y. Zhao, Y. Zhang, A. Konarov, M. Sadhu, R. Tangirala, P. Chen, *J. Power Sources* **2013**, *241*, 61.
- [209] M. R. Kaiser, X. Liang, H.-K. Liu, S.-X. Dou, J.-Z. Wang, *Carbon* **2016**, *103*, 163.
- [210] J. Wang, S. Cheng, W. Li, S. Zhang, H. Li, Z. Zheng, F. Li, L. Shi, H. Lin, Y. Zhang, *J. Power Sources* **2016**, *321*, 193.
- [211] S. H. Cho, S. M. Cho, K. Y. Bae, B. H. Kim, W. Y. Yoon, *J. Power Sources* **2017**, *341*, 366.
- [212] X.-B. Cheng, H.-J. Peng, J.-Q. Huang, L. Zhu, S.-H. Yang, Y. Liu, H.-W. Zhang, W. Zhu, F. Wei, Q. Zhang, *J. Power Sources* **2014**, *261*, 264.
- [213] H. Nara, T. Yokoshima, H. Mikuriya, S. Tsuda, T. Momma, T. Osaka, *J. Electrochem. Soc.* **2017**, *164*, A5026.
- [214] S.-H. Chung, A. Manthiram, *Electrochem. Commun.* **2014**, *38*, 91.
- [215] S.-H. Chung, A. Manthiram, *J. Mater. Chem. A* **2013**, *1*, 9590.
- [216] S. S. Zhang, J. A. Read, *J. Power Sources* **2012**, *200*, 77.
- [217] N. He, L. Zhong, M. Xiao, S. Wang, D. Han, Y. Meng, *Sci. Rep.* **2016**, *6*, 33871.
- [218] S. Walus, C. Barchasz, R. Bouchet, J. F. Martin, J. C. Lepretre, F. Alloin, *Electrochim. Acta* **2016**, *211*, 697.
- [219] C. Barchasz, F. Mesguich, J. Dijon, J.-C. Lepretre, S. Patoux, F. Alloin, *J. Power Sources* **2012**, *217*, 19.
- [220] a) Q. Pang, L. F. Nazar, *ACS Nano* **2016**, *10*, 4111; b) Q. Pang, J. Tang, H. Huang, X. Liang, C. Hart, K. C. Tam, L. F. Nazar, *Adv. Mater.* **2015**, *27*, 6021; c) X. Liang, Y. Rangom, C. Y. Kwok, Q. Pang, L. F. Nazar, *Adv. Mater.* **2017**, *29*, 1603040.
- [221] a) K. Jiang, J. Wang, Q. Li, L. Liu, C. Liu, S. Fan, *Adv. Mater.* **2011**, *23*, 1154; b) Q. Zhang, J.-Q. Huang, W.-Z. Qian, Y.-Y. Zhang, F. Wei, *Small* **2013**, *9*, 1237.
- [222] L. Li, Z. P. Wu, H. Sun, D. Chen, J. Gao, S. Suresh, P. Chow, C. V. Singh, N. Koratkar, *ACS Nano* **2015**, *9*, 11342.
- [223] R. Fang, S. Zhao, P. Hou, M. Cheng, S. Wang, H.-M. Cheng, C. Liu, F. Li, *Adv. Mater.* **2016**, *28*, 3374.
- [224] F. Wu, E. Zhao, D. Gordon, Y. Xiao, C. Hu, G. Yushin, *Adv. Mater.* **2016**, *28*, 6365.
- [225] Z. Chen, W. Ren, L. Gao, B. Liu, S. Pei, H.-M. Cheng, *Nat. Mater.* **2011**, *10*, 424.
- [226] G. Hu, C. Xu, Z. Sun, S. Wang, H.-M. Cheng, F. Li, W. Ren, *Adv. Mater.* **2016**, *28*, 1603.
- [227] G. Ren, S. Li, Z.-X. Fan, J. Warzywoda, Z. Fan, *J. Mater. Chem. A* **2016**, *4*, 16507.
- [228] L. Zielke, C. Barchasz, S. Walus, F. Alloin, J. C. Lepretre, A. Spettl, V. Schmidt, A. Hilger, I. Manke, J. Banhart, R. Zengerle, S. Thiele, *Sci. Rep.* **2015**, *5*, 10921.
- [229] R. D. Rauh, K. M. Abraham, G. F. Pearson, J. K. Surprenant, S. B. Brummer, *J. Electrochem. Soc.* **1979**, *126*, 523.
- [230] S. S. Zhang, D. T. Tran, *J. Power Sources* **2012**, *211*, 169.
- [231] Y. Fu, Y.-S. Su, A. Manthiram, *Angew. Chem., Int. Ed.* **2013**, *52*, 6930.
- [232] S.-H. Chung, C.-H. Chang, A. Manthiram, *ACS Nano* **2016**, *10*, 10462.
- [233] H. Yao, G. Zheng, P.-C. Hsu, D. Kong, J. J. Cha, W. Li, Z. W. Seh, M. T. McDowell, K. Yan, Z. Liang, V. K. Narasimhan, Y. Cui, *Nat. Commun.* **2014**, *5*, 3943.
- [234] C. Zu, L. Li, J. Guo, S. Wang, D. Fan, A. Manthiram, *J. Phys. Chem. Lett.* **2016**, *7*, 1392.
- [235] G. Zhou, Y. Zhao, C. Zu, A. Manthiram, *Nano Energy* **2015**, *12*, 240.
- [236] X. Wang, T. Gao, F. Han, Z. Ma, Z. Zhang, J. Li, C. Wang, *Nano Energy* **2016**, *30*, 700.
- [237] S. Li, T. Mou, G. Ren, J. Warzywoda, Z. Wei, B. Wang, Z. Fan, *J. Mater. Chem. A* **2017**, *5*, 1650.
- [238] X.-W. Wu, H. Xie, Q. Deng, H.-X. Wang, H. Sheng, Y.-X. Yin, W.-X. Zhou, R.-L. Li, Y.-G. Guo, *ACS Appl. Mater. Interfaces* **2017**, *9*, 1553.
- [239] H. Xu, L. Qie, A. Manthiram, *Nano Energy* **2016**, *26*, 224.
- [240] Z. Chang, H. Dou, B. Ding, J. Wang, Y. Wang, X. Hao, D. R. MacFarlane, *J. Mater. Chem. A* **2017**, *5*, 250.
- [241] L. Fan, H. L. Zhuang, K. Zhang, V. R. Cooper, Q. Li, Y. Lu, *Adv. Sci.* **2016**, *3*, 1600175.
- [242] L. Li, L. Chen, S. Mukherjee, J. Gao, H. Sun, Z. Liu, X. Ma, T. Gupta, C. V. Singh, W. Ren, H.-M. Cheng, N. Koratkar, *Adv. Mater.* **2017**, *29*, 1602734.
- [243] J. Gao, M. A. Lowe, Y. Kiya, H. D. Abruna, *J. Phys. Chem. C* **2011**, *115*, 25132.
- [244] B. Zhang, X. Qin, G. R. Li, X. P. Gao, *Energy Environ. Sci.* **2010**, *3*, 1531.
- [245] C.-P. Yang, Y.-X. Yin, Y.-G. Guo, L.-J. Wan, *J. Am. Chem. Soc.* **2015**, *137*, 2215.
- [246] Z. Li, L. Yuan, Z. Yi, Y. Sun, Y. Liu, Y. Jiang, Y. Shen, Y. Xin, Z. Zhang, Y. Huang, *Adv. Energy Mater.* **2014**, *4*, 1301473.
- [247] a) E. Markevich, G. Salitra, A. Rosenman, Y. Talyosef, F. Chesneau, D. Aurbach, *J. Mater. Chem. A* **2015**, *3*, 19873; b) D.-W. Wang, G. Zhou, F. Li, K.-H. Wu, G. Q. Lu, H.-M. Cheng, I. R. Gentle, *Phys. Chem. Chem. Phys.* **2012**, *14*, 8703; c) Y. Xu, Y. Wen, Y. Zhu, K. Gaskell, K. A. Cychosz, B. Eichhorn, K. Xu, C. Wang, *Adv. Funct. Mater.* **2015**, *25*, 4312; d) C. Fu, B. M. Wong, K. N. Bozhilov, J. Guo, *Chem. Sci.* **2016**, *7*, 1224.
- [248] a) W. Xu, J. Wang, F. Ding, X. Chen, E. Nasybutin, Y. Zhang, J.-G. Zhang, *Energy Environ. Sci.* **2014**, *7*, 513; b) H. Kim, G. Jeong, Y.-U. Kim, J.-H. Kim, C.-M. Park, H.-J. Sohn, *Chem. Soc. Rev.* **2013**, *42*, 9011; c) M. D. Tikekar, S. Choudhury, Z. Tu, L. A. Archer, *Nat. Energy* **2016**, *1*, 16114; d) J. Lang, L. Qi, Y. Luo, H. Wu, *Energy Storage Mater.* **2017**, *7*, 115; e) J.-G. Zhang, W. Xu, W. A. Henderson, *Lithium Metal Anodes and Rechargeable Lithium Metal Batteries*, Vol. 249, Springer, **2017**.
- [249] X.-B. Cheng, R. Zhang, C.-Z. Zhao, F. Wei, J.-G. Zhang, Q. Zhang, *Adv. Sci.* **2016**, *3*, 1500213.

- [250] Z. Li, S. Zhang, S. Terada, X. Ma, K. Ikeda, Y. Kamei, C. Zhang, K. Dokko, M. Watanabe, *ACS Appl. Mater. Interfaces* **2016**, *8*, 16053.
- [251] J. Brueckner, S. Thieme, F. Boettger-Hiller, I. Bauer, H. T. Grossmann, P. Strubel, H. Althues, S. Spange, S. Kaskel, *Adv. Funct. Mater.* **2014**, *24*, 1284.
- [252] D. Lv, P. Yan, Y. Shao, Q. Li, S. Ferrara, H. Pan, G. L. Graff, B. Polzin, C. Wang, J.-g. Zhang, J. Liu, J. Xiao, *Chem. Commun.* **2015**, *51*, 13454.
- [253] A. Bhargav, M. Wu, Y. Fu, *J. Electrochem. Soc.* **2016**, *163*, A1543.
- [254] Y. Yang, M. T. McDowell, A. Jackson, J. J. Cha, S. S. Hong, Y. Cui, *Nano Lett.* **2010**, *10*, 1486.
- [255] M. Hagen, E. Quiroga-Gonzalez, S. Doerfler, G. Fahrer, J. Tuebke, M. J. Hoffmann, H. Althues, R. Speck, M. Krampfert, S. Kaskel, H. Foell, *J. Power Sources* **2014**, *248*, 1058.
- [256] J. Hassoun, B. Scrosati, *Angew. Chem., Int. Ed.* **2010**, *49*, 2371.
- [257] B. Duan, W. Wang, A. Wang, Z. Yu, H. Zhao, Y. Yang, *J. Mater. Chem. A* **2014**, *2*, 308.
- [258] W. Cai, J. Zhou, G. Li, K. Zhang, X. Liu, C. Wang, H. Zhou, Y. Zhu, Y. Qian, *ACS Appl. Mater. Interfaces* **2016**, *8*, 27679.
- [259] D. Lv, Y. Shao, T. Lozano, W. D. Bennett, G. L. Graff, B. Polzin, J. Zhang, M. H. Engelhard, N. T. Saenz, W. A. Henderson, P. Bhattacharya, J. Liu, J. Xiao, *Adv. Energy Mater.* **2015**, *5*, 1400993.
- [260] L. Qie, C. Zu, A. Manthiram, *Adv. Energy Mater.* **2016**, *6*, 1502459.
- [261] X.-B. Cheng, C. Yan, J.-Q. Huang, P. Li, L. Zhu, L. Zhao, Y. Zhang, W. Zhu, S.-T. Yang, Q. Zhang, *Energy Storage Mater.* **2017**, *6*, 18.
- [262] a) C. Brissot, M. Rosso, J. N. Chazalviel, P. Baudry, S. Lascaud, *Electrochim. Acta* **1998**, *43*, 1569; b) V. Fleury, J. N. Chazalviel, M. Rosso, B. Sapoval, *J. Electroanal. Chem.* **1990**, *290*, 249; c) J. N. Chazalviel, *Phys. Rev. A* **1990**, *42*, 7355.
- [263] J. Heine, S. Krueger, C. Hartnig, U. Wietelmann, M. Winter, P. Bieker, *Adv. Energy Mater.* **2014**, *4*, 1300815.
- [264] M.-H. Ryou, Y. M. Lee, Y. Lee, M. Winter, P. Bieker, *Adv. Funct. Mater.* **2015**, *25*, 834.
- [265] C.-P. Yang, Y.-X. Yin, S.-F. Zhang, N.-W. Li, Y.-G. Guo, *Nat. Commun.* **2015**, *6*, 8058.
- [266] Q. Yun, Y.-B. He, W. Lv, Y. Zhao, B. Li, F. Kang, Q.-H. Yang, *Adv. Mater.* **2016**, *28*, 6932.
- [267] L. L. Lu, J. Ge, J.-N. Yang, S.-M. Chen, H.-B. Yao, F. Zhou, S.-H. Yu, *Nano Lett.* **2016**, *16*, 4431.
- [268] K. Yan, Z. Lu, H.-W. Lee, F. Xiong, P.-C. Hsu, Y. Li, J. Zhao, S. Chu, Y. Cui, *Nat. Energy* **2016**, *1*, 16010.
- [269] X.-B. Cheng, H.-J. Peng, J.-Q. Huang, R. Zhang, C.-Z. Zhao, Q. Zhang, *ACS Nano* **2015**, *9*, 6373.
- [270] R. Zhang, X.-B. Cheng, C.-Z. Zhao, H.-J. Peng, J.-L. Shi, J.-Q. Huang, J. Wang, F. Wei, Q. Zhang, *Adv. Mater.* **2016**, *28*, 2155.
- [271] X. Ji, D.-Y. Liu, D. G. Prendiville, Y. Zhang, X. Liu, G. D. Stucky, *Nano Today* **2012**, *7*, 10.
- [272] Z. Liang, G. Zheng, C. Liu, N. Liu, W. Li, K. Yan, H. Yao, P.-C. Hsu, S. Chu, Y. Cui, *Nano Lett.* **2015**, *15*, 2910.
- [273] X.-B. Cheng, T.-Z. Hou, R. Zhang, H.-J. Peng, C.-Z. Zhao, J.-Q. Huang, Q. Zhang, *Adv. Mater.* **2016**, *28*, 2888.
- [274] Z. Liang, D. Lin, J. Zhao, Z. Lu, Y. Liu, C. Liu, Y. Lu, H. Wang, K. Yan, X. Tao, Y. Cui, *Proc. Natl. Acad. Sci. U. S. A.* **2016**, *113*, 2862.
- [275] Y. Liu, D. Lin, Z. Liang, J. Zhao, K. Yan, Y. Cui, *Nat. Commun.* **2016**, *7*, 10992.
- [276] D. Lin, Y. Liu, Z. Liang, H.-W. Lee, J. Sun, H. Wang, K. Yan, J. Xie, Y. Cui, *Nat. Nanotechnol.* **2016**, *11*, 626.
- [277] X.-B. Cheng, H.-J. Peng, J.-Q. Huang, F. Wei, Q. Zhang, *Small* **2014**, *10*, 4257.
- [278] X. Zhang, W. Wang, A. Wang, Y. Huang, K. Yuan, Z. Yu, J. Qiu, Y. Yang, *J. Mater. Chem. A* **2014**, *2*, 11660.
- [279] S. Jin, S. Xin, L. Wang, Z. Du, L. Cao, J. Chen, X. Kong, M. Gong, J. Lu, Y. Zhu, H. Ji, R. S. Ruoff, *Adv. Mater.* **2016**, *28*, 9094.
- [280] E. Peled, *J. Electrochem. Soc.* **1979**, *126*, 2047.
- [281] D. Wang, W. Zhang, W. Zheng, X. Cui, T. Rojo, Q. Zhang, *Adv. Sci.* **2017**, *4*, 1600168.
- [282] D. Aurbach, E. Pollak, R. Elazari, G. Salitra, C. S. Kelley, J. Affinito, *J. Electrochem. Soc.* **2009**, *156*, A694.
- [283] S. S. Zhang, *Electrochim. Acta* **2012**, *70*, 344.
- [284] S. Xiong, K. Xie, Y. Diao, X. Hong, *J. Power Sources* **2013**, *236*, 181.
- [285] S. Xiong, K. Xie, Y. Diao, X. Hong, *J. Power Sources* **2014**, *246*, 840.
- [286] W. Li, H. Yao, K. Yan, G. Zheng, Z. Liang, Y.-M. Chiang, Y. Cui, *Nat. Commun.* **2015**, *6*, 7436.
- [287] C.-Z. Zhao, X.-B. Cheng, R. Zhang, H.-J. Peng, J.-Q. Huang, R. Ran, Z.-H. Huang, F. Wei, Q. Zhang, *Energy Storage Mater.* **2016**, *3*, 77.
- [288] C. Yan, X.-B. Cheng, C.-Z. Zhao, J.-Q. Huang, S.-T. Yang, Q. Zhang, *J. Power Sources* **2016**, *327*, 212.
- [289] X.-B. Cheng, C. Yan, X. Chen, C. Guan, J.-Q. Huang, H.-J. Peng, R. Zhang, S.-T. Yang, Q. Zhang, *Chem* **2017**, *2*, 258.
- [290] a) S. S. Zhang, *J. Power Sources* **2016**, *322*, 99; b) N. Ding, L. Zhou, C. Zhou, D. Geng, J. Yang, S. W. Chien, Z. Liu, M.-F. Ng, A. Yu, T. S. A. Hor, M. B. Sullivan, Y. Zong, *Sci. Rep.* **2016**, *6*, 33154.
- [291] A. Jozwiuk, B. B. Berkes, T. Weiss, H. Sommer, J. Janek, T. Brezesinski, *Energy Environ. Sci.* **2016**, *9*, 2603.
- [292] X. Chen, T.-Z. Hou, B. Li, C. Yan, L. Zhu, C. Guan, X.-B. Cheng, H.-J. Peng, J.-Q. Huang, Q. Zhang, *Energy Storage Mater.* **2017**, DOI: 10.1016/j.ensm.2017.01.003.
- [293] F. Ding, W. Xu, G. L. Graff, J. Zhang, M. L. Sushko, X. Chen, Y. Shao, M. H. Engelhard, Z. Nie, J. Xiao, X. Liu, P. V. Sushko, J. Liu, J.-G. Zhang, *J. Am. Chem. Soc.* **2013**, *135*, 4450.
- [294] Y. Lu, Z. Tu, L. A. Archer, *Nat. Mater.* **2014**, *13*, 961.
- [295] R. Miao, J. Yang, X. Feng, H. Jia, J. Wang, Y. Nuli, *J. Power Sources* **2014**, *271*, 291.
- [296] J. Chen, K. S. Han, W. A. Henderson, K. C. Lau, M. Vijayakumar, T. Dzwiniel, H. Pan, L. A. Curtiss, J. Xiao, K. T. Mueller, Y. Shao, J. Liu, *Adv. Energy Mater.* **2016**, *6*, 1600160.
- [297] Q. Ma, B. Tong, Z. Fang, X. Qi, W. Feng, J. Nie, Y.-S. Hu, H. Li, X. Huang, L. Chen, Z. Zhou, *J. Electrochem. Soc.* **2016**, *163*, A1776.
- [298] F. Wu, J. Qian, R. Chen, J. Lu, L. Li, H. Wu, J. Chen, T. Zhao, Y. Ye, K. Amine, *ACS Appl. Mater. Interfaces* **2014**, *6*, 15542.
- [299] a) J. Heine, P. Hilbig, X. Qi, P. Niehoff, M. Winter, P. Bieker, *J. Electrochem. Soc.* **2015**, *162*, A1094; b) X.-Q. Zhang, X.-B. Cheng, X. Chen, C. Yan, Q. Zhang, *Adv. Funct. Mater.* **2017**, *27*, 1605989.
- [300] a) Y. Yamada, K. Furukawa, K. Sodeyama, K. Kikuchi, M. Yaegashi, Y. Tateyama, A. Yamada, *J. Am. Chem. Soc.* **2014**, *136*, 5039; b) Q. Ma, Z. Fang, P. Liu, J. Ma, X. Qi, W. Feng, J. Nie, Y.-S. Hu, H. Li, X. Huang, L. Chen, Z. Zhou, *ChemElectroChem* **2016**, *3*, 531; c) P. Liu, Q. Ma, Z. Fang, J. Ma, Y.-S. Hu, Z.-B. Zhou, H. Li, X.-J. Huang, L.-Q. Chen, *Chinese Phys. B* **2016**, *25*, 078203.
- [301] a) J. H. Shin, E. J. Cairns, *J. Power Sources* **2008**, *177*, 537; b) L. Wang, J. Liu, S. Yuan, Y. Wang, Y. Xia, *Energy Environ. Sci.* **2016**, *9*, 224.
- [302] J. Qian, W. A. Henderson, W. Xu, P. Bhattacharya, M. Engelhard, O. Borodin, J.-G. Zhang, *Nat. Commun.* **2015**, *6*, 6362.
- [303] L. Suo, Y.-S. Hu, H. Li, M. Armand, L. Chen, *Nat. Commun.* **2013**, *4*, 1481.
- [304] J. Zheng, M. Gu, H. Chen, P. Meduri, M. H. Engelhard, J.-G. Zhang, J. Liu, J. Xiao, *J. Mater. Chem. A* **2013**, *1*, 8464.
- [305] F. Wu, Q. Zhu, R. Chen, N. Chen, Y. Chen, L. Li, *Electrochim. Acta* **2015**, *184*, 356.
- [306] F. Wu, Q. Zhu, R. Chen, N. Chen, Y. Chen, Y. Ye, J. Qian, L. Li, *J. Power Sources* **2015**, *296*, 10.
- [307] W. Weng, V. G. Pol, K. Amine, *Adv. Mater.* **2013**, *25*, 1608.
- [308] M. L. Gordin, F. Dai, S. Chen, T. Xu, J. Song, D. Tang, N. Azimi, Z. Zhang, D. Wang, *ACS Appl. Mater. Interfaces* **2014**, *6*, 8006.
- [309] N. Azimi, Z. Xue, I. Bloom, M. L. Gordin, D. Wang, T. Daniel, C. Takoudis, Z. Zhang, *ACS Appl. Mater. Interfaces* **2015**, *7*, 9169.

- [310] C. Zu, N. Azimi, Z. Zhang, A. Manthiram, *J. Mater. Chem. A* **2015**, *3*, 14864.
- [311] J. J. Hu, G. K. Long, S. Liu, G. R. Li, X. P. Gao, *Chem. Commun.* **2014**, *50*, 14647.
- [312] H. Kim, F. Wu, J. T. Lee, N. Nitta, H.-T. Lin, M. Oschatz, W. I. Cho, S. Kaskel, O. Borodin, G. Yushin, *Adv. Energy Mater.* **2015**, *5*, 1401792.
- [313] R. Cao, J. Chen, K. S. Han, W. Xu, D. Mei, P. Bhattacharya, M. H. Engelhard, K. T. Mueller, J. Liu, J.-G. Zhang, *Adv. Funct. Mater.* **2016**, *26*, 3059.
- [314] Z. Lin, Z. Liu, W. Fu, N. J. Dudney, C. Liang, *Adv. Funct. Mater.* **2013**, *23*, 1064.
- [315] Z. Lin, Z. Liu, N. J. Dudney, C. Liang, *ACS Nano* **2013**, *7*, 2829.
- [316] C. Zu, A. Manthiram, *J. Phys. Chem. Lett.* **2014**, *5*, 2522.
- [317] C. Zu, A. Dolocan, P. Xiao, S. Stauffer, G. Henkelman, A. Manthiram, *Adv. Energy Mater.* **2016**, *6*, 1501933.
- [318] G. Zheng, S. W. Lee, Z. Liang, H.-W. Lee, K. Yan, H. Yao, H. Wang, W. Li, S. Chu, Y. Cui, *Nat. Nanotechnol.* **2014**, *9*, 618.
- [319] N.-W. Li, Y.-X. Yin, C.-P. Yang, Y.-G. Guo, *Adv. Mater.* **2016**, *28*, 1853.
- [320] H.-K. Jing, L.-L. Kong, S. Liu, G.-R. Li, X.-P. Gao, *J. Mater. Chem. A* **2015**, *3*, 12213.
- [321] A. C. Kozen, C.-F. Lin, A. J. Pearse, M. A. Schroeder, X. Han, L. Hu, S.-B. Lee, G. W. Rubloff, M. Noked, *ACS Nano* **2015**, *9*, 5884.
- [322] C. Huang, J. Xiao, Y. Shao, J. Zheng, W. D. Bennett, D. Lu, L. V. Saraf, M. Engelhard, L. Ji, J. Zhang, X. Li, G. L. Graff, J. Liu, *Nat. Commun.* **2014**, *5*, 3015.
- [323] G. Ma, Z. Wen, M. Wu, C. Shen, Q. Wang, J. Jin, X. Wu, *Chem. Commun.* **2014**, *50*, 14209.
- [324] G. Ma, Z. Wen, Q. Wang, C. Shen, J. Jin, X. Wu, *J. Mater. Chem. A* **2014**, *2*, 19355.
- [325] S.-K. Lee, S.-M. Oh, E. Park, B. Scrosati, J. Hassoun, M.-S. Park, Y.-J. Kim, H. Kim, I. Belharouak, Y.-K. Sun, *Nano Lett.* **2015**, *15*, 2863.
- [326] B. Li, S. Li, J. Xu, S. Yang, *Energy Environ. Sci.* **2016**, *9*, 2025.
- [327] a) H. Lee, M. Yanilmaz, O. Toprakci, K. Fu, X. Zhang, *Energy Environ. Sci.* **2014**, *7*, 3857; b) S. S. Zhang, *J. Power Sources* **2007**, *164*, 351.
- [328] J.-Q. Huang, Q. Zhang, H.-J. Peng, X.-Y. Liu, W.-Z. Qian, F. Wei, *Energy Environ. Sci.* **2014**, *7*, 347.
- [329] I. Bauer, S. Thieme, J. Brueckner, H. Althues, S. Kaskel, *J. Power Sources* **2014**, *251*, 417.
- [330] J. Conder, A. Forner-Cuenca, E. M. Gubler, L. Gubler, P. Novak, S. Trabesinger, *ACS Appl. Mater. Interfaces* **2016**, *8*, 18822.
- [331] Y.-S. Su, A. Manthiram, *Nat. Commun.* **2012**, *3*, 1166.
- [332] C. Li, A. L. Ward, S. E. Doris, T. A. Pascal, D. Prendergast, B. A. Helms, *Nano Lett.* **2015**, *15*, 5724.
- [333] Q. Wang, J. Jin, X. Wu, G. Ma, J. Yang, Z. Wen, *Phys. Chem. Chem. Phys.* **2014**, *16*, 21225.
- [334] J.-Q. Huang, T.-Z. Zhuang, Q. Zhang, H.-J. Peng, C.-M. Chen, F. Wei, *ACS Nano* **2015**, *9*, 3002.
- [335] S. Bai, X. Liu, K. Zhu, S. Wu, H. Zhou, *Nat. Energy* **2016**, *1*, 16094.
- [336] Z. Jin, K. Xie, X. Hong, *RSC Adv.* **2013**, *3*, 8889.
- [337] L. Wang, Y. Wang, Y. Xia, *Energy Environ. Sci.* **2015**, *8*, 1551.
- [338] X. Yu, Z. Bi, F. Zhao, A. Manthiram, *ACS Appl. Mater. Interfaces* **2015**, *7*, 16625.
- [339] X. Yu, Z. Bi, F. Zhao, A. Manthiram, *Adv. Energy Mater.* **2016**, *6*, 1601392.
- [340] F. Zeng, Z. Jin, K. Yuan, S. Liu, X. Cheng, A. Wang, W. Wang, Y.-s. Yang, *J. Mater. Chem. A* **2016**, *4*, 12319.
- [341] T. Yim, S. H. Han, N. H. Park, M.-S. Park, J. H. Lee, J. Shin, J. W. Choi, Y. Jung, Y. N. Jo, J.-S. Yu, K. J. Kim, *Adv. Funct. Mater.* **2016**, *26*, 7817.
- [342] T.-Z. Zhuang, J.-Q. Huang, H.-J. Peng, L.-Y. He, X.-B. Cheng, C.-M. Chen, Q. Zhang, *Small* **2016**, *12*, 381.
- [343] Y.-S. Su, A. Manthiram, *Chem. Commun.* **2012**, *48*, 8817.
- [344] H. Yao, K. Yan, W. Li, G. Zheng, D. Kong, Z. W. Seh, V. K. Narasimhan, Z. Liang, Y. Cui, *Energy Environ. Sci.* **2014**, *7*, 3381.
- [345] a) S.-H. Chung, A. Manthiram, *Adv. Funct. Mater.* **2014**, *24*, 5299; b) H. Wei, J. Ma, B. Li, Y. Zuo, D. Xia, *ACS Appl. Mater. Interfaces* **2014**, *6*, 20276.
- [346] a) S.-H. Chung, A. Manthiram, *J. Phys. Chem. Lett.* **2014**, *5*, 1978; b) C. Jin, W. Zhang, Z. Zhuang, J. Wang, H. Huang, Y. Gan, Y. Xia, C. Liang, J. Zhang, X. Tao, *J. Mater. Chem. A* **2017**, *5*, 632.
- [347] a) L. Wang, Z. Yang, H. Nie, C. Gu, W. Hua, X. Xu, X. a. Chen, Y. Chen, S. Huang, *J. Mater. Chem. A* **2016**, *4*, 15343; b) X. Gu, C.-j. Tong, C. Lai, J. Qiu, X. Huang, W. Yang, B. Wen, L.-m. Liu, Y. Hou, S. Zhang, *J. Mater. Chem. A* **2015**, *3*, 16670.
- [348] S.-H. Chung, P. Han, R. Singhal, V. Kalra, A. Manthiram, *Adv. Energy Mater.* **2015**, *5*, 1500738.
- [349] a) Z. Xiao, Z. Yang, L. Wang, H. Nie, M. e. Zhong, Q. Lai, X. Xu, L. Zhang, S. Huang, *Adv. Mater.* **2015**, *27*, 2891; b) S.-H. Chung, A. Manthiram, *Adv. Mater.* **2014**, *26*, 7352; c) G. Wang, Y. Lai, Z. Zhang, J. Li, Z. Zhang, *J. Mater. Chem. A* **2015**, *3*, 7139.
- [350] S.-H. Chung, A. Manthiram, *Chem. Commun.* **2014**, *50*, 4184.
- [351] C.-H. Chang, S.-H. Chung, A. Manthiram, *Small* **2016**, *12*, 174.
- [352] J. Balach, T. Jaumann, M. Klose, S. Oswald, J. Eckert, L. Giebeler, *Adv. Funct. Mater.* **2015**, *25*, 5285.
- [353] J. Balach, T. Jaumann, M. Klose, S. Oswald, J. Eckert, L. Giebeler, *J. Phys. Chem. C* **2015**, *119*, 4580.
- [354] J. Balach, T. Jaumann, M. Klose, S. Oswald, J. Eckert, L. Giebeler, *J. Power Sources* **2016**, *303*, 317.
- [355] J. Balach, H. K. Singh, S. Gomoll, T. Jaumann, M. Klose, S. Oswald, M. Richter, J. Eckert, L. Giebeler, *ACS Appl. Mater. Interfaces* **2016**, *8*, 14586.
- [356] H.-J. Peng, D.-W. Wang, J.-Q. Huang, X.-B. Cheng, Z. Yuan, F. Wei, Q. Zhang, *Adv. Sci.* **2016**, *3*, 1500268.
- [357] N. Liu, B. Huang, W. Wang, H. Shao, C. Li, H. Zhang, A. Wang, K. Yuan, Y. Huang, *ACS Appl. Mater. Interfaces* **2016**, *8*, 16101.
- [358] P.-Y. Zhai, H.-J. Peng, X.-B. Cheng, L. Zhu, J.-Q. Huang, W. Zhu, Q. Zhang, *Energy Storage Mater.* **2017**, *7*, 56.
- [359] J. H. Kim, J. Seo, J. Choi, D. Shin, M. Carter, Y. Jeon, C. Wang, L. Hu, U. Paik, *ACS Appl. Mater. Interfaces* **2016**, *8*, 20092.
- [360] S. A. Abbas, M. A. Ibrahim, L.-H. Hu, C.-N. Lin, J. Fang, K. M. Boopathi, P.-C. Wang, L.-J. Li, C.-W. Chu, *J. Mater. Chem. A* **2016**, *4*, 9661.
- [361] L. Luo, S.-H. Chung, A. Manthiram, *J. Mater. Chem. A* **2016**, *4*, 16805.
- [362] G. Ma, Z. Wen, J. Jin, M. Wu, X. Wu, J. Zhang, *J. Power Sources* **2014**, *267*, 542.
- [363] C.-Y. Fan, H.-Y. Yuan, H.-H. Li, H.-F. Wang, W.-L. Li, H.-Z. Sun, X.-L. Wu, J.-P. Zhang, *ACS Appl. Mater. Interfaces* **2016**, *8*, 16108.
- [364] J.-Q. Huang, B. Zhang, Z.-L. Xu, S. Abouali, M. A. Garakani, J. Huang, J.-K. Kim, *J. Power Sources* **2015**, *285*, 43.
- [365] T. Zhao, Y. Ye, X. Peng, G. Divitini, H.-K. Kim, C.-Y. Lao, P. R. Coxon, K. Xi, Y. Liu, C. Ducati, R. Chen, R. V. Kumar, *Adv. Funct. Mater.* **2016**, *26*, 8418.
- [366] J. Liu, L. Yuan, K. Yuan, Z. Li, Z. Hao, J. Xiang, Y. Huang, *Nanoscale* **2016**, *8*, 13638.
- [367] J. Balach, T. Jaumann, S. Muehlenhoff, J. Eckert, L. Giebeler, *Chem. Commun.* **2016**, *52*, 8134.
- [368] N. Liu, F. Ai, W. Wang, H. Shao, H. Zhang, A. Wang, Z. J. Xu, Y. Huang, *Electrochim. Acta* **2016**, *215*, 162.
- [369] H.-J. Peng, Z.-W. Zhang, J.-Q. Huang, G. Zhang, J. Xie, W.-T. Xu, J.-L. Shi, X. Chen, X.-B. Cheng, Q. Zhang, *Adv. Mater.* **2016**, *28*, 9551.
- [370] S. Niu, W. Lv, G. Zhou, H. Shi, X. Qin, C. Zheng, T. Zhou, C. Luo, Y. Deng, B. Li, F. Kang, Q.-H. Yang, *Nano Energy* **2016**, *30*, 138.
- [371] M. S. Kim, L. Ma, S. Choudhury, L. A. Archer, *Adv. Mater. Interfaces* **2016**, *3*, 1600450.

- [372] M. S. Kim, L. Ma, S. Choudhury, S. S. Moganty, S. Wei, L. A. Archer, *J. Mater. Chem. A* **2016**, *4*, 14709.
- [373] a) M.-H. Ryou, D. J. Lee, J.-N. Lee, Y. M. Lee, J.-K. Park, J. W. Choi, *Adv. Energy Mater.* **2012**, *2*, 645; b) M.-H. Ryou, Y. M. Lee, J.-K. Park, J. W. Choi, *Adv. Mater.* **2011**, *23*, 3066.
- [374] J.-S. Kim, T. H. Hwang, B. G. Kim, J. Min, J. W. Choi, *Adv. Funct. Mater.* **2014**, *24*, 5359.
- [375] J.-S. Kim, D.-J. Yoo, J. Min, R. A. Shakoor, R. Kahraman, J. W. Choi, *ChemNanoMat* **2015**, *1*, 240.
- [376] Z. Zhang, Z. Zhang, J. Li, Y. Lai, *J. Solid State Electrochem.* **2015**, *19*, 1709.
- [377] R. Song, R. Fang, L. Wen, Y. Shi, S. Wang, F. Li, *J. Power Sources* **2016**, *301*, 179.
- [378] B.-C. Yu, K. Park, J.-H. Jang, J. B. Goodenough, *ACS Energy Lett.* **2016**, *1*, 633.
- [379] W. Luo, L. Zhou, K. Fu, Z. Yang, J. Wan, M. Manno, Y. Yao, H. Zhu, B. Yang, L. Hu, *Nano Lett.* **2015**, *15*, 6149.
- [380] D. Lin, D. Zhuo, Y. Liu, Y. Cui, *J. Am. Chem. Soc.* **2016**, *138*, 11044.
- [381] H. M. Kim, H.-H. Sun, I. Belharouak, A. Manthiram, Y.-K. Sun, *ACS Energy Lett.* **2016**, *1*, 136.
- [382] J.-Y. Hwang, H. M. Kim, S.-K. Lee, J.-H. Lee, A. Abouimrane, M. A. Khaleel, I. Belharouak, A. Manthiram, Y.-K. Sun, *Adv. Energy Mater.* **2016**, *6*, 1501480.
- [383] H.-S. Kang, Y.-K. Sun, *Adv. Funct. Mater.* **2016**, *26*, 1225.
- [384] C.-Y. Fan, S.-Y. Liu, H.-H. Li, H.-F. Wang, H.-C. Wang, X.-L. Wu, H.-Z. Sun, J.-P. Zhang, *ACS Appl. Mater. Interfaces* **2016**, *8*, 28689.
- [385] L. Qie, A. Manthiram, *ACS Energy Lett.* **2016**, *1*, 46.
- [386] Y. Zhang, K. Li, H. Li, Y. Peng, Y. Wang, J. Wang, J. Zhao, *J. Mater. Chem. A* **2017**, *5*, 97.
- [387] C. Wu, L. Yuan, Z. Li, Z. Yi, Y. Li, R. Zeng, W. Zhang, Y. Huang, *RSC Adv.* **2015**, *5*, 14196.
- [388] Z. Liu, X. Zheng, N.-y. Yuan, J.-n. Ding, *J. Mater. Chem. A* **2017**, *5*, 942.
- [389] G. Zhou, L. Li, D.-W. Wang, X.-y. Shan, S. Pei, F. Li, H.-M. Cheng, *Adv. Mater.* **2015**, *27*, 641.
- [390] R. Fang, S. Zhao, S. Pei, Y. Cheng, P. Hou, M. Liu, H.-M. Cheng, C. Liu, F. Li, *Carbon* **2016**, *109*, 719.
- [391] Y. Fu, Y.-S. Su, A. Manthiram, *Adv. Energy Mater.* **2014**, *4*, 1300655.
- [392] G. Zhou, S. Pei, L. Li, D.-W. Wang, S. Wang, K. Huang, L.-C. Yin, F. Li, H.-M. Cheng, *Adv. Mater.* **2014**, *26*, 625.
- [393] S.-H. Chung, A. Manthiram, *Adv. Mater.* **2014**, *26*, 1360.
- [394] a) H. Wang, W. Zhang, H. Liu, Z. Guo, *Angew. Chem., Int. Ed.* **2016**, *55*, 3992; b) J. Song, Z. Yu, T. Xu, S. Chen, H. Sohn, M. Regula, D. Wang, *J. Mater. Chem. A* **2014**, *2*, 8623.
- [395] J. Yan, X. Liu, H. Qi, W. Li, Y. Zhou, M. Yao, B. Li, *Chem. Mater.* **2015**, *27*, 6394.
- [396] S.-H. Chung, C.-H. Chang, A. Manthiram, *Small* **2016**, *12*, 939.
- [397] Y. Yang, W. Sun, J. Zhang, X. Yue, Z. Wang, K. Sun, *Electrochim. Acta* **2016**, *209*, 691.
- [398] M. Yu, J. Ma, M. Xie, H. Song, F. Tian, S. Xu, Y. Zhou, B. Li, D. Wu, H. Qiu, R. Wang, *Adv. Energy Mater.* **2017**, *7*, 1602347.
- [399] C. Zu, A. Manthiram, *Adv. Energy Mater.* **2014**, *4*, 1400897.
- [400] R. Fang, S. Zhao, S. Pei, X. Qian, P.-X. Hou, H.-M. Cheng, C. Liu, F. Li, *ACS Nano* **2016**, *10*, 8676.
- [401] S. Li, T. Mou, G. Ren, J. Warzywoda, B. Wang, Z. Fan, *ACS Energy Lett.* **2016**, *1*, 481.
- [402] C.-H. Chang, S.-H. Chung, A. Manthiram, *Mater. Horiz.* **2017**, DOI: 10.1039/c6mh00426a.
- [403] J. Song, M.-J. Choo, H. Noh, J.-K. Park, H.-T. Kim, *ChemSusChem* **2014**, *7*, 3341.
- [404] Z. Li, J. T. Zhang, Y. M. Chen, J. Li, X. W. Lou, *Nat. Commun.* **2015**, *6*, 8850.
- [405] S.-H. Chung, C.-H. Chang, A. Manthiram, *Energy Environ. Sci.* **2016**, *9*, 3188.
- [406] S.-H. Chung, C.-H. Chang, A. Manthiram, *J. Power Sources* **2016**, *334*, 179.
- [407] Y. Liu, D. Lin, P. Y. Yuen, K. Liu, J. Xie, R. H. Dauskardt, Y. Cui, *Adv. Mater.* **2017**, *29*, 1605531.
- [408] H. Al Salem, G. Babu, C. V. Rao, L. M. R. Arava, *J. Am. Chem. Soc.* **2015**, *137*, 11542.
- [409] Z. Wang, Y. Dong, H. Li, Z. Zhao, H. B. Wu, C. Hao, S. Liu, J. Qiu, X. W. Lou, *Nat. Commun.* **2014**, *5*, 5002.
- [410] a) W. J. Chung, J. J. Griebel, E. T. Kim, H. Yoon, A. G. Simmonds, H. J. Ji, P. T. Dirlam, R. S. Glass, J. J. Wie, N. A. Nguyen, B. W. Guralnick, J. Park, A. Somogyi, P. Theato, M. E. Mackay, Y.-E. Sung, K. Char, J. Pyun, *Nat. Chem.* **2013**, *5*, 518; b) H. Chen, C. Wang, C. Hu, J. Zhang, S. Gao, W. Lu, L. Chen, *J. Mater. Chem. A* **2015**, *3*, 1392.
- [411] S. N. Talapaneni, T. H. Hwang, S. H. Je, O. Buyukcakir, J. W. Choi, A. Coskun, *Angew. Chem., Int. Ed.* **2016**, *55*, 3106.
- [412] a) S. Chen, F. Dai, M. L. Gordin, Z. Yu, Y. Gao, J. Song, D. Wang, *Angew. Chem., Int. Ed.* **2016**, *55*, 4231; b) M. Wu, Y. Cui, A. Bhargava, Y. Losovyj, A. Siegel, M. Agarwal, Y. Ma, Y. Fu, *Angew. Chem., Int. Ed.* **2016**, *55*, 10027; c) W. Hua, Z. Yang, H. Nie, Z. Li, J. Yang, Z. Guo, C. Ruan, X. a. Chen, S. Huang, *ACS Nano* **2017**, DOI: 10.1021/acsnano.6b08627.
- [413] N. Xu, T. Qian, X. Liu, J. Liu, Y. Chen, C. Yan, *Nano Lett.* **2017**, *17*, 538.
- [414] S. Chen, Y. Gao, Z. Yu, M. L. Gordin, J. Song, D. Wang, *Nano Energy* **2017**, *31*, 418.
- [415] a) Z. Lin, Z. Liu, W. Fu, N. J. Dudney, C. Liang, *Angew. Chem., Int. Ed.* **2013**, *52*, 7460; b) H. Nagata, Y. Chikusa, *J. Power Sources* **2014**, *264*, 206; c) F. Han, J. Yue, X. Fan, T. Gao, C. Luo, Z. Ma, L. Suo, C. Wang, *Nano Lett.* **2016**, *16*, 4521.
- [416] X. Han, Y. Gong, K. K. Fu, X. He, G. T. Hitz, J. Dai, A. Pearse, B. Liu, H. Wang, G. Rubloff, Y. Mo, V. Thangadurai, E. D. Wachsman, L. Hu, *Nat. Mater.* **2017**, DOI: 10.1038/nmat4821.